M&D Modelle & Daten

Technical Report

No. 3

Support for Climate- and Earth System Research at the Max Planck Institute for Meteorology, Hamburg

Ensemble Simulations over Europe with the Regional Climate Model CLM forced with IPCC AR4 Global Scenarios

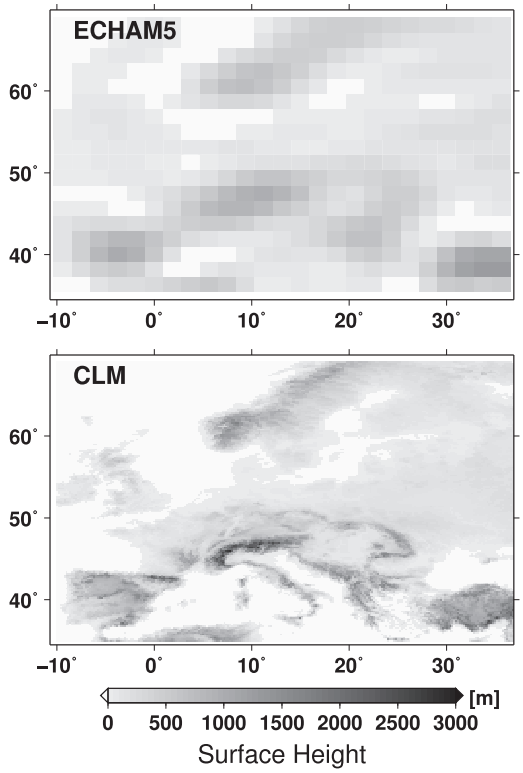

by

Heinz-Dieter Hollweg, Uwe Böhm, Irina Fast, Barbara Hennemuth, Klaus Keuler, Elke Keup-Thiel, Michael Lautenschlager, Stephanie Legutke, Kai Radtke, Burkhardt Rockel, Martina Schubert, Andreas Will, Michael Woldt, Claudia Wunram

Hamburg, December 2008

Support for Climate- and Earth System Research at the Max Planck Institute for Meteorology, Hamburg

Office address

Max-Planck-Institut für Meteorologie
Gruppe Modelle & Daten
Beim Schlump 58
20144 Hamburg

Post address

Max-Planck Institut für Meteorologie
Gruppe Modelle & Daten
Bundesstrasse 53
D-20146 Hamburg
Germany

Contact via e-Mail

Contact the office: mad_office@dkrz.de
Contact the Model-Section: model@dkrz.de
Contact the Data-Section: data@dkrz.de

Phone/Fax

Tel: +49 (40) 411 73 - 189
Fax: +49 (40) 411 73 - 476

Internet

Home Page: http://www.mad.zmaw.de

Cover figure (figure 2): Surface height. Top: ECHAM5/MPIOM: assessed from the surface geopotential (see text). Bottom: CLM parameter HSURF for D3 assigned from nearest D2 neighbour grid-box.

Technical Report

No. 3

Gruppe Modelle & Daten

Support for Climate- and Earth System Research at the Max Planck Institute for Meteorology, Hamburg

Ensemble Simulations over Europe with the Regional Climate Model CLM forced with IPCC AR4 Global Scenarios

Heinz-Dieter Hollweg [1], Uwe Böhm [2], Irina Fast [1], Barbara Hennemuth [1], Klaus Keuler [3], Elke Keup-Thiel [1], Michael Lautenschlager [1], Stephanie Legutke [1], Kai Radtke [3], Burkhardt Rockel [4], Martina Schubert [1], Andreas Will [3], Michael Woldt [3], Claudia Wunram [1]

corresponding author: Stephanie Legutke, Max-Planck-Institut für Meteorologie, Gruppe Modelle & Daten. Postal address: Bundesstrasse 53, D-20146 Hamburg, Germany,

e-mail: stephanie.legutke@zmaw.de

[1] Model and Data group, Max Planck Institute for Meteorology, Hamburg, Germany
[2] Potsdam Institute for Climate Impact Research (PIK)
[3] Brandenburgische Technische Universität Cottbus (BTU)
[4] GKSS-Forschungszentrum Geesthacht

ISSN 1619-2257

Hamburg, December 2008

Ensemble Simulations over Europe with the Regional Climate Model CLM forced with IPCC AR4 Global Scenarios

Heinz-Dieter Hollweg[1], Uwe Böhm[2], Irina Fast[1], Barbara Hennemuth[1], Klaus Keuler[3], Elke Keup-Thiel[1], Michael Lautenschlager[1], Stephanie Legutke[*,1], Kai Radtke[3], Burkhardt Rockel[4], Martina Schubert[1], Andreas Will[3], Michael Woldt[3], Claudia Wunram[1]

[*]corresponding author: Stephanie Legutke, Max-Planck-Institut für Meteorologie, Gruppe Modelle & Daten. Postal address: Bundesstrasse 53, D-20146 Hamburg, Germany, e-mail: stephanie.legutke@zmaw.de

[1]Model and Data group, Max Planck Institute for Meteorology, Hamburg, Germany

[2]Potsdam Institute for Climate Impact Research (PIK)

[3]Brandenburgische Technische Universität Cottbus (BTU)

[4]GKSS-Forschungszentrum Geesthacht

CLM Technical Report

Date: 2008-11-10

Abstract

Regional climate projections have been performed for Europe with the climate version CLM (version 3.1) of the 'Lokal-Modell' (LM) of the German Meteorological Service. CLM has been forced with output of the ECHAM5/MPIOM global climate model of the Max Planck Institute for Meteorology, which contributed to the fourth climate assessment report (AR4) of the International Panel on Climate Change (IPCC). The results of the global model for the IPCC A1B and B1 scenarios as well as the reconstruction of the last four decades of the 20th century (20C3M) for the AR4 are dynamically scaled down to the CLM grid cell size of about 18×18 km^2. Climatological parameters including all model variables and additional quantities characterising the climate are available from the World Data Centre for Climate database run by the German climate service group Model & Data. They can be accessed by the general public at no costs with the help of M&D. In particular, the 'Service Group Adaptation' (SGA) has been established at M&D to assist adaptation projects funded by the German Federal Ministry of Education and Research (BMBF) giving advice on the interpretation of the CLM model results.

Contents

1 Introduction

The Intergovernmental Panel on Climate Change (IPCC) has established the current understanding of climate change in its fourth assessment report AR4 (IPCC, 2007). In the "Special Report on Emissions Scenarios" (SRES), available from *http://www.grida.no/climate/ipcc/emission/index.htm*, emission scenarios are defined, which are based on different assumptions for economic and population growth, implementation rates of energy-efficient technologies, and convergence of national economy levels. The conversion from emissions to atmospheric concentrations of greenhouse gases and sulphate aerosols is described in chapter 10 and illustrated by Figure 10.26 of the IPCC AR4.

Projections of the climate in the next century have been calculated for the AR4 with 23 Global Climate Models (GCM) for a number of scenarios. However, results from GCMs have a coarse resolution and regional effects are poorly represented. Assessing regional aspects of climate change requires downscaling from the global resolution to smaller scales. Giorgi et al. (2001) discuss statistical and dynamical downscaling methods in the 'Third Assessment Report of IPCC'. Statistical downscaling, since it relies on data of the past, may not be applicable to future projections, because these may not have the same statistical relationships (Leung et al., 2003). Dynamical downscaling describes the nesting of a Regional Climate Model (RCM) into the grid of a GCM where the output of the global model supplies the regional model with boundary conditions (Mearns et al., 2003, *http://www.ipcc-data.org/guidelines/index.html).*

Most of the dynamical downscaling studies perform time slice experiments and simulate typically two periods of 30 years, one period in the past and one period in the future. In the study presented here, a small ensemble of transient regional climate simulations has been generated over Europe from 1960 to 2100 with different boundary conditions representing different realisations of the present day climate and of the future climate on a rotated spherical grid of 0.165°with 257x271 grid points. The simulations have no feed-back from the regional model to the global scale. This would require synchronously two-way nested model runs, which are demanding in computing resources and difficult to accomplish with the available computing facilities. It should be noticed that the downscaling method cannot amend systematic errors in the driving GCM output, however, it can improve the reproduction of patterns on smaller scales not represented by the coarse-resolution of a GCM (Giorgi et al., 2001).

The transient ensemble climate-change simulations described here were performed with the climate version CLM of the "Lokal-Modell" (LM). The LM was originally developed by the German Meteorological Service (DWD) (Steppeler et al., 2002) and is now further developed by COSMO, the

consortium of national weather services for small scale modelling. The CLM (Will et al., 2008, Boehm et al., 2006) was developed by the CLM-Community, an international network of scientists from universities and research centers (*http://www.clm-community.eu*).

Simulation results of the coupled atmosphere-ocean global climate model ECHAM5/MPIOM for the last four decades of the 20th century (IPCC AR4 20C3M climate reconstruction experiments) and for the IPCC scenarios A1B and B1 were used to drive the regional climate simulations. In the global simulations, the atmospheric model component ECHAM5 has a horizontal resolution of approximately 200 km (T63) and 31 vertical levels. The horizontal resolution of the ocean component model MPIOM varies regionally between approximately 10 km and 150 km. The GCM ECHAM5/MPIOM and its components were developed by the Max Planck Institute for Meteorology in Hamburg. It is described in a special section of the Journal of Climate (see e.g. Jungclaus et al., 2006).

Data and documentation of the ECHAM5/MPIOM global IPCC AR4 climate projections are available at the World Data Centre for Climate (WDCC) and can be accessed from *http://ipcc.wdc-climate.de*. These global experiments are summarised in Roeckner et al. (2006).

The German Federal Ministry of Education and Research (BMBF) promotes within the "Funding Priority 'klima*zwei*' Research for Climate Protection and Protection from Climate Impacts" interdisciplinary projects with various thematic backgrounds. The projects aim to develop strategies and techniques on how to adapt to the imminent regional climate change in the upcoming decades. Emphasis is on project schemes with an application oriented approach. Having members from several disciplines, the joint projects address various aspects of suitable adaptation processes in different geographical regions. Thus, the Service Group Adaptation has been established at M&D (SGA-Hamburg) and the DWD (SGA-Offenbach) as interface between modellers and the project partners. Consulting and supporting the interdisciplinary project partners is understood to be the comprehensive purpose of SGA's work. Another goal is to facilitate the communication between climate experts having a modelling background and climate data users from all parts of society aiming at application oriented strategies. SGA communicates both, simulated regional model products as well as climatological observations. The latter is carried out by the DWD in close cooperation with the SGA.

This report has six main parts. In section 2 the regional climate model CLM and its configuration developed by members of the CLM-Community (BTU, GKSS, PIK) used for the simulations is described. In section 3 the in- and output and different aspects of the conduction of the experiments are given by the M&D group. In section 4 the concept of the quality control of the original model output performed at BTU Cottbus and of the visual and automated inspection of the data performed by M&D is described. Section 5 gives a detailed description of the model output and postprocessing

products available from the CERA archive on behalf of SGA and of the inspection of all output data types. Section 6 contains results of the quality control of the model output for selected variables and regions. Finally, a list of the model output variables together with a short description are found in the Appendix.

2 The configuration of the regional climate model CLM

After the ambitious decision to downscale the ECHAM5/MPIOM IPCC AR4 scenario simulations for a large model domain of roughly 4500 km × 5000 km to a grid resolution of approximately 18 km conducting transient model runs from 1960 to 2100 for different IPCC scenarios with the regional community model CLM, the developers of the Climate version of the 'Lokal Modell' (CLM) had to find an appropriate configuration and model version for these ensemble simulations. This configuration will be named in the following CLM_3-K

Three groups within the community undertook the task: BTU Cottbus, GKSS and PIK. It was a challenge in several respects. First, the CLM is a new model and it has never before been used for climate change simulations. Second, all previous CLM evaluation runs have been done over a time scale of 15 years only. Third, the domain size of CLM_3-K is substantially larger than that of any previous evaluation run, although these have had already a size of 3500 km × 3900 km. Fourth, no other non-hydrostatic regional climate model had been used before to perform such simulations.

In the following the configuration CLM_3-K of the CLM_3.1 model version used for the experiments is described in four paragraphs. At first the external fields are described characterising the properties of the land surface and of the deep soil. Then, the fields used as initial and boundary conditions at the lateral, lower, and upper boundaries of the model domain are specified. Here after, the definition of the model grid is given followed by the settings of the other steering parameters (namelist parameters) affecting the model dynamics and model physics. Finally, the initialisation of the runs is described.

2.1 Input fields, initial and boundary conditions

The standard interpolation program *int2clm2* is used to generate the initial and boundary fields of the CLM grid from the original grid of the driving model. The *int2clm2* program is based on the *int2lm1.1* program of the German Meteorological Service (see Schaettler, 2005, for details).

The constant external fields, characterising the properties of earth's surface and of the deep soil, are taken from the DWD global data set. The fields are listed in Table 1.

The ECHAM5/MPIOM results are used to generate the atmospheric initial and boundary conditions of the CLM simulation. They are described in section 3 in this report. Table 1 gives an overview of the ECHAM5/MPIOM AR4 control and scenario simulation fields used as boundary and/or as initial conditions of the CLM atmosphere.

Table 1 Data used for CLM simulations. Land surface and soil data from DWD data set: land fraction (FRLAND), surface height above sea level (HSURF), surface roughness length (Z0), leaf area index (LAI), plant cover / vegetation area fraction (PLCOV), root depth (ROOTDP), soil type (STYPE) and the temperature of the deepest soil layer (T_CL). ECHAM5/MPIOM fields used as initial and/or boundary conditions: temperature (T), horizontal wind (U,V), pressure (P), specific humidity (QV), liquid water content (QC), land surface temperature (T_S), sea surface temperature (SST), snow water content (W_SNOW), snow surface temperature (T_SNOW).

DWD external fields	**ECHAM5/MPIOM sim. results**		
2D Initial & Boundary	**3D Initial & Boundary**	**2D Initial & Boundary**	**2D Initial**
FRLAND	T	SST	T_S
HSURF	U,V	T_SNOW	
Z0	P	W_SNOW	
LAI	QV		
PLCOV	QC		
ROOTDP			
STYPE			
T_CL			

All dynamical variables of the CLM model have to be initialised at all grid points of the model domain from the forcing fields. They have been updated every 6h (time increment) at the lateral, upper and lower (only Sea Surface Temperatures) boundaries of the CLM model domain and interpolated at each time step.

The CLM soil model TERRA is a multi layer model with a constant temperature lower boundary condition (see Table 2 for the configuration of the soil). The ECHAM5/MPIOM used a 3 m deep soil with a zero flux lower boundary condition. Furthermore, the distribution of the soil types in the model domain was different in the regional and in the global model. Therefore, an initialisation of the CLM soil using the ECHAM5/MPIOM profiles was not useful. The soil temperature has been initialised as solution of the heat conduction equation between the land surface temperature at initial time and the prescribed temperature of the deepest soil layer (T_{CL}). The latter has been calculated as the 1961-1990 mean of the CRU 2 m temperature. The lower boundary condition T_{CL} was kept

constant over the whole simulation period. The soil water content was initialised with 75% of the pore volume (PV) of the soil at each grid cell. However, the specific PV depends on the soil type.

Two additional modifications of the external fields have been performed. First, the standard root depth has been stretched in order to obtain the same mean root depth as in the ECOCLIMAP data set. This avoids the drying of the upper soil layers due to strong evapo-transpiration.
The second modification was a substantial reduction of the height of the Caucasus Mountains to the constant height of 150 m, which is the mean height in the ECHAM5/MPIOM model for that region. Therefore, it is recommended not to use the results in that region for further studies. The reduction of the Caucasus orography became necessary, because the mountains cross the eastern boundary. Two problems could be solved, which originated from the height difference of the Caucasus Mountains in the ECHAM5 grid (far below 500 m) and in the CLM grid (above 2000 m). First, there is no method to generate the prescribed boundary values of the dynamical fields in steep orography from the velocities in flat orography. Second, the mass flux through the eastern boundary was systematically smaller in the CLM than in the ECHAM5 model due to prescribed velocities and pressure boundary conditions (no mass flux through the mountain). Over long time scales a positive pressure bias would occur within the CLM model domain.
No height correction of the deep soil temperature T_CL was applied in the Caucasus Mountains after reduction of their height. This caused unrealistically low deep soil temperatures at 150 m above sea level and caused an unphysical cooling of the surface temperatures. However, a direct comparison of the average daily maximum temperature at 2 m (see Fig.17) and other variables for the CLM050 evaluation run with CRU data exhibited no anomaly in that region, which could be caused by the low deep soil temperatures. Furthermore, the dominating westerlies prevented a transport of the effect of the modification into the model domain. A significant effect on any of the regions selected for the quality control (see Table 8) can therefore be excluded.

2.2 Model grid

The horizontal model domain of the experiments was decided to be very similar to the model domain of the ENSEMBLES project. It covers Europe nearly entirely, including the Iberian Peninsula, the Mediterranean, the Black Sea, Great Britain, and Scandinavia. Especially, the extension of the domain to the northern part of Africa and over the Atlantic to obtain a 500 km distance to the Iberian coast is substantial in comparison with previous simulations not only with the CLM.

The definition of the model grid is done by setting model parameters of the `LMGRID` namelist

(www.clm-community.eu → Model System → COSMO-CLM → Configuration of CLM). The model grid orography and the geographic coordinates (black lines) are given in Figure 1. The details of the model grid are summarised in Table 2.

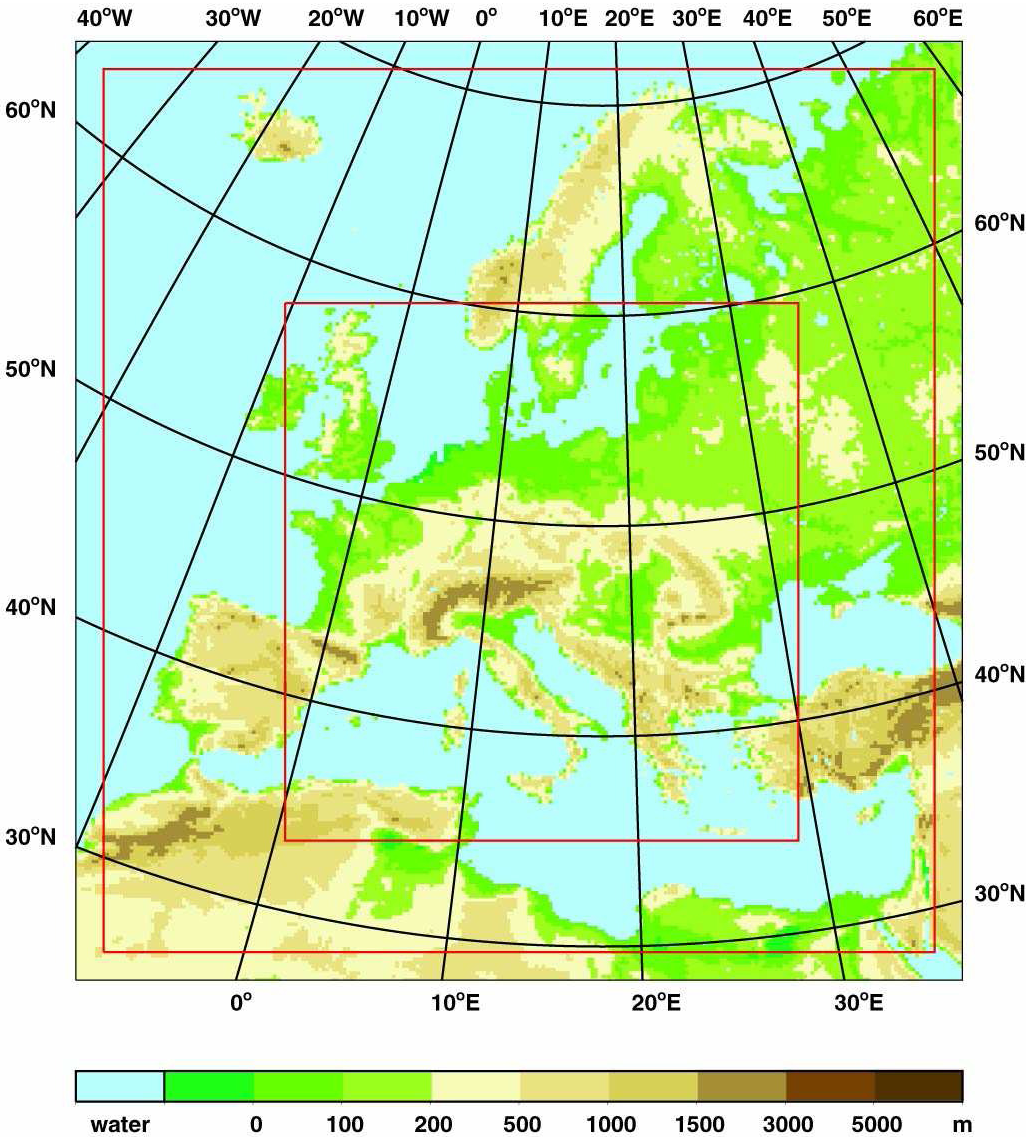

Figure 1 The orography of the experiments in the model domain. The outer red line separates the relaxation zone from the inner model domain and follow the model grid lines. The black lines show the geographical grid.

Table 2 Model Grid. *rlon*: longitudes of the rotated grid. *rlat*: latitudes of the rotated grid. The vertical height of the levels is calculated assuming the dry-adiabatic stratification of the standard atmosphere. The height of the levels is given in [Pa/Pa], which is the factor P_f in $P(z) = P_f(z) \times P_0$ with the standard pressure at sea level P_0, and in [m], which is the corresponding absolute height.

Atmospheric Grid		
Rotated location of north pole	longitude: -162	latitude: 39.25
Horizontal Grid	rlon	rlat
Extension	- 25.0475 to 17.1925	-22.1925 to 22.3575
Resolution	0.165	0.165
Number of grid points	257	271
Vertical Grid	32 layers	
Height of layer: 32 to 25 [Pa/Pa] 24 to 18 [Pa/Pa] 17 to 10 [Pa/Pa] 9 to 1 [Pa/Pa]	 0.992, 0.982, 0.970, 0.956, 0.940, 0.922, 0.903, 0.883, 0.862, 0.839, 0.813, 0.783, 0.749, 0.712, 0.673, 0.633, 0.593, 0.553, 0.513, 0.473, 0.433, 0.393, 0.353, 0.313, 0.273, 0.233, 0.193, 0.153, 0.113, 0.077, 0.046, 0.020	
Height of layer: 32 to 25 [m] 24 to 17 [m]	 67.7, 152.9, 256.2, 378.2, 519.4, 680.7, 853.9, 1039.6, 1238.5, 1461.2, 1719.2, 2015.4, 2353,2, 2725.8	
Soil Grid		
Number of layers	10	
Mean depth of layers	0.01, 0.04, 0.10, 0.22, 0.46, 0.94, 1.90, 3.82, 7.66, 15.34	

The CLM uses terrain-following, rotated spherical height coordinates (see Doms and Schaettler (2003). The vertical coordinate is parallel to the gravitational force. The horizontal coordinates are indicated by the red lines in Figure 1. One of the advantages of the rotated spherical grid is a horizontal grid stretching close to unity in the model domain. Hereto the location of the rotated north pole is chosen in such a way that the equator of the rotated grid divides the model domain in two nearly equal parts.

The spatial resolution and the time scale of the integration are substantially increased compared to the ENSEMBLES simulations. The horizontal resolution of the model grid ($\Delta\lambda = \Delta\phi = 1/6^\circ$) is

chosen to be the same as in the CLM evaluation runs (CLM_3-E) and results in 257 $\times$ 271 horizontal grid points.
The calculation of the downscaling factor S can be estimated as quotient of the resolved wave lengths of the global and of the regional model simulations. As shown by Laprise (1992) the method for the calculation of the spectral resolution on the sphere is not unique. Here we use the definition for maximal wave number representation. In grid space models two grid points are required for the representation of a wave. The minimal wavelength represented by spectral models with triangular truncation may be estimated by the wave length of the zonal wave with highest wave number at the equator. The resulting downscaling factor is:

$$\begin{aligned}
\text{ECHAM5 (T63):} \quad & L_{ECHAM} = \frac{2\pi R}{63} = 635,41 \text{ km} \\
\text{CLM } (1/6^\circ): \quad & L_{CLM} = 2\Delta x = 2\frac{2\pi R}{360^\circ}\Delta\lambda = 37,07 \text{ km} \\
\rightarrow \textbf{downscaling factor:} \quad & \mathbf{S = L_{ECHAM}/L_{CLM} = \frac{360^\circ}{2 \cdot 63 \Delta\lambda} \simeq 17} \\
\text{with} \quad & R = 6371.229 \text{ km}
\end{aligned}$$

The vertical of the simulations is resolved by 32 layers. This is more than in CLM_3-E (20 layers) and similar to ECHAM5/MPIOM.

2.3 Configuration (namelist) parameters

The period of each simulation was planned to be roughly 140 years in comparison with 30 years of time slice experiments and 15 years of CLM_3-E. Never before was an ensemble of regional climate simulations conducted over such a long period using a horizontal resolution of $1/6^\circ \simeq 18$ km in such a large model domain of roughly 4500×5000 km^2. It appeared to be a challenge to find an appropriate configuration for the simulations.

The CLM has more than 150 external (namelist) parameters affecting the model physics, dynamics, input and output. Overall tested configurations are given on the CLM-homepage (www.clm-community.eu $\rightarrow$ Model System $\rightarrow$ CLM $\rightarrow$ Configuration of CLM-namelist). These are the evaluation configurations CLM_3-E and CLM_4-E and the configuration of the scenario simulations presented here (CLM_3-K). These configurations are based on the COSMO-EU (previously LME) or COSMO-DE (previously LMK) configurations, which have been developed by the German Weather Service (DWD) for operational weather prediction They can be found on the COSMO homepage (www.cosmo-model.org). The set of parameters is arranged in the following 12 `NAMELIST` groups:

LMGRID	the domain and the size of the grid
RUNCTL	organising of the model run
TUNING	the tuning of model equations
DYNCTL	the adiabatic model dynamics
PHYCTL	the diabatic model physics
DIACTL	the diagnostic calculations
NUDGING	the data assimilation
INICTL	initialisation of the model variables
IOCTL	controlling the in- and output
DATABASE	specification of the database job
GRIBIN	specification of the model input
GRIBOUT	specification of the model output

The LMGRID parameters define the model grid and have been discussed in the previous paragraph. The DATABASE and the NUDGING namelist groups are needed for operational weather prediction only. The parameters contained in the remaining nine namelist groups can not be discussed in detail here. The meaning of the single settings is explained shortly in the online documentation mentioned above and in more detail in the model external documentation (see Schaettler et al., 2006, and the other parts of the documentation).

The most important setting in the CLM_3-K configuration is the selection of the time step $\Delta t = 75$ s instead of the 90 s standard time step of the leapfrog scheme for 18 km horizontal resolution, also used in CLM_3-E. Using the standard time step an instability occurred in the large CLM_3-K model domain, which did not occur for integration times typical in the numerical weather prediction mode neither for coarse horizontal resolutions of 50 km nor for the standard domain size of CLM_3-E. This instability originates probably in the standard splitting of fast waves and slow modes used in the leap-frog scheme.

There are several further settings of minor relevance affecting the results in some respects. Here the settings of four parameters are discussed, which might be of interest to the data user.

The time increment of updating the boundary fields (see GRIBIN, the `HINCBOUND` parameter) of the simulation has been set to 6 hours, which is the time increment of the forcing fields from ECHAM5/ MPIOM. Between the update times a linear interpolation of the boundary fields is applied.

The standard width of the lateral boundary relaxation zone, in which the CLM solution is relaxed to the ECHAM5/MPIOM fields, are 8 grid boxes for numerical weather prediction applications. The standard value was confirmed to be optimal in the climate mode for the 18 km resolution.

The parameter `rat_sea` in `PHYCTL` determines the evaporation over sea. However, there are no reliable observations of evaporation over sea and the integral variable is not very well known. Therefore, it has to be adjusted to obtain observed precipitation over land. The parameter `rat_sea` was increased from 10 to 20 in order to reduce the overestimation of precipitation found in the evaluation simulations.

Finally, the `ico2_rad` parameter in `PHYCTL` sets the radiatively effective CO_2 concentration for the different greenhouse gas scenarios. This approximates the radiative effect of all greenhouse gases. Notice that only the radiative effect of CO_2 is implemented in CLM.

2.4 Initialisation of the simulations

The simulation of the 20th century control climate started at 1 January 1955 00:00 UTC. The model results are made available from 1 January 1960 00:00 UTC. The first 5 years of the simulation are the spin-up phase.

As already described on page 12 in subsection 2.1, the initial condition for the dynamical variables of the 15 m deep soil has been chosen artificially. In order to avoid an influence of this unphysical initial conditions on model results, a five year spin-up phase between 1955 and 1959 was introduced for the development of the vertical soil temperature and soil water content profile at each grid point consistent with the model physics and dynamics.

3 Description of the experiments

3.1 Input and forcing data

The IPCC AR4 experiment output of the GCM ECHAM5/MPIOM supplying the forcing data is stored in binary GRIB format in the World Data Centre for Climate (WDCC) database. Table 3 gives an overview of the ECHAM5/MPIOM experiments related to the regional projections described here.

Table 3 ECHAM5/MPIOM IPCC AR4 forcing for CLM.

Name	Period	Description
EH5-T63L31_OM-GR1.5L40_CTL	2150-2655	Pre-industrial control experiment (CTL).
EH5-T63L31_OM-GR1.5L40_20C_1	1860-2000	20th century reconstruction (20C3M) with anthropogenic forcing (greenhouse gases, sulfate) initialised in the year 2190 of the CTL.
EH5-T63L31_OM-GR1.5L40_20C_2	1860-2000	2. realisation of 20C3M (yr 2215 of CTL).
EH5-T63L31_OM-GR1.5L40_20C_3	1860-2000	3. realisation of 20C3M (yr 2240 of CTL).
EH5-T63L31_OM-GR1.5L40_A1B_1	2001-2100	SRES Scenario: A1B (initialised with yr 2000 of 20C_1).
EH5-T63L31_OM-GR1.5L40_A1B_2	2001-2100	2. realisation (yr 2000 of 20C_2).
EH5-T63L31_OM-GR1.5L40_B1_1	2001-2100	SRES Scenario B1 (yr 2000 of 20C_1).
EH5-T63L31_OM-GR1.5L40_B1_2	2001-2100	2. realisation (yr 2000 of 20C_2).

The first column displays the names associated with the data in the WDCC. All global experiments are started from model states obtained in a 505–year long integration of the coupled global model with pre-industrial conditions. In that 'control' experiment (CTL), the concentrations of well-mixed greenhouse gases have been specified at the observed levels of 1860 and sulphate aerosols are not included. This reconstruction of a non-drifting climate is representative for the middle of the 19th century and provides the initial fields for the 20th century AR4 20C3M global ensemble simulations (rows 2–4 in Table 3). Fields from different years of CTL are used to initialise the different 20C3M realisations. The state of each 20C3M global ensemble realisation at the end of year 2000 is used to initialise the IPCC AR4 climate projections.

Dynamical downscaling of the data from the three 20C3M global ensemble members was performed for the last four decades of the 20th century (1960–2000). These regional simulations will be denoted by CLM_C20 in the following. Analogously, CLM_C20 provides initial driving fields for the realisations of the regional climate projections A1B and B1. The downscaling was performed for the full 100 years simulation period of the global projections A1B and B1. The forcing data from the ECHAM5/MPIOM experiments was supplied to CLM at 6–hourly intervals, interpolated to the CLM horizontal grid and vertical levels. The forcing was linearly interpolated to the regional model time level in CLM.

3.2 Examples of dynamical downscaling

The effect of downscaling is demonstrated for the temperature at 2 m height and total precipitation, contrasting the driving fields from ECHAM5/MPIOM and the CLM output, which is given on a geographical grid (details on page 49 in section 5). Before going into detail, it is pointed out that, although differences are expected, it should be kept in mind that the RCM is forced at the boundaries by 6 hourly GCM fields.

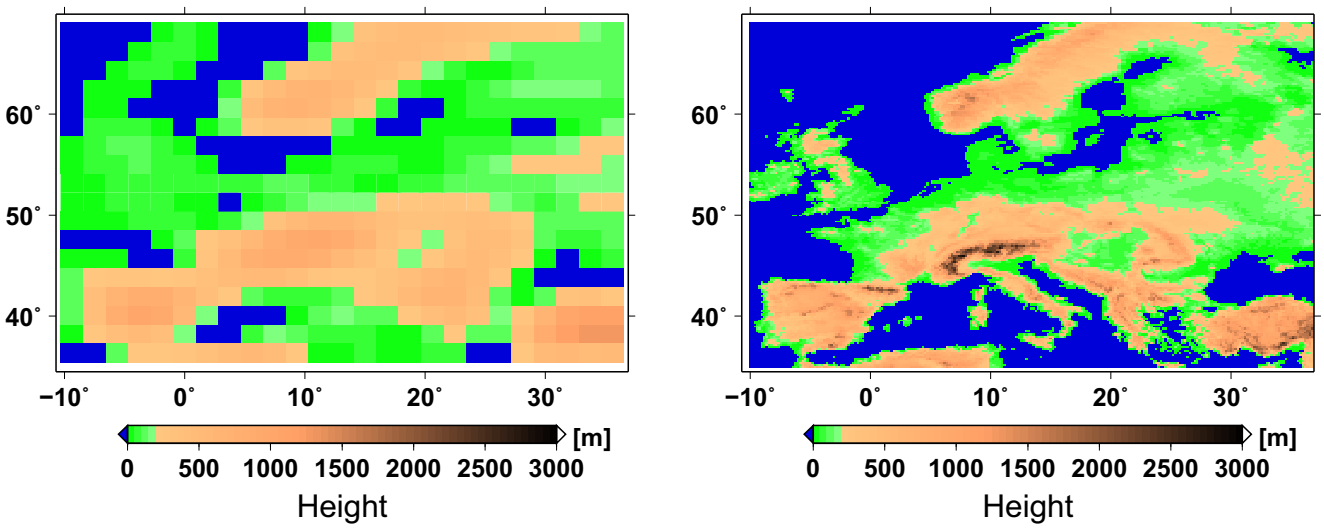

Figure 2 Surface height.
Left: ECHAM5/MPIOM: assessed from the surface geopotential (see text).
Right: CLM parameter HSURF for D3 assigned from nearest D2 neighbour grid-box.

For the analysis in the following, the global fields used to drive CLM are not interpolated to the CLM grid, but used with their original resolution of ECHAM5/MPIOM. Furthermore, it is ignored that the edges of the CLM domain do not exactly match those of the European sub-domain of the GCM used in the analyses. Figure 2 shows a field of the surface height of Europe on both the RCM and the GCM grid. On the regional grid, details of orography and coastlines come out more distinctly. For CLM, the data was assigned to each D3 grid-box from its nearest neighbouring D2 grid-box. The minimum is about -4 m located in Ireland. The minimum for ECHAM5/MPIOM was found to be about -150 m (note that the height was estimated from the geopotential applying a latitude of 50 °N). The magnitude of minimum value is presumably due to spectral truncation. The maximum height in CLM is approx. 2861 m, whereas a maximum of 1257 m was derived for ECHAM5.

Time series of daily-mean temperatures at 2 m height averaged over the European land surface were calculated for both the CLM 20th century runs and the corresponding fields of ECHAM5/MPIOM from all three ensemble runs. The difference ΔT of the CLM minus the ECHAM5/MPIOM data was determined, but only the extremes within blocks of 50 days are shown in Figure 3. The bias derived from the entire set of daily data is drawn in grey. Apparently, CLM obtains a higher mean temperature for the European land than the GCM with a value of about 0.27 K. However, this warm

bias turns into a cold one of -0.08 K, if the CLM D3 data is transformed to the T63 grid resolution of ECHAM5/MPIOM by bilinear interpolation and the land/sea fraction of ECHAM5/MPIOM is applied.

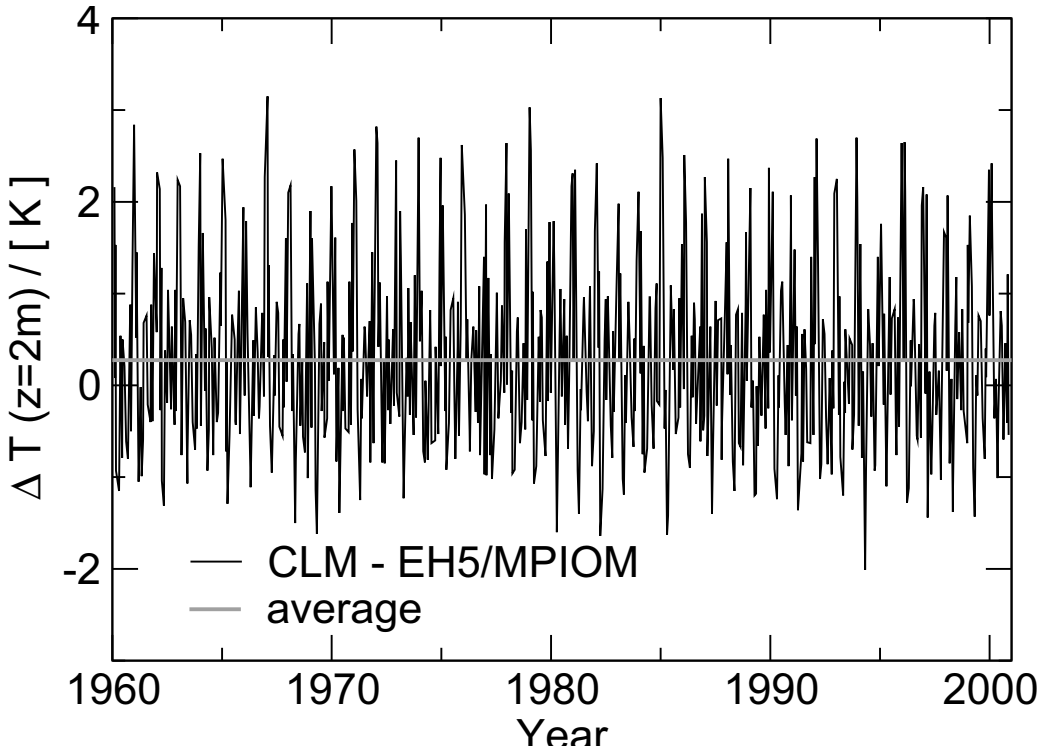

Figure 3 Deviation of daily mean temperature at 2 m height (black curve) averaged over Europe (land only) of the 20th century climate reconstructed by CLM and ECHAM5/MPIOM from the mean of the three ensemble runs, respectively. The bias of the mean daily temperature in grey.

The mean temperature over Europe gives no information about differences between the RCM and the GCM fields on smaller scales. Therefore, a frequency distribution was calculated for both from the three ensemble runs. The frequency distribution in Figure 4 was normalised with respect to the area of each grid-box within the domain and to the time span. Due to the different spatial resolution of the GCM and CLM, the least lower bound of the frequency is different; it is approx. 7×10^{-8} for the smallest GCM grid-cell and approx. 9×10^{-10} for CLM considering daily values over a period of 41 years.

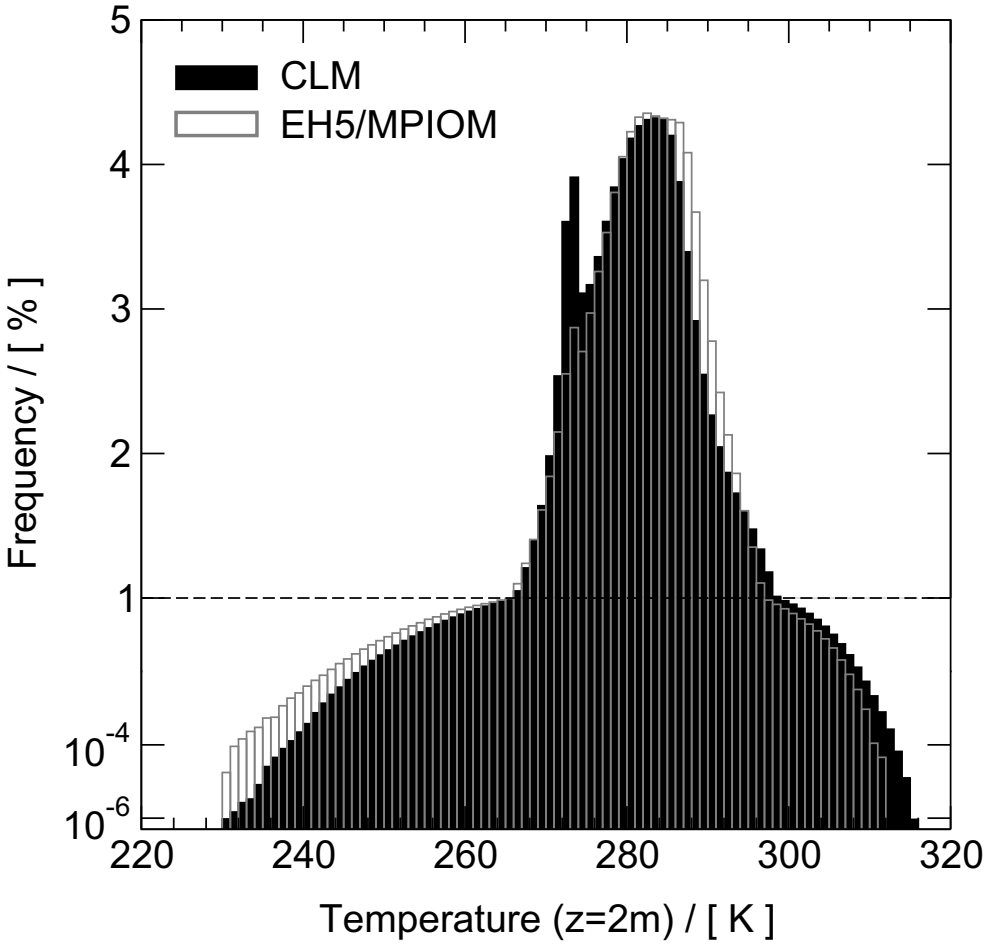

Figure 4 Frequency distribution of daily temperature at 2 m height for all grid cells of the European land surface from CLM_C20 and for the corresponding GCM IPCC AR4 experiment (three ensemble runs for each). The temperature class size is 1 K. Note that the ordinate is split into an upper linear and lower logarithmic scale.

The logarithmic portion of the ordinate brings out rare events. Temperatures below 250 K have a higher frequency in the ECHAM5/MPIOM data, while the opposite is found for the extreme high temperatures. Maximum temperature given by CLM exceeds that of the GCM.

Some 90 % of the mean daily temperature events occurs in classes with a frequency above 1 % . The linear portion of the ordinate shows that the frequency distribution for ECHAM5/MPIOM appears shifted to higher temperatures, i.e. values between 285 K and 300 K are more frequently obtained by the GCM than by CLM and vice versa between 265 K and 300 K. CLM exhibits a peak about 273 K,

which is weaker present in the ECHAM5/MPIOM data. This peak will be discussed further in the following subsection.

Next, we consider diurnal total precipitation, which is the sum of convective and large scale rain and snow fall. Again, all three ensemble runs are taken into account with precipitation over land only.

The daily average of total precipitation on the European surface is about 1.3×10^{13}kg from ECHAM5. This is out valued by CLM by some 28%, where the land area of Europe is about 12 % larger in CLM. Thus, CLM simulates more precipitation than the GCM with lower resolution. Again, additional details are given by the frequency distribution evaluated for the values in all grid boxes as shown in Figure 5.

In this presentation, both ordinate and abscissa are split into a linearly and logarithmically scaled part, i.e. the upper-left panel displays the most frequently occupied classes in a linear – linear scale and the lower-right panel presents the extreme events logarithmically. Additionally, the frequency of non-precipitation events is shown by a singular histogram bar.

The most common case is precipitation of small amounts shown in the upper-left panel. The frequency of the class with diurnal precipitation of $0 < \mathrm{P} \leq 1$ mm is higher for ECHAM5 than for CLM. The frequencies of the other classes for precipitation in the upper left panel are similar.

Precipitation in ECHAM5 rarely exceeds 100 mm per day (given in the lower-right panel), but the CLM results are beyond this with values exceeding occasionally 400 mm. The maximum of precipitation occurred between Sicily and Tunisia on the simulation date Oct. 8, 1981. The corresponding fields of mean sea-level pressure, specific humidity at 850 hPa, and wind suggest that CLM calculated a small-scale cyclone.

Steppeler et al. (2003) discussed the precipitation algorithm of the 'Lokal-Modell' in relation with a detected large overestimation of the precipitation maximum in the Black Forest region. Such overestimations of maximum precipitation values have also been detected for some precipitation events in northern Portugal by comparing statistics of the CLM downscaling simulations with those from observations provided by the Global Precipitation Climate Centre (*http://www.dwd.de/en/FundE/Klima/KLIS/int/GPCC/GPCC.htm*).

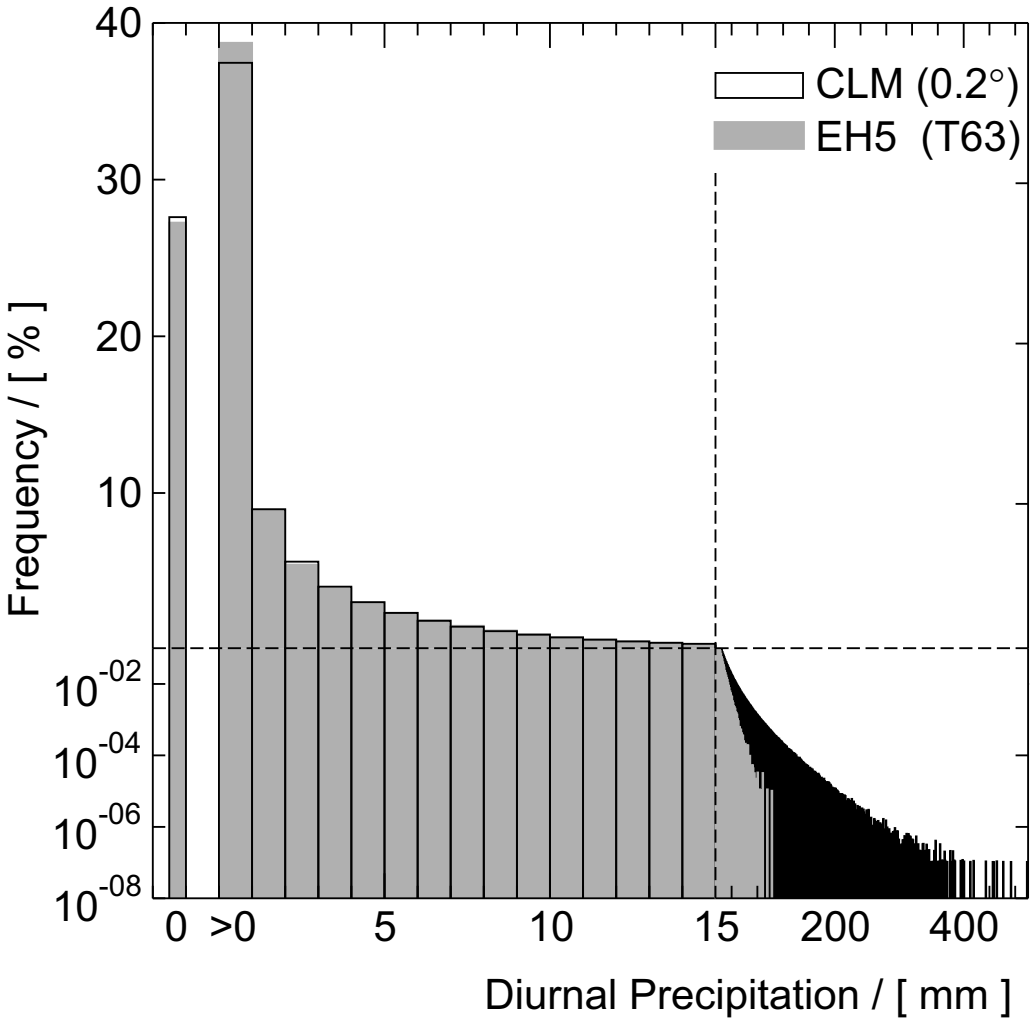

Figure 5 Frequency distribution of diurnal total precipitation. Open black bars are for the CLM_C20_1 data (geographical grid) and grey bars for the corresponding realisation of the AR4 20C3M ECHAM5/MPIOM 20th century climate reconstruction. Non-precipitation cases are indicated by the separated bar. Different scaling of ordinate/abscissa in the quadrants separated by the dashed lines: linear/linear (upper left), logarithmic/linear (lower left), and log/log (lower right).

3.3 Execution of experiments: M&D Modelling Environment

The consortium IPCC AR4 dynamical downscaling experiments with CLM described here have been conducted by the M&D group as a service to the wider German Earth system research community. They have been run within the modelling environment of M&D on NEC SX-6 machines, mainly at German Climate Computing Centre (DKRZ), but also at the HLRS (High Performance Computing Center) of the University of Stuttgart. The modelling environment is a toolkit that can be used to compile (Standard Compile Environment 'SCE') and execute (Standard Run Environment 'SRE') Earth System models and also includes data aspects (postprocessing, archiving, WDCC data base filling facilities) (*http://mad.zmaw.de/imdi*).

It was initially developed by M&D in the European FP5 PRISM project (Project for Integrated Earth System Modelling). Developments since the end of PRISM concentrate on data management aspects. Emphasis is on efficient use of resources, in this case of the DKRZ and HLRS infrastructures.

The modelling environment toolkit and the model source code, as well as some input data, can be downloaded from the SVN repository of M&D, provided that authentification and access authorisation is recognised. In practice, this means that a person interested in downloading the model and tools should contact M&D (model@dkrz.de) to obtain an SVN user account and required access rights.

The model and environment version that was used for the experiments is tagged in the SVN repository with '`clm2.4.11_ipcc_070925`' which reads "model version 2.4.11, configured for IPCC consortium experiments, and with version from 25 September 2007". Due to the license conditions for CLM, access can only be provided to persons authorised to use CLM as laid down in the 'CLM Community Agreement' (*http://clm-community.eu*).

The command to download is:

```
svn checkout \
   http://svn-mad.zmaw.de/svn/mad/Model/IMDI/tags/clm2.4.11_ipcc_070925 \
   dir          or
svn export \
   http://svn-mad.zmaw.de/svn/mad/Model/IMDI/tags/clm2.4.11_ipcc_070925 \
   dir
```
[1].

The tagged revision `clm2.4.11_ipcc_070925` is then copied into the specified directory `./dir`.

[1] All file, variable and command names are written in typewriter font. User-specific parts are in italic.

If no target directory is given, the base name of the tagged revision will be used. The 'checkout' command copies the SVN administration files together with the source and script code. The second version using 'export' does not include copies of these files.

The base directory name *dir*, together with the name of the working directory from which the download was triggered is called */rootdir* in the following.
The source code of CLM is contained in the sub-directory */rootdir*/src/mod/clm and related libraries (grib1 and nccf) in sub-directories of */rootdir*/src/lib. Source code for the preparation of driving data, i.e. of the converter and preprocessor programs ieee2nc and int2clm2, reside in sub-directories of */rootdir*/src/mod/processing. The directory */rootdir*/util contains script code used for the generation of compile and run scripts and is accordingly separated into compile and running branches. The directory */rootdir*/data holds additional input data required for preprocessing and postprocessing.

If no SVN client is installed on your system, a tar file with the CLM package is provided by M&D.

The scripts to set up and run the experiment described in this report are called as indicated below. Detailed information is provided in technical handbooks residing in the directories
/rootdir/compile/doc and */rootdir*/running/doc
and in a 'HowTo' document in */rootdir*/src/mod/clm/doc.

Compilation

A model package including the M&D modelling environment does not contain any ready-to-use scripts for compilation. Instead it provides a toolkit to generate them and a collection of script code fragments, called include files, from which the scripts are assembled. Some of the include files are model and/or platform (site) dependent, and the scripts are generated specifically for the model (here CLM) and the platform by selecting the appropriate source code fragments, as required by the user when calling the tools.

CLM and associated compile scripts have been created by calling
./Create_COMP_cpl_models.ksh clm [--id *ID* [--node ds]]
in the SCE toolkit directory */rootdir*/util/compile/tools.

The parameter clm is mandatory and specifies the name of the model. With the option --id a configuration acronym '*ID*' is specified which was chosen to be 2.4.11 for the consortium IPCC AR4 experiments. The CLM model has been cross-compiled for execution on SX-6 machines on ia64 Linux nodes with hostnames with a leading 'ds' literal at DKRZ. The pre- and postprocessor executables have been compiled and executed on the ia64 Linux nodes. As the compile scripts have

been generated on one such node, the correct compilers are selected without further specification and the scripts are correctly configured for the platforms[2,3].

The script creates a compile script for CLM as well as a compile script for the format converter ieee2nc, the preprocessor int2clm2, and some postprocessing tools. Also, scripts for the compilation of libraries linked to the model and preprocessor are created.
The scripts are named

`/rootdir/src/mod/clm/COMP_clm_ID.ksh`	*CLM compile script*
`/rootdir/src/mod/processing/COMP_processing_ID.ksh`	*preprocessor compile script*
`/rootdir/src/lib/COMP_libs_ds.ksh`	*library compile script (SX-6)*
`/rootdir/src/lib/COMP_libs_cross.ksh`	*library compile script (ia64)*

The CLM model is compiled calling
`/rootdir/src/mod/clm/COMP_clm_ID.ksh`
and the preprocessor and postprocessing tools by calling
`/rootdir/src/mod/processing/COMP_processing_ID.ksh -t int2clm`
`/rootdir/src/mod/processing/COMP_processing_ID.ksh -t ieee2nc`
`/rootdir/src/mod/processing/COMP_processing_ID.ksh -t ptools` where the option `-t` specifies the compilation target. The executables generated, i.e. `clm_2.4.11.x`, `int2clm.x`, `ieee2nc.x`, and postprocessing programs are archived together with the experiment data.

Execution

The CLM experiments consisted of the following tasks:

(*i*) preprocessing, (*ii*) model integration, (*iii*) postprocessing, and (*iv*) archiving.

The task scripts are created calling a SRE tool in `/rootdir/util/running/tools`:

```
./Create_TASKS.frm clm ID.
```

The second parameter is a tag for the experiment. The experiment is further configured by editing the created setup file `/rootdir/running/setup/setup_clm_ID`. The setup file is divided into several logically related sections. In the block `"TASK SPECIFICATION"` the (optional) pre-

[2]If the scripts are generated on a different machine (e.g. the user's workstation) the first part of the node names 'ds' has to be provided with the `--node` option as indicated above.

[3]The CLM model version tagged `clm2.4.11_ipcc_070925` is configured only for SX-6/ia64 machines of the computing centres DKRZ and HLRS. Configuration for other platforms is not possible within the M&D modelling environment. This is however possible (e.g. for Linux cluster, IBM) for the next major version of CLM.

processing, postprocessing, and archiving tasks have been switched on. In the section "COMPONENT MODELS" the model configuration parameter 'atmvers' was changed. If the same *ID* is specified as for the generation of compile scripts, the scripts are inter operable in the sense that the run script uses the executable clm_*ID*.x. Otherwise, e.g. if experiments tagged with different experiment configuration *ID*s are run with the same executable, as was the case for the consortium experiments, the parameter atmvers has to be changed from the respective experiment *ID* to a different model configuration *ID* (here 2.4.11). In the following part "TIME CONTROL" of file setup_clm_*ID*, initial and final dates of the experiment are set. In section "PRE PROCESSING", the ID of the experiment that created the global ECHAM5/MPIOM forcing data and the path to the forcing data is set. In the section "FILE SYSTEM" the permanent script directory (called home), to where the tasks scripts are moved, a short term data storage directory (data), and an archiving directory (archive) are specified. Section "PLATFORM DEPENDEND SPECIFICATIONS" offers the possibility to set email address, account and finally the queue for NQSII.

The scripts, when created in the SRE are preconfigured for the consortium experiments as performed by M&D. This primarily concerns the CLM namelists (model domain and resolution, output variables and frequencies etc.) and the input and output data. The model was forced by 6-hourly data, produced by the global coupled model ECHAM5/MPIOM in IPCC AR4 experiments to simulate the climate of the second half of the 20th century (20C3M) and SRES scenarios A1B and B1 for Europe. The simulated periods were 1960-2000 and 2001-2100 respectively.

A CLM experiment consists of several consecutive runs. The default duration of each run is one month. The experiment work flow is as follows: The run script submits the preprocessing script for the next run (for prep_offset=1[4]). If driving data for the current run are not available, the preprocessing script is also submitted for the current run and the run task is suspended until the input data are ready. When the model integration of the first run is completed, the run script submits the postprocessing script and re-submits itself for the integration of the next run. Upon completion, the postprocessing script submits the archiving script. In case of errors, the archiving script resubmits itself until all files are saved successfully.

Some of the experiments have been executed in a distributed computing environment (pre- and postprocessing on the DKRZ ia64 machines in Hamburg, and CLM integration on a SX-6 node at the HLRS in Stuttgart). The corresponding setup file has been configured accordingly (preprocessing=remote and postprocessing=remote). After creation, the scripts have

[4] prep_offset specifies the number of months the forcing data are generated in advance.

been copied to the place where they are run, `pre/postprocessing=yes` and `pre/postproc_mode=chain` are set, and the paths were adjusted.

Care had to be taken of sufficient disk capacity for the short range data storage (defined by variable `data`).

The disk space requirements (per simulated month) are: 22 GB for raw data, 1.4 GB for restart files, 3x5 GB for data streams 1-3, and 9 GB for driving data. The model has been run on 1 node with 8 dedicated processors of the NEC SX-6. It takes about 4 1/2 hours wall-clock-time to simulate one month.
This makes a total of at least 1170 days for the complete realisations of C20 (3×), A1B (2×), and B1 (2×) on a single node.

Work flows
Below, the experiment work flow is schematically described.

Preprocessing
The preprocessing tasks were all executed on the 'cross' Linux ia64 machine at DKRZ. In the first step, the global ECHAM5/MPIOM data are converted from IEEE-format into netCDF-format using the program `ieee2nc` (see above). Thereafter, the preprocessor `int2clm` prepares the initial and boundary conditions by interpolating the global data (resolution T63) onto the rotated CLM grid (resolution 0.165°). At the same time some climatological or fixed domain parameters (land fraction, surface roughness length, soil type etc.) are included in the generated data files:

ECHAM5 data (ieee) → ieee2nc → ECHAM5 data (netCDF) → int2clm → ECHAM5 data on CLM-grid

CLM integration
The preprocessed data are used for the model integration. The integration was performed on NEC SX-6 nodes, either at the DKRZ, or at the HLRS. The CLM raw output is netCDF. It is written in 6 different channels (`out01,...,out06`):

ECHAM5 data on CLM-grid → clm_2.4.11.x → CLM raw output data: `out01,...,out06`

Postprocessing
The postprocessing tasks, similar to the preprocessing, were all executed on the 'cross' Linux ia64 machine at DKRZ. For the generation of the final products in the postprocessing task, the Climate Data Operator software package CDO
(*http://www.mpimet.mpg.de/fileadmin/software/cdo/*) developed by U. Schulzweida at the MPI-M

was intensively employed. The postprocessing script produces three additional data stages (D*n*): (*i*) 3-dimensional data on a sub-domain of the CLM grid that can be used e.g. to drive finer resolved models (D1), (*ii*) time series of output variables on the CLM grid excluding a lateral sponge zone[5] (D2), and (*iii*) a selected sub-set of variables from D2 interpolated on a regular geographical grid with a 0.2° grid spacing (D3) in both the north-south and east-west directions (see column 2 of Table 11). The interpolation method was bi-linear except for the parameters depending on soil properties. These were assigned the nearest-neighbour value.

For D3 a number of derived variables and climatological indices (e.g. frost days, tropical nights etc.) is calculated and, where appropriate, daily/monthly/yearly means/sums/minima/maxima are composed:

Data stage 1 (D1)	Data stage 2 (D2)	Data stage 3 (D3)
CLM 3D data (channel out01 - 02) on CLM grid (sub-domain)	time series (channel out03 - 06) on CLM grid without sponge zone	selected variables from D2 on a regular 0.2° grid as well as derived variables and indices

Archiving

Finally, postprocessed and raw output data as well as restart files are archived in the UniTree archive at DKRZ in Hamburg. During experiment execution additional files have been created in the script directory
`$home/ID/scripts`. Notably *ID*`.log`, which provides information on the progress of the experiment, and job log files *ID*`.run*`, which contain script messages and CLM standard and error output. These files are stored in the DKRZ file archive together with the model output.

Restart files	CLM raw output data	Data stream 1,2, and 3	additional files

Archiving in WDCC data base

For ease of use, time series of a number of variables are archived in the WDCC on both the model grid and the geographical grid. They are provided on several time scales ranging from hourly up to yearly information. Variables include atmospheric and surface states, precipitation, energy fluxes, and the like. Characteristic numbers such as the number of days with snow-cover are only provided on the geographical grid. Additionally, all model raw output is stored in the DKRZ file archive.

Access to data

The data are accessible from the WDCC together with its meta data by the general public. The convention for table names and filenames in the CERA data model used by the WDCC is: CLM_*sce_rls*_D*n*

[5]The sponge zone covers 8 grid boxes on all lateral boundaries of the modelling domain.

where *sce*=(C20, A1B, B1) denotes the experiment class, *rls*=(1, 2, 3) gives the realisation number, and *n* indicates whether the data are given on the model grid (D2) (*n*=2) or geographical grid (*n*=3).

For accessing CLM data, the terms of use have to be signed, which can be downloaded from *http://www.mad.zmaw.de/projects-at-md/sg-adaptation/clm/clm-data-access*. After receiving an account access the data will be free. However, there is free access to information and meta-data about the CLM AR4 climate change projections and provided variables without any account via the WDCC catalogue interface (*http://cera.wdc-climate.de*).

4 Quality control

Quality control considers both the quality of the original model results and the technical inspection of the archived data. The quality of the original model results is analyzed by comparisons with observations and by the detection of deviations between different simulations (e.g. global and regional, present-day and scenario runs). This quality control has been conducted by the colleagues from BTU Cottbus. The methodology is presented in section 4.1. The results are discussed in section 6. The technical inspection of the data covers different aspects of data quality of the original model output and of the transformed data in other formats and on other grids, such as completeness, consistency (which is also model part of the evaluation), and outlier occurrences. It is ensured by M&D applying two control techniques: automated and visual inspection (see sections 4.2 and 5 for details).

4.1 Strategy for quality control

The data quality of the executed simulations is checked by an extensive climatological evaluation. It is based on both the comparison of the simulation results with reference data derived from observations and the comparison of the regional simulations among each other and with the results of the corresponding global simulations.

The quality of the regional climate simulations essentially depends on two factors:

- the quality of the regional model itself,
- the influence of the global simulation results which force the regional simulations by time-dependent lateral and lower boundary values.

Additionally, the internal variability of the reproduced climate system on different time-scales has to be taken into account with the interpretation of the climate change signals.

In order to ensure the quality of the regional climate model CLM, an additional simulation (evaluation run CLM050) with present-day climate conditions was performed for the time period from 1979 to 1998. Model domain and configuration were identical to the climate simulations (CLM-C20). However, in contrast to the CLM-C20 simulations, which were driven by the results of a global climate run, the evaluation run was using three-dimensional weather analysis – so-called reanalysis ERA40 (Uppala et al., 2005) – of the European Centre of Medium-Range Weather Forecasts (ECMWF) as time-dependent boundary values. Through this the evaluation run (CLM050) represents the course

of the real weather conditions of the simulated time period while the climate runs (CLM-C20) create courses of fictitious weather conditions of the given climate period.

Table 4 provides a summary of the nomenclature used to identify the different simulations. Altogether, the analysis of the simulation-quality is based on five different comparisons between these simulations, which are schematically presented in Figure 6. All comparisons aim on a quantification of the simulation-quality by determining ranges of uncertainty or variability.

Table 4 Labelling of simulations and simulated periods used for the quality control.

Global simulations	ERA40	EC-C20	EC-CCS
Global realisations		ECC201, ECC202,	ECA1B1, ECA1B2
Regional simulations	CLM050	CLM-C20	CLM-CCS
Simulation periods	1979 – 1998	1961 – 2000	2001 – 2100
Regional realisations		C20_1, C20_2	A1B_1, A1B_2

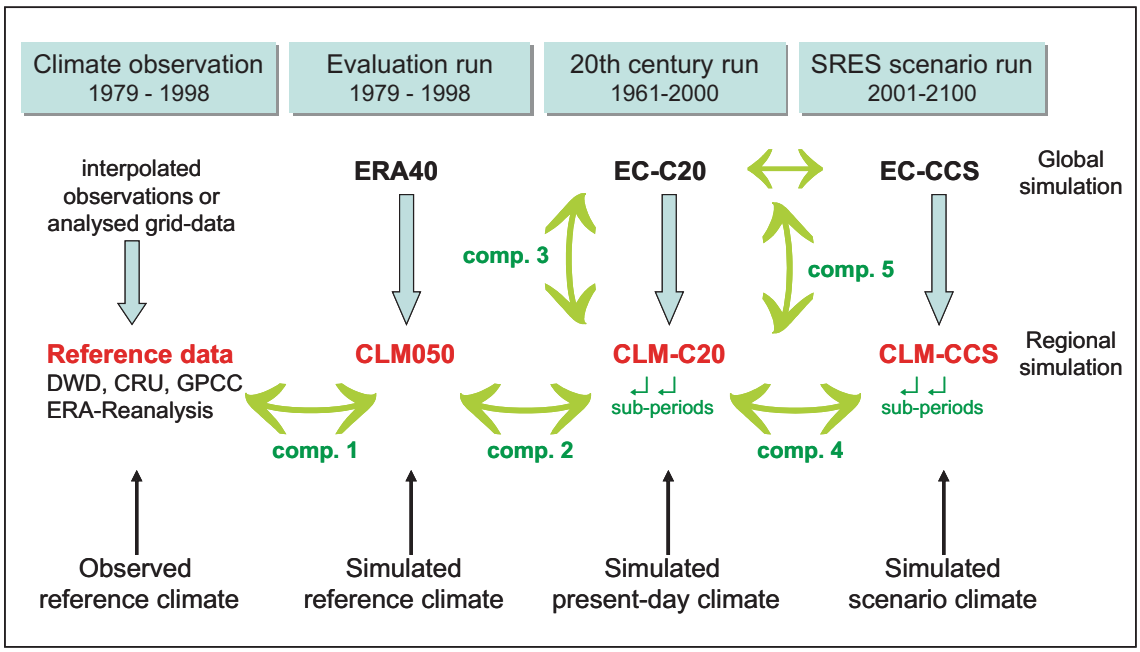

Figure 6 Outline for the quality control of the CLM climate simulations.

4.1.1 Comparisons

Comparison 1, the model evaluation, forms the basis of the quality control of the CLM. In principle, the regional simulation CLM050 should provide the best possible representation of climate within the simulated domain. Therefore, this simulation serves as a reference-run for all further model simulations. The quantitative comparison of this run with different reference datasets determines the quality of the regional climate model itself. The examination also considers deviations between different reference data of the same climatological quantity (if available), i.e. the influence of the uncertainty about the knowledge of the actual climate state on the quality control.

Comparison 2 investigates the quality of the regional present-day climate simulation (CLM-C20). The differences to the evaluation run CLM050 demonstrate the influence of the global climate simulations on the regional climate reconstruction. The combination of this comparison with comparison 1 yields the modification of quality in the 20th century climate runs. Furthermore, the comparison captures the internal climate variability on the considered time-scale. Since no time-period of the two CLM-C20 simulations can be exactly identified with the reference period 1979–1998, four different 20-year long simulation periods of the C20-runs are compared with the evaluation run (see Table 5).

Table 5 Scheme of paired comparisons between the forty-year long 20th century climate simulations CLM-C20 and the twenty-year long evaluation run CLM050.

Reference climate	20th century climate	
CLM050	C20_1 (1961 – 1980)	C20_1 (1981 – 2000)
1979 – 1998	C20_2 (1961 – 1980)	C20_2 (1981 – 2000)

The range of variation between these 20-year climate means provides an impression of the potential variability of the simulated present-day climate state. The mean deviations between CLM-C20 and CLM050, which are only caused by the driving global simulation results, must be assessed with respect to this climate variability. The deviations from the simulated reference climate (CLM050) must be taken into account if the data are used in subsequent applications. This comparison allows the user to estimate the potential quality loss if the absolute values of the simulated 20th century climate are used and analysed instead of those of the evaluation simulation. However for some quantities or some regions, the C20-simulation may agree better with observations than the CLM050-simulation. In this case, the errors induced by the global and the regional simulation partly cancel each other coincidentally.

Comparison 3 helps to identify the properties of the regional present-day climate simulation caused by the global model. It shows the differences between the regional (CLM-C20) and the global (EC-C20) simulations. On the one hand, this comparison allows conclusions to what extent the deviations of the regional present-day climate simulation from the reference climate, which have been analysed in comparison 2, are caused by the global driving data. On the other hand, it shows where and how the higher resolution modifies the climatological fields of the corresponding global simulation. The analysis is based on 4 pairwise comparisons of twenty-year long time periods between the two global and regional 20th century simulations as depicted in Table 6.

Table 6 Scheme of paired comparisons between the regional and the global 20th century simulations.

	ECHAM5-simulation EC-C20			
CLM-simulation	ECC201 (1961–'80)	ECC202 (1961–'80)	ECC201 (1981–'00)	ECC202 (1981–'00)
C20_1 (1961–'80)	X			
C20_2 (1961–'80)		X		
C20_1 (1981–'00)			X	
C20_2 (1981–'00)				X

Comparison 4 investigates the regional climate change. The comparison of four twenty-year long time periods of the scenario runs (CLM-CCS) with corresponding periods of the 20th century runs (CLM-C20), as indicated in Table 7, allows conclusions about the intensity and stability of the simulated climate change.

The analysis is restricted to the A1B-scenario, because here two realisations of the same scenario had already been completely available at the time of investigation. The time lag of each comparison is 50 years, e.g. 2011–2030 vs. 1961–1980 and all comparisons are repeated with a time shift of 20 years (2031–2050 vs. 1981–2000). The results provide a first impression of the expected climate change for the A1B-scenario on a 50-year time-scale and of the potential uncertainty of the detected changes due to the internal variability of the climate system.

Table 7 Scheme of paired comparisons between twenty-year climate means used for the assessment of climate changes over a time lag of 50 years (1961–2000 vs. 2011–2050, etc.). The confrontation of the comparisons marked by 'X' with those marked by '+' demonstrates the stability or variability of the climate change signal with time.

CLM-simulation CLM-C20	CLM-simulation CLM-CCS			
	A1B_1 (2011–'30)	A1B_2 (2011–'30)	A1B_1 (2031–'50)	A1B_2 (2031–'50)
C20_1 (1961–'80)	X	X		
C20_2 (1961–'80)	X	X		
C20_1 (1981–'00)			+	+
C20_2 (1981–'00)			+	+

Comparison 5 addresses the differences between the climate change of the global simulations and that of the regional ones. For this reason, all comparisons which have been listed in Table 7 are repeated with the corresponding results of the global runs (EC-C20 and EC-CCS). The resulting climate change signals are then compared in pairs with those of the associated regional comparisons. This approach allows to prove the consistency of the regional and the global climate simulations. It also shows how far deviations of the regional simulations from the global ones are stable along a transient climate change and it provides an estimate on the added value of the regional simulation.

4.1.2 Types of analysis and presentations

The analysis of the comparisons illustrated above is essentially based on three different types of presentation: difference plots, bias-tables, and mean annual cycles. The *difference plots* show the spatial distribution of the deviations between the twenty-year means of two simulations or time periods for a selected climate variable over the whole model domain. They are generally prepared for the annual means and the monthly means of January and July. In order to obtain a more detailed and quantitative regional analysis, the model domain is sub-divided into a number of sub-areas (see Table 8) representing different geographical and climatological regions on different spatial scales. For every sub-region, the difference of the area averages is calculated for all pairs of compared twenty-year means. The ranges between the smallest and the largest difference of all comparisons are given in the *bias-tables* for the annual values and for the mid-season months January, April, July, and October. Furthermore, the *annual cycles* of the monthly means of a sub-region are plotted or, alternatively, the difference between two mean *annual cycles* of a comparison.

The comparisons 1, 2, and 4 are executed for 35 different sub-regions (see Figure 7 and Table 8) defined on the regional model grid. On the first level, the model domain is sub-divided into Northern and Southern Europe as well as land and water surfaces. These regions are further sub-divided into smaller sub-areas (level 2). The third level includes sub-regions, which are either characterised by special geographical features (Po valley, Alps, etc.) or which have been used as sub-national areas in previous studies so that substantial experiences are available for these regions regarding the quality of regional climate simulations.

Table 8 Labelling of sub-regions with the number of associated grid-points on the regional and the global model grid (Figure 7 and Figure 8). To be continued.

Labelling of sub-regions	Number of grid-points in regional model	global model	Description
Level 1			
NEU	23125	376	Northern Europe (NEL+NEW)
NEL	14024	214	Northern Europe land area
NEW	9101	162	Northern Europe water area
SEU	23888	238	Southern Europa (SEL+SEW)
SEL	13361	127	Southern Europe land area
SEW	10527	111	Southern Europe water area
Level 2			
SCA	3510	67	Scandinavia
NWE	1330	16	North-western Europe
MEU	2068	27	Central Europe
SWE	2245	20	South-western Europe
EEU	3516	46	Eastern Europe
SUE	3809	38	Southern Europe
NEE	1066	23	North-eastern Europe
RUS	2527	35	Western Russia
VAS	2340	27	South-western Asia
NAF	4961	42	Northern Africa
MED	7824	77	Mediterranean Sea
OSS	1426	17	Baltic Sea
NOS	1531	22	North Sea
SWM	1297	15	Black Sea
NOA	3336	69	North Atlantic
BIS	2354	32	Bay of Biscay

Continuation of Table 8.

Labelling of sub-regions	Number of grid-points in regional model	global model	Description
Level 3			
NSK	758	not def.	Northern Scandinavia
SSK	2752	"	Southern Scandinavia
ALP	627	"	Alps (grid-points above 500 m)
POE	135	"	Po valley (grid-points below 300 m)
UNG	667	"	Pannonian Basin (grid-points below 300 m)
DTL	1067	"	Germany
SLW	49	"	Region around Schleswig
ESS	49	"	Region around Essen
LIN	49	"	Region around Lindenberg
MEI	49	"	Region around Meiningen
MUN	49	"	Region around Munich
STU	49	"	Region around Stuttgart
SAX	55	"	Saxony

The comparisons 3 and 5 are performed on the grid of the global model instead of the regional one. Because of the much coarser resolution of this model, all analyses are carried out only for the sub-regions of level 1 and 2 (see Figure 8, Table 8). These regions, which are originally defined on the regional grid, are approximately transferred to the global grid. Because grid-size, coordinate system, and land-sea-distribution of the global model differ substantially from those of the regional one, the transfer of the sub-regions necessitates an adjustment to the global grid structure. This leads to small differences in location and size of the regions between both grid representations, which are however irrelevant for the findings.

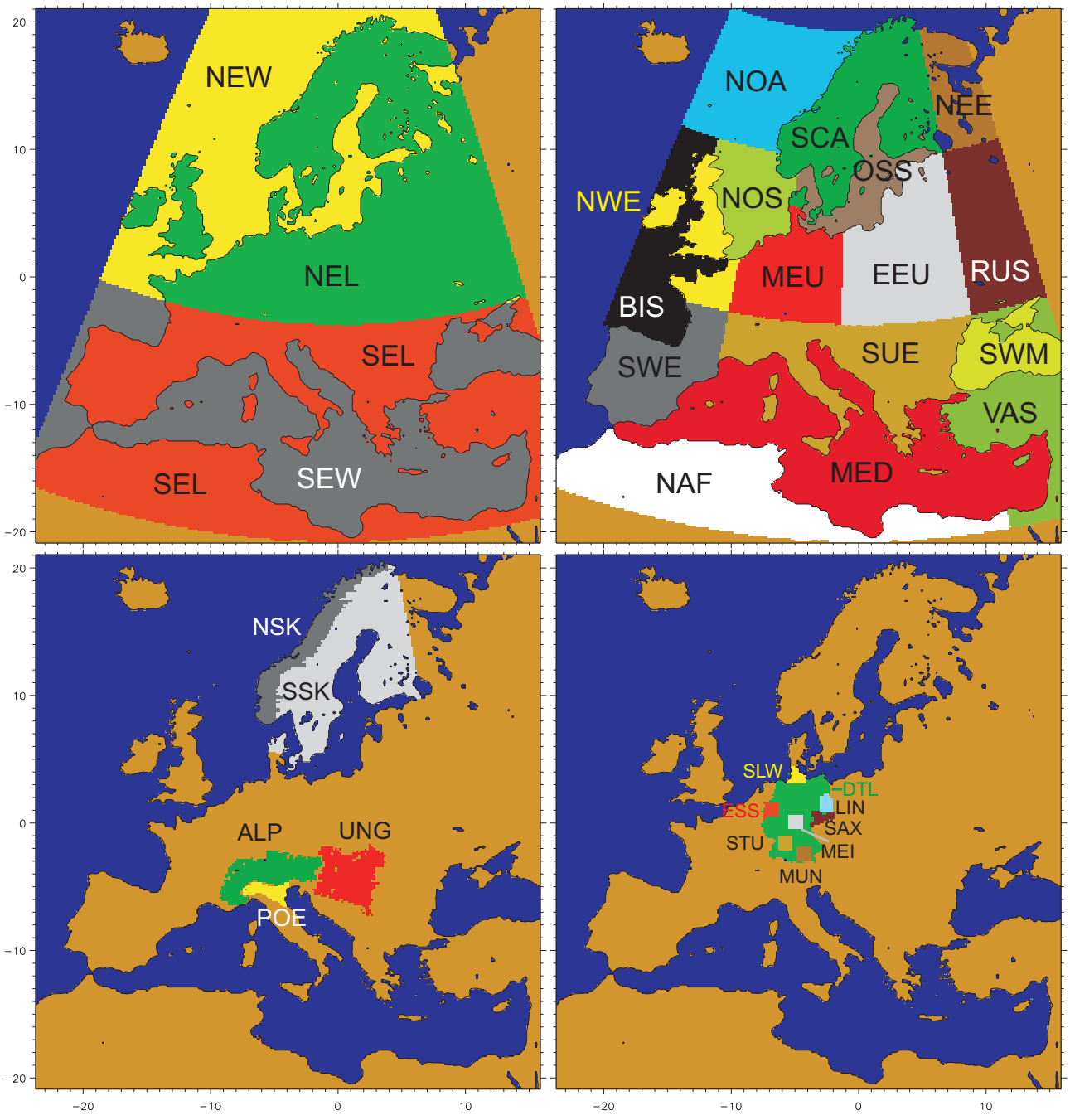

Figure 7 Location and size of the sub-regions being used for the comparisons 1, 2, and 4 on the regional model grid (for meaning of labels see Table 8).

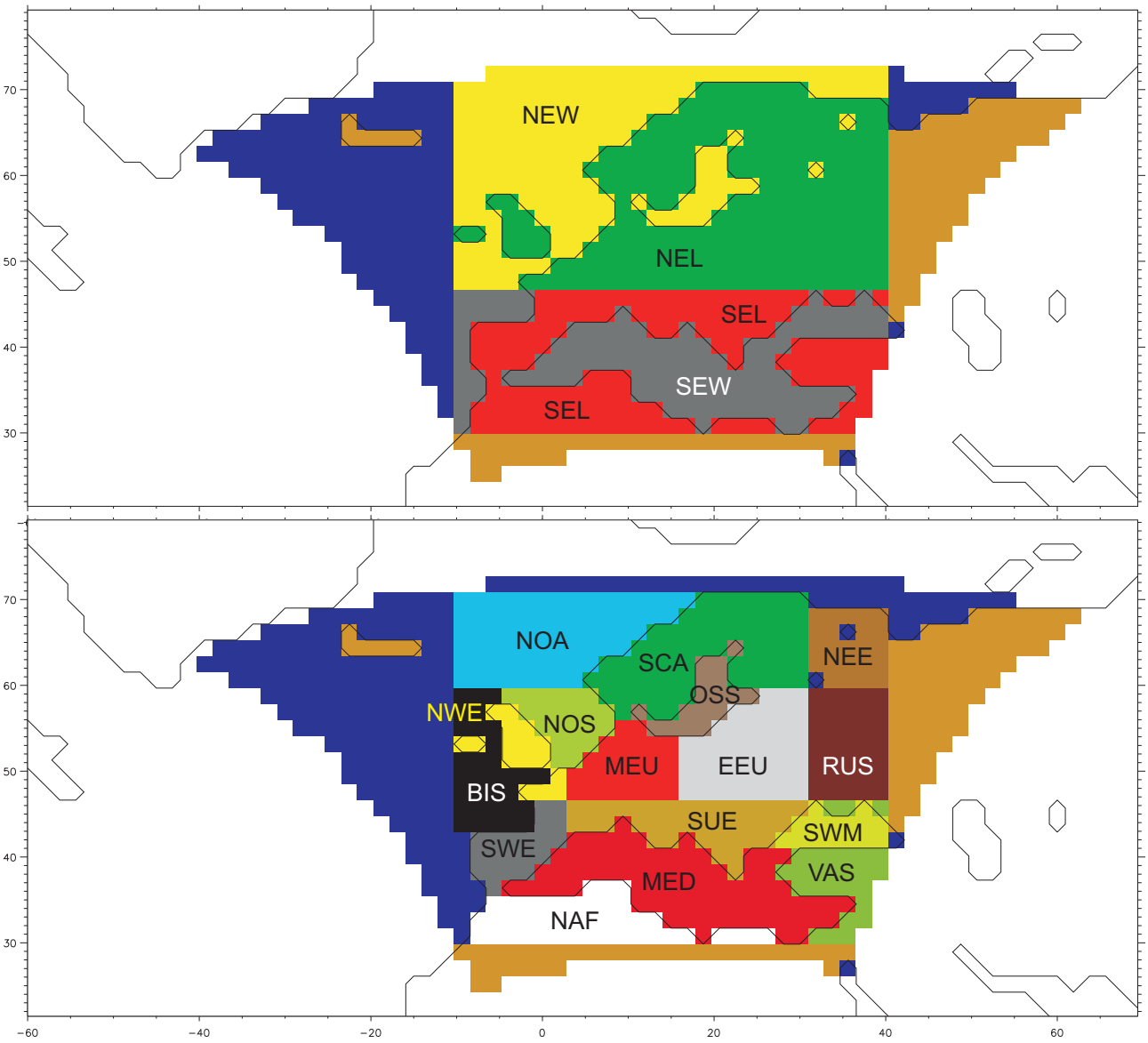

Figure 8 Location and size of the sub-regions being used for the comparisons 3 and 5 on the global model grid (for meaning of labels see Table 8). The coloured background represents the regional model domain in the geographical coordinate system of the global model.

If data sets being compared are given on different grids – e.g. the regional or global model grid or various grids for reference data – they are projected from the original grids onto a common evaluation grid – which is the regional model grid for comparisons 1, 2, and 4 and the global model grid for comparisons 3 and 5. The projection is done by an area-weighted averaging of the original grid-values. The weights of this averaging are determined for each cell of the evaluation grid by the relative area-fractions of the overlapping cells of the original grid. For the comparison of temperature values, the horizontal grid-projection is followed by an additional height correction accounting for the strong height-dependence of this quantity. For this purpose, the same projection method is applied to the corresponding surface elevations (orography) of the data sets. The resulting differences in surface heights on the evaluation grid are then used for the height correction of the projected temperature values by a linear regression approach. The projection procedure does not account for differences in the land-see-distribution of the two grids being compared. If, for instance, land-points of the original grid are projected to a cell of the evaluation grid (e.g. the global model grid) representing a see-point, considerable differences may occur between the two data sets. This can lead to grid-cell wide bands along coastlines with noticeable values in the difference plots, in particular for quantities related to near-surface temperature.

Some special features must be considered for comparison 1, since appropriate reference data are not available for all climate variables or sub-regions. If a projected data set covers less than 95% of a sub-region on the evaluation grid, the comparison is not preformed for that sub-region. This can lead to empty lines in the bias-table or to a reduction in the number of comparisons contributing to the calculation of the ranges of uncertainties (see below) for that particular region. Table 9 and Table 10 give an overview which data sets are available for which climate variable and sub-region.

All five comparisons are executed for the subsequently listed climate variables:

- daily mean of air temperature (**T-mean**)
- daily maximum of air temperature (**T-max**)
- daily minimum of air temperature (**T-min**)
- precipitation sum (**PREC**)
- wind speed 10 m above ground (**V 10m**)
- mean sea level pressure (**MSLP**)
- number of summer days (**NSD**, T-max > 25 °C)
- number of frost days (**NFD**, T-min < 0 °C)
- number of days with intensive precipitation (**NIPD**, PREC > 10 mm/d)
- frequency distribution of daily precipitation (**FDP**)
- persistence of dry days (**PDD**)

Only some of the comparisons are executed to investigate selected aspects of near-surface humidity and coastal wind variability (see sections 6.12 and 6.13).

The occurrence of specific weather events like summer and frost days is analysed on the basis of yearly frequencies. Therefore, no annual cycles are available for these quantities. An important feature of the bias-tables and the figures of annual cycles is the presentation of the ranges of uncertainties. These ranges result from differences in the comparisons between all possible pairs of twenty-year means.

Altogether, a large number of detailed analyses for several climate variables and many sub-regions has been carried out. In section 6 some selected results of the different comparisons described above are presented. They summarise the essential results of the quality control and give an impression of the scope of available data evaluations.

A complete presentation of all aspects of quality for different regions and possibly interesting climate variables is not feasible at all in such a summary report. The variety of interests of potential users of these data may require additional and more specific investigations which have to be executed with adequate care by the user himself. In order to support this work, the authors provide an extensive number of systematic data preparations in form of tables and plots in addition to the original and processed output data in the different data streams. The complete analysis with presentations of all executed comparisons for all variables and sub-regions are available via the CERA database.

Exemplary results are discussed in section 6. For each comparison and each type of presentation figures are shown. The discussion is focused on Germany.

Table 9 Availability of reference data (see also Table 10) for model evaluation (comparison 1). The numbers indicate the data sets which are used for the evaluation of a certain variable (see text on page 45) on a given sub-region (Table 8). To be continued.

Region	PREC	T-mean	T-min	T-max	V 10m	MSLP	NFD	NSD	NIPD	FPD	PDD
NEU		2	2	2	2	2					
NEL	4,5,6	2,4	2,4,7	2,4,7	2,7	2	7	7	7	7	7
NEW		2	2	2	2	2					
SEU		2	2	2	2	2					
SEL	4,5,6	2,4	2,4	2,4	2	2					
SEW		2	2	2	2	2					
SCA	3,4,5,6	2,3,4	2,4,7	2,4,7	2,7	2	7	7	7	7	7
NWE	3,4,5,6	2,3,4	2,4,7	2,4,7	2,7	2	7	7	7	7	7
MEU	3,4,5,6	2,3,4	2,4,7	2,4,7	2,7	2	7	7	7	7	7
SWE	3,4,5,6	2,3,4	2,4,7	2,4,7	2,7	2	7	7	7	7	7
EEU	3,4,5,6	2,3,4	2,4,7	2,4,7	2,7	2	7	7	7	7	7
SUE	3,4,5,6	2,3,4	2,4,7	2,4,7	2,7	2	7	7	7	7	7
NEE	4,5,6	2,4	2,4,7	2,4,7	2,7	2				7	7
RUS	4,5,6	2,4	2,4,7	2,4,7	2,7	2	7	7	7	7	7
VAS	4,5,6	2,4	2,4	2,4	2	2					
NAF	4,5,6	2,4	2,4	2,4	2	2					
MED		2	2	2	2	2					
OSS		2	2	2	2	2					
NOS		2	2	2	2	2					
SWM		2	2	2	2	2					
NOA		2	2	2	2	2					
BIS		2	2	2	2	2					

Continuation of Table 9.

Region	PREC	T-mean	T-min	T-max	V 10m	MSLP	NFD	NSD	NIPD	FPD	PDD
NSK	3,4,5,6	2,3,4	2,4,7	2,4,7	2,7	2	7	7	7	7	7
SSK	3,4,5,6	2,3,4	2,4,7	2,4,7	2,7	2	7	7	7	7	7
UNG	3,4,5,6	2,3,4	2,4,7	2,4,7	2,7	2	7	7	7	7	7
ALP	3,4,5,6,8,9	2,3,4	2,4,7	2,4,7	2,7	2	7	7	7	7	7
POE	3,4,5,6,9	2,3,4	2,4,7	2,4,7	2,7	2	7	7	7	7	7
DTL	1,3,4,5,6	1,2,3,4	1,2,4,7	1,2,4,7	1,2,7	1,2	1,7	1,7	1,7	7	7
SLW	1,3,4,5,6	1,2,3,4	1,2,4,7	1,2,4,7	1,2,7	1,2	1,7	1,7	1,7	7	7
ESS	1,3,4,5,6	1,2,3,4	1,2,4,7	1,2,4,7	1,2,7	1,2	1,7	1,7	1,7	7	7
LIN	1,3,4,5,6	1,2,3,4	1,2,4,7	1,2,4,7	1,2,7	1,2	1,7	1,7	1,7	7	7
MEI	1,3,4,5,6	1,2,3,4	1,2,4,7	1,2,4,7	1,2,7	1,2	1,7	1,7	1,7	7	7
STU	1,3,4,5,6	1,2,3,4	1,2,4,7	1,2,4,7	1,2,7	1,2	1,7	1,7	1,7	7	7
MUN	1,3,4,5,6,8,9	1,2,3,4	1,2,4,7	1,2,4,7	1,2,7	1,2	1,7	1,7	1,7	7	7
SAX	1,3,4,5,6	1,2,3,4	1,2,4,7	1,2,4,7	1,2,7	1,2	1,7	1,7	1,7	7	7

Table 10 Description of the data set numbers used in Table 9. The column 'Label' contains the abbreviations of the data sets by which they are referenced in text and figures.

Used reference data			
No.	Data set	Label	Reference
1	DWD climate data	DWD001, DWD003, DWD006, DWD007	Walter et al., 2006
2	ECMWF reanalysis	ERA040	Uppala et al., 2005
3	CRU climate data [TS1.2]	CRU005	New et al., 2002
4	CRU climate data [TS2.1]	CRU007	Mitchell and Jones, 2005
5	GPCC precipitation data [VASClimo V1.1]	GPC003	Beck et al., 2003
6	GPCC precipitation data [Full Data V3]	GPC004	Fuchs et al., 2007
7	MARS climate data	MARS01, MARS05	v.d. Goot and Orlandi, 2003
8	ETH precipitation data	ALP003	Frei and Schär, 1998
9	HISTALP precipitation data	ALP002	Auer et al., 2005

4.2 Visual and automated quality control

In addition to the extended scientific quality control described in subsection 4.1, an automated operation is conducted by scripts that access the NetCDF files for each CLM variable and verifies the availability of every record in the database system. Invalid time stamps in the NetCDF files are detected and corrected. The minimum, average, standard deviation, and maximum of the entire domain are calculated for each time record. Numerical errors, manifested in conspicuous outliers, would be notified. Additionally, frequency distributions for the entire simulation period are built from the values of all grid points. Examples are shown in section 5.

The human eye may detect patterns which an automated procedure is not instructed to look for. Therefore, time series and 2–dimensional graphs of selected key parameters at different time levels for selected periods are checked additionally by visual inspection with focus on specific regions. The visual inspection is intended to find irregularities in the 2–dimensional fields of parameters, which are documented by SGA if they have the potential to cause irritations of users not familiar with model results. These includes peculiar features due to weaknesses in the model design such as occasionally unrealistic wind speed and gust in some regions.

Quality control at M&D includes a check of the meta data in the WDCC database system as well. It is checked whether the content of meta data items like description, unit, grid and level information, time step, and the type of data (i.e. mean, extreme, or accumulated) is set correctly.

The quality control of CLM data at M&D only ensures that the information content of some 60 terabyte in the database is technically sound. Additional quality considerations are left to ongoing research projects. Relevant information to each model parameter, emerging from the quality control, can be accessed via Table 14 starting on page 59.

5 Description of model grid and geographical grid

Running the model and postprocessing comes about in four stages, which are also called 'streams' for historical reasons. They are numbered serially from D0 to D3. As noted before, the raw output (D0) of the model is calculated on the rotated grid with zero-latitude in the middle of the domain. The result, a large file comprising all data for each model-month, is stored in the archiving file system. Stage one (D1) is designated for nesting experiments. Stage D2 is obtained by removing the relaxation layer and separating the climatological variables into self-contained files. Finally, stage D3 is given by the back transformation to the geographical grid. Only D2 and D3 are accessible from the WDCC data base.

The properties of the model grid have been already presented on page 15 in Table 2. The characteristics of the CLM D2 and D3 grid are summarised in Table 11. The extent displayed in Table 11 does not include the relaxation zone of 8 grid cells at all 4 sides of the model domain where the output is considered to be too much influenced or distorted by the boundaries. Atmospheric variables are defined on the pressure levels: 200, 500, 700, 850, 925, and 1000 hPa; they have been interpolated out of the 32 original model levels. Available layers of the soil are between the depths: 0, 0.01, 0.04, 0.1, 0.22, 0.46, 0.94, 1.9, 3.82 m (two additional layers down to 7.66 and 15.34 m form the lower boundaries of the soil model).

Table 11 CLM data grids. Longitudes and latitudes are denoted by lon/lat in geographical coordinates and by rlon/rlat for the rotated grid.

	model grid of stage D2	**geographical grid of stage D3**
Domain	Europe	Europe
Grid Size	0.165°	0.2°
Extent in longitudes	rlon: -23.810° to 15.955°	lon: -10.7° to 36.9°
Extent in latitudes	rlat: -20.955° to 21.12°	lat: 34.5° to 69.9°
Number of Grid Cells	241 × 255	238 × 177
Position of Rotated North Pole	lon: -162.0°, lat: 39.25°	–

An overview of parameters available from the WDCC database is given in Table 12, where the first column indicates whether it is present for D2, D3 or both. The complete list of parameters is presented

in Table 14 in a separate subsection, where the table is subdivided by grouping the output parameters with respect to the atmosphere, near-surface, and soil components of the model output.

Table 12 CLM output parameters and postprocessed fields.

General:	
D2+D3	latitude, longitude, area of grid box, land-sea fraction
D2	bounds of latitude and longitude
Atmosphere:	
D2+D3	cloudiness, radiation at top, temperature, wind components, heights of particular features, ozone amount, etc.
D2	hydrological parameters, convective mass flux density
D3	precipitation, wind speed and direction, humidity
Near-Surface:	
D2+D3	temperature, wind, precipitation components, runoff, air pressure, net radiation, albedo, photo synthetic active radiation, sunshine duration, heat flux, canopy water amount, vegetation cover, leaf area index, surface roughness length, snow surface temperature
D2	surface pressure
D3	evaporation, climate indices, total precipitation
Soil:	
D2+D3	temperature, water content, root depth, type
D3	number of days with frozen soil

The D2 domain is composed out of approx. equal-area grid-cells around the equator in rotated coordinates. The transformation into the geographical coordinates of D3 expands a grid-cell in terms of angles of latitudes (a given distance in kilometres covers more degrees at higher latitudes than next to the equator). In order to provide a geographical grid completely filled with values, parts from the edges of D2 have to be cut, in particular in the north-west and north-east. The different domains of D2 and D3 are shown in Figure 9 using the example of the temperature at 2 m height. The two domains are projected with latitude and longitude as Cartesian coordinates. Obviously, studies including Iceland or requiring the Mediterranean with its full extend have to use the D2 domain, optionally rotated, but then with curvilinear edges of grid cells.

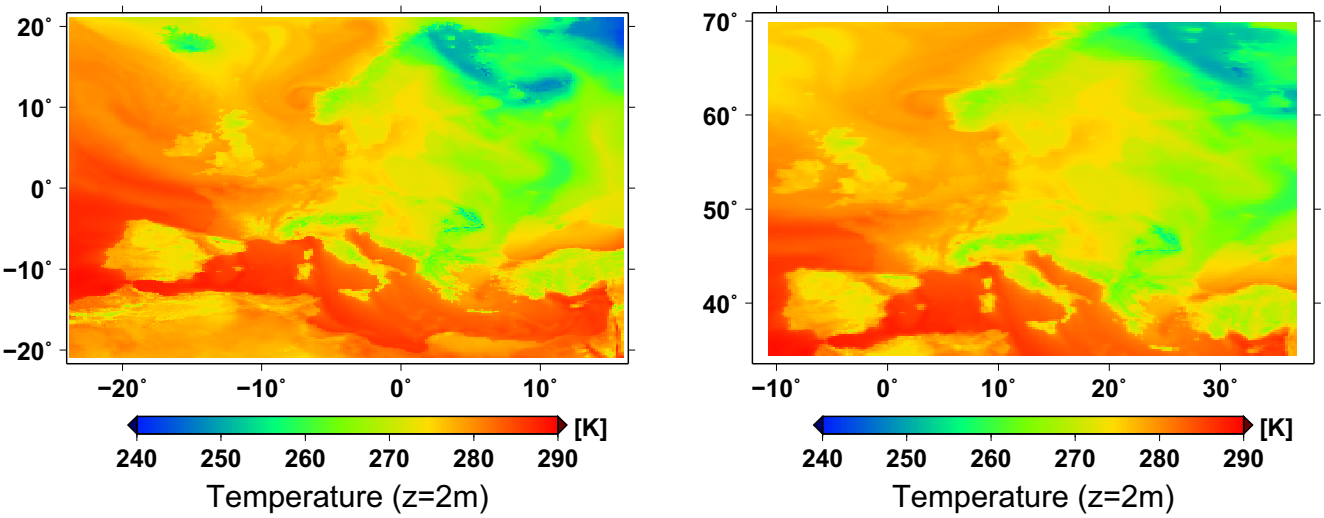

Figure 9 Temperature at 2 m height for the date 1984-01-07 06:00h obtained in the first realisation of the reconstruction of the climate of the 20th century. *Left:* D2 domain in the rotated coordinate system. *Right:* D3 domain.

A few examples are presented in the following subsections to demonstrate ways to extract properties from the huge amount of data. At first, regional effects from the A1B scenario are given for precipitation and temperature, followed by graphs about a climatological change, and finally, the effect on two climate indices is shown. All results, presented in the following, are prepared with the CLM output fields interpolated to the geographical (0.2°) grid (see Table 11) and for the first realisation of the respective experiments.

5.1 Regional effects of the A1B scenario

The impact of the A1B scenario is demonstrated in Figure 10 showing the time series of minimum and maximum temperatures, respectively, averaged over a $1° \times 1°$ box in Northern Italy for the four seasons. The dashed line separates the C20_1 20th century reconstruction run from the A1B_1 scenario.

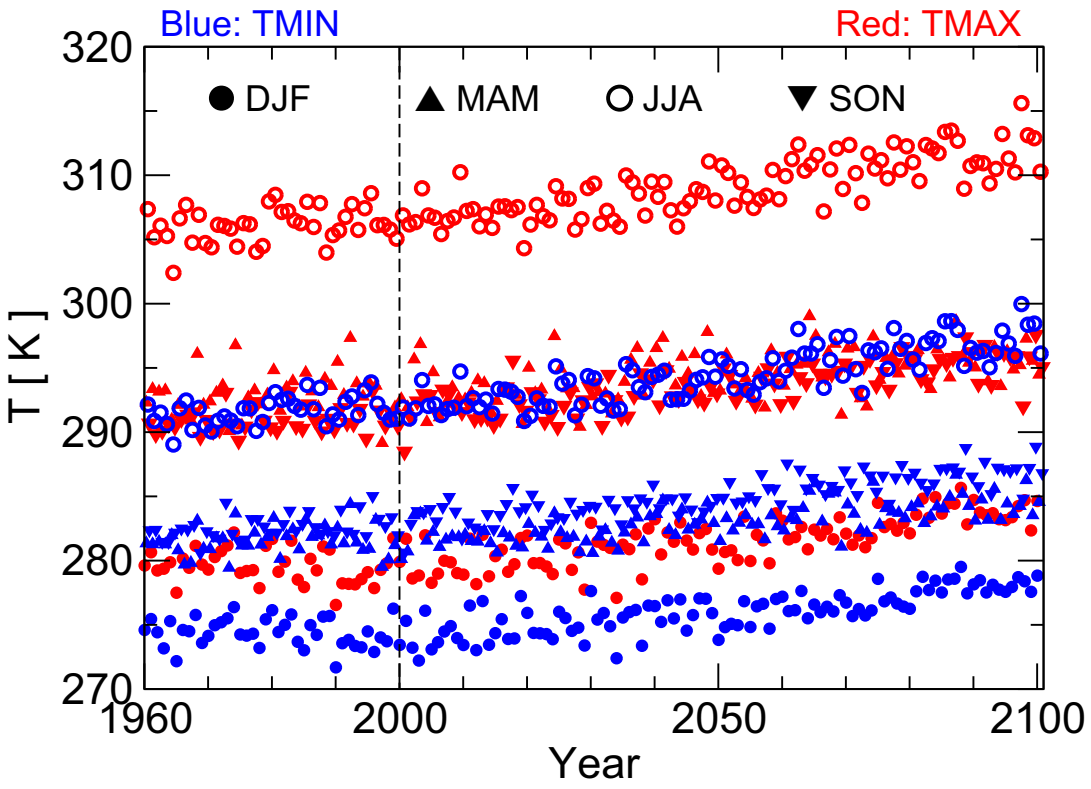

Figure 10 Seasonal minimum and maximum temperature at 2 m height, respectively, for C20_1 and A1B_1 scenario averaged over a region of 1°x1° in size with centre at longitude 11°E and latitude 45°N (Northern Italy).

Apparently, there is a similar increase of temperature (this holds also for the mean temperature not shown in the graph) for each season. The least square regression technique was applied to the daily mean temperature. Table 13 summarises the increase over 41–year periods for the ranges 1960 –

2000, 2001 – 2041, and 2060 – 2100 for the Italian and two other regions (around Lüchow in Northern Germany and in East-Bavaria).

Table 13 Change of temperature [K] at 2 m height over periods of 41–years for selected regions of $1° \times 1°$ size (Northern and Southern Germany and Northern Italy) from least square regression. Given is coefficient a_1 for the runs of the C20 and A1B scenarios of CLM daily mean temperature (geographical grid).

	1960 – 2000			**2001 – 2041**		**2060 – 2100**	
	run 1	run 2	run 3	run 1	run 2	run 1	run 2
11°E, 53°N	0.55	0.47	0.40	1.18	0.97	1.71	1.07
11°E, 49°N	0.72	0.38	0.68	1.34	1.08	1.76	1.48
11°E, 45°N	0.59	0.64	0.94	1.40	0.84	1.81	1.69

Although the coefficients of the linear least-square regression are not scientifically sound, because the annual cycle was not removed and significance was not tested, they give a first impression of what can be expected due to the scenario. In fact, all regions experience a temperature increase, even in the late 20th century. Note that the increase at the end of the 21st century is even higher than before, although the A1B greenhouse gas concentration increase is decreasing in the second half of the 21st century. Also, the variations between the runs appear to be rather high, which expresses the influence of long term variability (natural or in the driving model) of different realisations of the same climate scenario.

Frequency distributions as shown in Figures 4 and 5 are not suitable to demonstrate tendencies or seasonal properties. However, differences of frequency distributions from different periods can reveal changes. Therefore, the frequency distribution of the last four decades of the 20th century from the CLM_C20 data was chosen as reference for the distributions of the CLM_A1B results from the periods 2001–2041 and 2060–2100, respectively.

The frequency distribution of temperature at 2 m height for two regions (Northern Italy and Northern Germany) from the CLM_C20 run is shown in Figure 11.

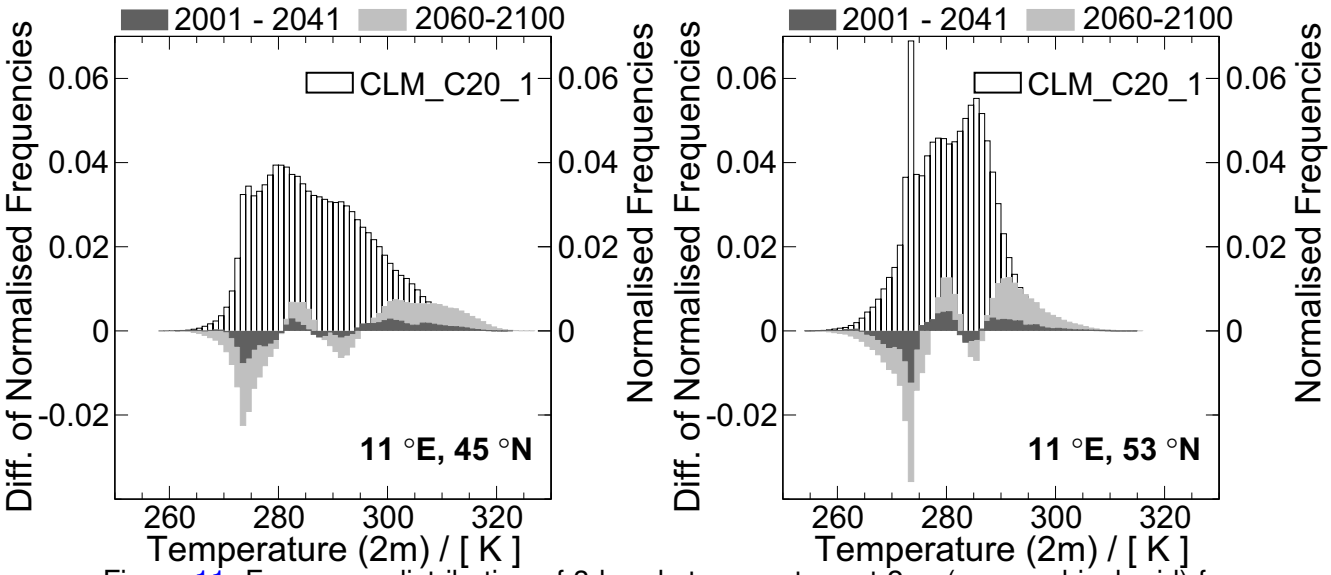

Figure 11 Frequency distribution of 3-hourly temperature at 2 m (geographical grid) for the region of 1°×1° around 11 °E and 45 °N. *Right Ordinate:* Distribution of CLM_C20_1 data (open bars) for the period 1960–2000. *Left Ordinate:* Deviations of frequency distributions of the CLM_A1B_1 scenario from CLM_C20_1 for the model-period 2001–2041 (dark grey) and 2060–2100 (light grey).

Additionally, the deviations of the two periods of the CLM_A1B_1 runs from the reference distribution are displayed, i.e. the frequencies of CLM_A1B_1 data minus those of CLM_C20_1. The dark grey areas in the figure express changes between 1960–2000 and the projection for the period 2001–2041, whereas the light grey area is for the period 2060–2100 of the CLM_A1B projection. The frequency distributions of 3–hourly temperatures from the CLM_C20 run exhibit a peak around 0 °C, which is very prominent for the German region. Although a peak could be explained due to persisting temperatures about 0 °C as long as snow and ice are melting, the peak was not confirmed by observations for the site of Lüchow provided by SGA-Offenbach shown in Appendix A. Temperature at the height of 2 m is not a variable given directly in the output of CLM, but it is parameterised. If the peak of CLM is redistributed to the surrounding classes, the shape of the frequency distribution agrees fairly well with that for the observation. Additionally, the temperature range of 280–290 K exhibits a slightly higher frequency in the model results.

Temperatures lower than about 280 K are projected to occur less frequent in the first four decades of the CLM_A1B projection, a decrease that is continued during the whole simulation period (Figure 11). On the other hand, the positive areas for higher temperature indicate more frequent warm or

hot days in the later periods. Both tendencies, the decrease of the occurrence of low temperatures as well as the increase of high temperature events seem to accelerate in the course of the century.

A key parameter particularly relevant to climate change impact is precipitation. As for the temperatures, we show the relation of the CLM_A1B projection to the last four decades of the 20th century, whose frequency distributions of daily precipitation is given in the upper panels of Figure 12.

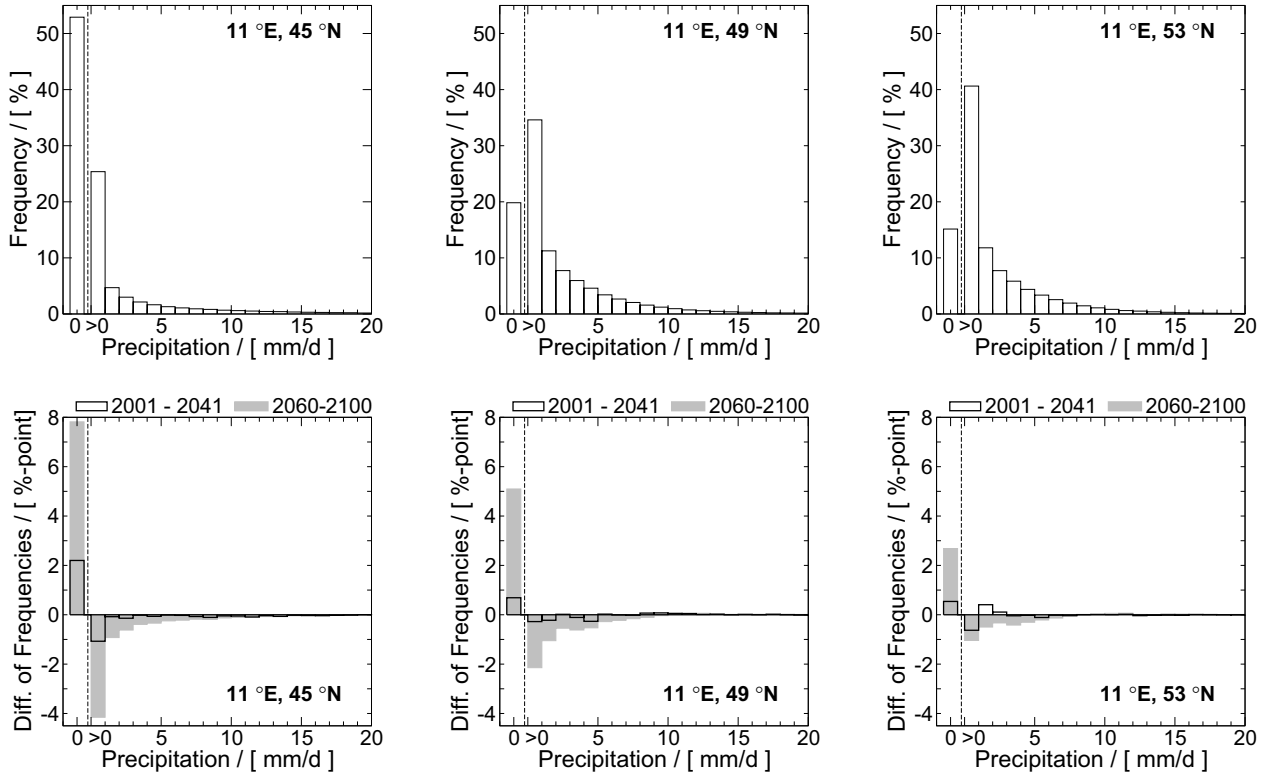

Figure 12 Frequency distribution of daily precipitation (geographical grid) for regions of $1° \times 1°$ in size with centres indicated in the panels. The dashed line separates the non-precipitation bar on its left from the precipitation classes.
Upper Row: Distribution for CLM_C20_1 (1960–2000).
Lower Row: Change of frequency distributions of the CLM_A1B_1 scenario from CLM_C20_1 for the model–period 2001–2041 (open black) and 2060–2100 (filled grey).

The most frequently occupied precipitation class is the one with values below 1 mm/d. The change due to the A1B projections for the periods 2001–2041 and 2060–2100 relative to the period of 1960–2000 is shown in the lower row of Figure 12. A change is depicted towards dryer conditions for all

three regions, but more pronounced for Northern Italy and for the second half of the 21st century. However, a slight increase of heavier precipitation is projected for classes above 10mm/d for the two regions in Germany.

5.2 Climatological change

Another method to investigate potential developments is in calculating differences of climatological means for different periods. Usually, periods of 30 years are taken. The difference between two of these climatological means would reveal whether anything has changed. Figure 13 (left) shows the change of precipitation over Europe between the climate of the last three decades of the 20th century and the last three decades for the A1B projection (only ensemble run 1).

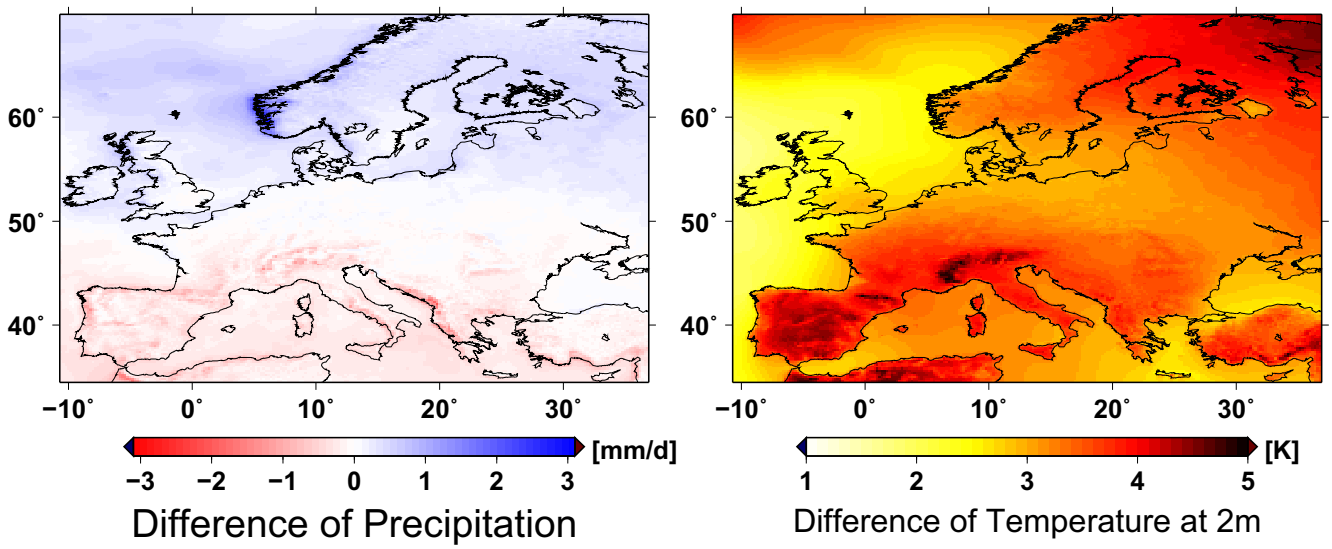

Figure 13 Change of 30–year climatological mean on the geographical grid. Deviation of CLM_A1B_1 projection data of 2070–2100 from CLM_C20_1 of 1960–1990. *Left:* Daily precipitation. *Right:* 3-hourly temperature at 2 m height.

A decrease of mean precipitation is prevalent in the southern half of the computational domain, in particular in the regions abutting on the Mediterranean, which already suffer from dry summers.

The analog picture for temperature is shown in the right panel. There is no change less than 1 K and a maximum of 4.9 K is found in the Pyrenees. Generally, the south and the north-east of Europe are more strongly affected.

5.3 Climate indices

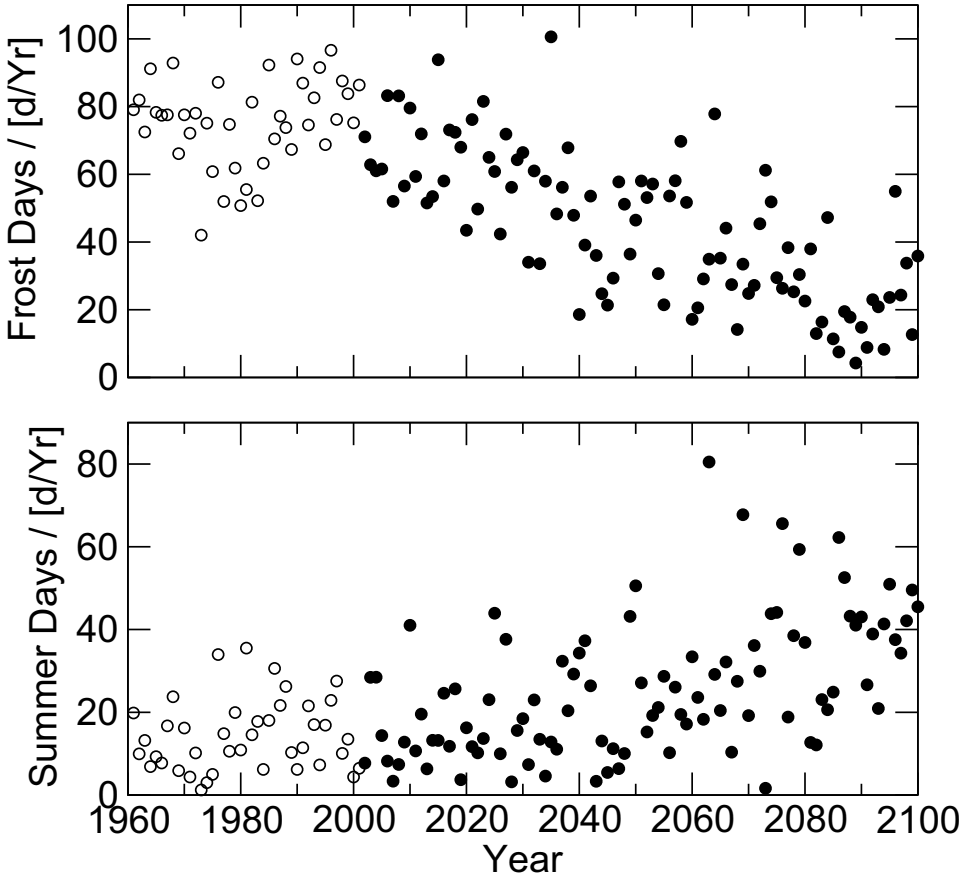

Figure 14 Number of frost days (top) and summer days (below) per year in the region centred next to Lüchow, Germany, (11°E, 53°N) with size 1°×1° for CLM_C20_1 (open circles) and the CLM_A1B_1 run (full circles).

The Service Group Adaptation calculated a set of parameters on the geographical grid which are characteristic for mid-latitude climate and useful in particular for climate change impact studies. It includes yearly and monthly numbers of days with snowfall, total precipitation and temperature exceeding certain thresholds, frozen soil, and snow-cover. The numbers were determined without normalising to a standard length of month or year, i.e. the month of January has a chance of 31 occurrences of an event and February only 28 or 29. These climate indices are available from the WDCC. As an example, the number of frost days defined by maximum temperatures below 0° C and summer days defined by minimum temperatures above 25° C, respectively, are presented in Figure 14 for the Northern German region around 53° N and 11° E. In particular, the decrease of the number of frost days per year is noticeable here.

5.4 Output variables for D2 and D3

Brief information is given in Table 14 about each variable provided on the D2 and D3 grid. Hyperlinks point from the table to Appendix A, if additional definitions, remarks, and figures from the quality control are provided. The tables will be updated taking into account new findings by M&D and responding users.

The following notation is applied to the table in order to characterise the valid output time intervals. Additionally, bi-linear interpolation from D2 to D3 is indicated by (B) and nearest-neighbour assignment by (N); non-interpolated variables of D2 are denoted by (-). Notice that variables, which are only provided for D3, have been derived from values on the geographical grid after bi-linear interpolation and nearest-neighbour assignment, respectively. This is indicated by $\mathbf{B}^*$ and $\mathbf{N}^*$.

For convenience, there is a link from each sub-table to this notation. For the sake of readability, the levels of the atmosphere and soil are given here again:

Atmosphere: 200, 500, 700, 850, 925, and 1000 hPa
Soil: 0, 0.01, 0.04, 0.1, 0.22, 0.46, 0.94, 1.9, 3.82 m

Notation:

x	mean over given period	1h/3h	one/three-hourly instantaneous value
$*$	sum over given period	1hc/3hc	accumulated over given period
#	number of days in given period	1hm/3hm	mean over given period
+	absolute maximum	d	instantaneous daily at 0 UTC
-	absolute minimum	dm	daily mean of the previous day
x+ and x-	both values available	dc	like dm, but accumulated
		f	fixed value

Variables, defined on levels, are indicated in the table by the superscript $^{\equiv}$.

Table 14 CLM output variables; click here for the notation.

Acronym	Description of Variables	Grid	Units	Time Step	D3 daily	D3 monthly	D3 yearly	Transf.
	General							
BOX_AREA	area of gridboxes	**D2&D3**	**m^2**	**f**				
FR_LAND	land-sea fraction	**D2&D3**	**1**	**f**				**B**
FR_LAND_NN	land-sea fraction	**D3**	**1**	**f**				**N**
HHL	height	**D2**	**m**	**f**				**-**
LAT	latitude	**D2&D3**	**deg**	**f**				
LAT_BNDS	latitude of bounds	**D2**	**deg**	**f**				
LON	longitude	**D2&D3**	**deg**	**f**				
LON_BNDS	longitude of the bounds	**D2**	**deg**	**f**				
	Atmosphere							
ASOB_T	net downward shortwave radiation (at model top)	**D2&D3**	**W/m^2**	**3hm**	**x**	**x**	**x**	**B**
ATHB_T	outgoing longwave radiation (at model top)	**D2&D3**	**W/m^2**	**3hm**	**x**	**x**	**x**	**B**
CAPE_CON	specific convectively available potential energy	**D2&D3**	**J/kg**	**3h**	**x**	**x**		**B**
CLCT	total cloud cover	**D2&D3**	**1**	**3h**	**x**	**x**		**B**
CLCH	high cloud cover	**D2&D3**	**1**	**3h**	**x**	**x**		**B**
CLCM	medium cloud cover	**D2&D3**	**1**	**3h**	**x**	**x**		**B**
CLCL	low cloud cover	**D2&D3**	**1**	**3h**	**x**	**x**		**B**
GPH $^{\equiv}$	geopotential	**D2&D3**	**m^2/s^2**	**3h**	**x**	**x**		**B**

Table 14 CLM output variables; click here for the notation.

Acronym	Description of Variables	Grid	Units	Time Step	D3 daily	D3 monthly	D3 yearly	Transf.
	Atmosphere continued							
HBAS_CON	height of convective cloud base	**D2**	**m**	**1h**				**-**
HMO3	air pressure at ozone maximum	**D2&D3**	**Pa**	**d**				**B**
HTOP_CON	height of convective cloud top	**D2**	**m**	**1h**				**-**
HZEROCL	height of freezing level	**D2&D3**	**m**	**d**				**B**
IDIV_HUM	atmosphere water divergence	**D2**	**kg/m^2**	**dc**				**-**
IWATER	cloud condensed water content	**D2**	**kg/m^2**	**3h**				**-**
IWV	precipitable water	**D2**	**kg/m^2**	**3h**				**-**
MFLX_CON	convective mass flux density	**D2**	**kg/m^{2}s**	**3h**				**-**
OMEGA $\equiv$	omega (dp/dt)	**D2&D3**	**Pa/s**	**3h**	**x**	**x**		**B**
QV $\equiv$	specific humidity	**D2&D3**	**kg/kg**	**3h**	**x**	**x**		**B**
T $\equiv$	air temperature	**D2&D3**	**K**	**3h**	**x**	**x**		**B**
U $\equiv$	u-component of the wind	**D2&D3**	**m/s**	**3h**	**x**	**x**		**B**
V $\equiv$	v-component of the wind	**D2&D3**	**m/s**	**3h**	**x**	**x**		**B**
VIO3	vertical integrated ozone amount	**D2&D3**	**Pa**	**d**				**B**

Table 14 CLM output variables; click here for the notation.

Acronym	Description of Variables				D3			
		Grid	Units	Time Step	daily	monthly	yearly	Transf.
Precipitation								
CON_TOT	convective precipitation	**D3**	**kg/m^2**	**1hc**	$*$	$*$	$*$	**B***
GSP_TOT	large scale precipitation	**D3**	**kg/m^2**	**1hc**	$*$	$*$	$*$	**B***
PRECIP_TOT	total precipitation	**D3**	**kg/m^2**	**1hc**	$*$	$*$	$*$	**B***
RAIN_CON	convective rainfall	**D2&D3**	**kg/m^2**	**1hc**	$*$	$*$	$*$	**B**
RAIN_GSP	large scale rainfall	**D2&D3**	**kg/m^2**	**1hc**	$*$	$*$	$*$	**B**
RAIN_TOT	rainfall	**D3**	**kg/m^2**	**1hc**	$*$	$*$	$*$	**B***
RR1MM	rain days	**D3**	**1**			**#**	**#**	**B***
R10MM	number of days with total precipitation $>$10 mm	**D3**	**1**			**#**	**#**	**B***
R20MM	number of days with total precipitation $>$20 mm	**D3**	**1**			**#**	**#**	**B***
SNOW_TOT	snowfall	**D3**	**kg/m^2**	**1hc**	$*$	$*$	$*$	**B***
SNOWLMT	height of the snowfall limit	**D2&D3**	**m**	**d**				**B**
SNOW_CON	convective snowfall	**D2&D3**	**kg/m^2**	**1hc**	$*$	$*$	$*$	**B**
SNOW_DAYS	number of days with snow	**D3**	**1**			**#**	**#**	**B***
SNOW_GSP	large scale snowfall	**D2&D3**	**kg/m^2**	**1hc**	$*$	$*$	$*$	**B**
Near-Surface								
AEVAP_S	evaporation	**D3**	**kg/m^2**	**3hc**	$*$	$*$	$*$	**B***
ALB	albedo	**D2&D3**	**1**	**3h**	**x**	**x**	**x**	**B**
ALB_NN	albedo	**D3**	**1**	**3h**	**x**	**x**	**x**	**N**

Table 14 CLM output variables; click here for the notation.

Acronym	Description of Variables	Grid	Units	Time Step	D3 daily	D3 monthly	D3 yearly	Transf.
	Near-Surface continued							
ALHFL_S	surface latent heat flux	**D2&D3**	**W/m^2**	**3hm**	**x**	**x**	**x**	**B**
APAB_S	surface photosynthetic active radiation	**D2&D3**	**W/m^2**	**dm**		**x**		**B**
ASOB_S	surface net downward shortwave radiation	**D2&D3**	**W/m^2**	**3hm**	**x**	**x**	**x**	**B**
ASHFL_S	surface sensible heat flux	**D2&D3**	**W/m^2**	**3hm**	**x**	**x**	**x**	**B**
ATHB_S	surface net downward longwave radiation	**D2&D3**	**W/m^2**	**3hm**	**x**	**x**	**x**	**B**
DURSUN	sunshine duration	**D2&D3**	**s**	**dc**		$*$	$*$	**B**
FD	frost days	**D3**	**1**			**#**	**#**	**B***
GZ0	surface roughness length	**D2&D3**	**m**	**d**				**N**
HSURF	surface height	**D2&D3**	**m**	**f**				**B**
HSURF_NN	surface height	**D3**	**m**	**f**				**N**
ID	ice days	**D3**	**1**			**#**	**#**	**B***
LAI	leaf area index	**D2&D3**	**1**	**d**				**N**
PLCOV	vegetation area fraction	**D2&D3**	**1**	**d**				**N**
PMSL	mean sea level pressure	**D2&D3**	**Pa**	**3h**	**x**	**x**		**B**
PS	surface pressure	**D2**	**Pa**	**d**				**-**
QV_S	surface specific humidity	**D2**	**kg/kg**	**d**				**-**
REL_HUM	relative humidity at 2 m	**D3**	**1**	**3h**				**B***

Table 14 CLM output variables; click here for the notation.

Acronym	Description of Variables	Grid	Units	Time Step	D3 daily	D3 monthly	D3 yearly	Transf.
	Near-Surface continued							
RUNOFF_S	surface runoff	**D2&D3**	**kg/m^2**	**1hc**	*	*		**B**
SNOW_COV	number of days with snow-cover	**D3**	**1**			**#**	**#**	**N***
SNOWFREQ	relative frequency of potential snowfall at surface	**D3**	**1**			*		**B***
SU	summer days	**D3**	**1**			**#**	**#**	**B***
TR	tropical nights	**D3**	**1**			**#**	**#**	**B***
T_G	grid mean surface temperature	**D2**	**K**	**3h**				**-**
T_SNOW	snow surface temperature	**D2&D3**	**K**	**d**		**x**	**x**	**N**
T_2M	instantaneous air temperature at 2 m	**D2&D3**	**K**	**3h**				**B**
T_2M_AV	average of air temperature at 2 m	**D2&D3**	**K**	**dm**		**x**	**x**	**B**
TD_2M	dew point temperature at 2 m	**D2&D3**	**K**	**3h**				**B**
TD_2M_AV	average of dew point temperature at 2 m	**D2&D3**	**K**	**dm**		**x**	**x**	**B**
TMAX_2M	maximum air temperature at 2 m	**D2&D3**	**K**	**dc**		**x+**		**B**
TMIN_2M	minimum air temperature at 2 m	**D2&D3**	**K**	**dc**		**x-**		**B**

Table 14 CLM output variables; click here for the notation.

Acronym	Description of Variables	Grid	Units	Time Step	D3 daily	D3 monthly	D3 yearly	Transf.
U_10M	u-component of wind at 10 m	**D2&D3**	**m/s**	**1h**	**x**	**x**	**x**	**B**
VMAX_10M	maximum wind speed at 10 m	**D2&D3**	**m/s**	**1hc**	**x+**	**x+**	**x+**	**B**
V_10M	v-component of wind at 10 m	**D2&D3**	**m/s**	**1h**	**x**	**x**	**x**	**B**
WIND_SPEED	wind speed at 10 m	**D3**	**m/s**	**1h**	**x**	**x**	**x**	**B***
WIND_DIR	wind direction at 10 m	**D3**	**deg**	**1h**				**B***
W_I	canopy water amount	**D2&D3**	**kg/m^2**	**d**		**x**	**x**	**N**
W_SNOW	surface snow amount	**D2&D3**	**m**	**d**		**x**		**N**
	Soil							
ROOTDP	root depth	**D2&D3**	**m**	**d**				**N**
RUNOFF_G	sub-surface runoff	**D2&D3**	**kg/m^2**	**dc**		*		**B**
SOILTYP	soil type	**D2**	**1**	**f**				-
SOILTYP_NN	soil type	**D3**	**1**	**f**				**N**
T_S	soil surface temperature	**D2**	**K**	**d**				**-**
T_SO ≡	soil temperature	**D2&D3**	**K**	**d**		**x**	**x**	**N**
W_ICE ≡	soil frozen water content	**D2&D3**	**m**	**d**		**x**	**x**	**N**
W_ICE_DAYS ≡	number of days with frozen soil	**D3**	**1**			**#**	**#**	**N***
W_SO ≡	soil water content	**D2&D3**	**m**	**d**		**x**	**x**	**N**

6 Discussion of the quality control results

The following sub-sections provide exemplary results of the scientific quality control which is based on the five different comparisons described in section 4.1.1. The results of these comparisons are illustrated by three different types of presentation as described in section 4.1.2. The discussion is restricted to Germany (sub-region DTL of Table 8 and Figure 7) for the comparisons 1, 2 and 4 and to Central Europe (MEU of Table 8 and Figure 7) for the comparisons 3 and 5, which are performed on the grid of the global model.

All considered annual or monthly average values are climatological averages over 20-year periods. The specific averaging periods for the various comparisons are described in section 4.1.1. Sections 6.10 and 6.11 present annual frequencies of specific events, which are climatological averages over 20-year periods, too. In contrast to the previous section, the following results were all obtained by an analysis of the raw output (D0) on the original model grid.

6.1 Daily mean of air temperature at 2 m height

This variable indicates the monthly or annual average of the daily mean of air temperature in 2 m above ground.

In COMPARISON 1 the evaluation run is compared to different reference data sets based on observations. Figure 15 (top left panel) exemplarily shows the deviation of the simulation to the CRU005 data set for the annual average temperature in 2 m above the surface. The simulated annual average temperature is too low in Central Europe. For Germany, this cold bias amounts -0.8 to -1.1 K depending on the considered reference data set. Hence, the error of the model is larger than the variability of the reference data for this region. Figure 16 (top left panel) shows the annual cycle of the deviation of the evaluation simulation to the reference data. The bars represent the range of the differences of the various reference data sets. The length of the bars indicates the differences between these reference data. Thus the bars quantify the uncertainty of knowledge about the real state of climate in the 20th century. The highest uncertainty is noticed in spring and autumn. For example the difference between the coldest and the warmest observation amounts to 0.59 K in September. The simulated daily means are too low, except in summer. The biggest deviations appear in winter. In this case the underestimation of the model is clearly larger than the variability of the reference data among themselves. For example in March, the model results are 1.87 K too low. The observations, however, only vary

up to 0.34 K. By contrast, the error of the simulation during the summer is low and smaller than the variability of the reference data.

COMPARISON 2 presents the influence of the forcing data (the results of the global model simulations) on the regional simulation. Figure 15 (middle left panel) shows the differences of an exemplary 20th century climate to the evaluation climate. The pattern of the deviations is similar for all four 20-year-realisations (see Table 5) of the 20th century climate. The difference between the various CLM-C20 climates and the evaluation climate varies between -0.08 and 0.18K for Germany. The annual cycle in Figure 16 (middle left panel), however shows much larger differences in the different seasons. In winter the 20th century climate runs are warmer and in summer colder. As a result, the cold-bias of the evaluation run is mostly compensated during winter in the CLM-C20 runs. But, the summer is simulated too cold. The variation of the deviations of the different 20th century climates to the evaluation climate in Figure 16 (middle left panel) gives evidences to the simulated internal climate variability of the current climate on the considered time scale. The variability from January to April and in June / July is relatively strong. The monthly averages vary up to 1.27 K between the different 20th century climates. The variability in September / October and in December (0.26 K) is the lowest. The use of different global forcing data in the regional model between evaluation and CLM-C20 runs causes differences in the simulated monthly averages up to 2.3 K. This amount is larger than the internal variability of the 20th century climates and comparable to the biggest difference of the monthly averages of the evaluation climate to the reference data.

COMPARISON 3 identifies the properties of the regional 20th century climate caused by the global model. Figure 15 (top right panel) exemplarily shows the difference of a regional CLM-C20 run to the corresponding global simulation. The spatial structure of the differences is similar for all four realisations (20 year climate averages) of the 20th century climate. The annual cycle in Figure 16 (top right panel) shows that in Central Europe the regional model usually simulates slightly lower temperatures. In the annual average the temperatures are 0.2 K lower than the temperatures of the global model. Only in the winter months the temperature in the regional model is a little bit higher. The differences are smaller than those in COMPARISON 2. This indicates that a large part of the differences shown in COMPARISON 2 are caused by the use of different global simulations forcing the regional model. A comparison of the forcing data (ECHAM5 versus ERA40) of CLM-C20 and evaluation runs (not shown here) shows in fact that the patterns of the deviations in COMPARISON 2 are already present in the global data.

COMPARISON 4 investigates the simulated climate change. Table 15 summarises the paired temperature changes of all considered simulations (paired comparisons of Table 7) for all sub-regions. An

increase of the annual average temperature appears in all paired comparisons across the whole model domain. Figure 15 (bottom left panel) presents an example of the horizontal structure of the climate warming. The comparison of the period 2011-2030 versus the period 1961-1980, which represents the mean climate change signal over the first 50 yr interval, yields a temperature increase for Germany of about 0.6 to 0.7 K. The temperature increase is more intensive (1.2 to 1.6 K), if the 20 yr periods of the second 50 yr interval (2031-2050 versus 1981-2000) are compared. This indicates that the change of the daily mean temperature is not constant in time. Figure 16 (bottom left panel) shows the annual cycle of the climate change separately for the first and the second interval. For the second interval the warming is stronger, in particular in autumn and winter. The temperature change varies considerably from month to month. The variability between the different pair comparisons is indicated by the bars in Figure 16 (bottom left panel). This variability represents the potential uncertainty of the climate change caused by the internal (or natural) variability of the climate system. Within this natural variation even a weak temperature decrease can appear in winter and spring within the first interval. In particular, the amount of the climate change (COMPARISON 4: 0.6 to 1.6 K) is higher than the uncertainty of the model (COMPARISON 1: -1.1 K to -0.8 K and COMPARISON 2: -0.1 K to 0.2 K). So, it can be stated as reliable change.

COMPARISON 5 investigates the consistency of and the differences between the climate change signals of the regional and of the global model. An example is presented in Figure 15 (bottom right panel). The differences are small over the sea. But, the temperature increase over land is lower in the regional model than in the global model all the year (see Figure 16 (bottom right panel)). The increase of the annual average in Central Europe in the regional model ranges from 0.6 to 1.5 K, but in the global model from 0.8 to 1.9 K. However, the shape of the annual cycle is the same in both models.

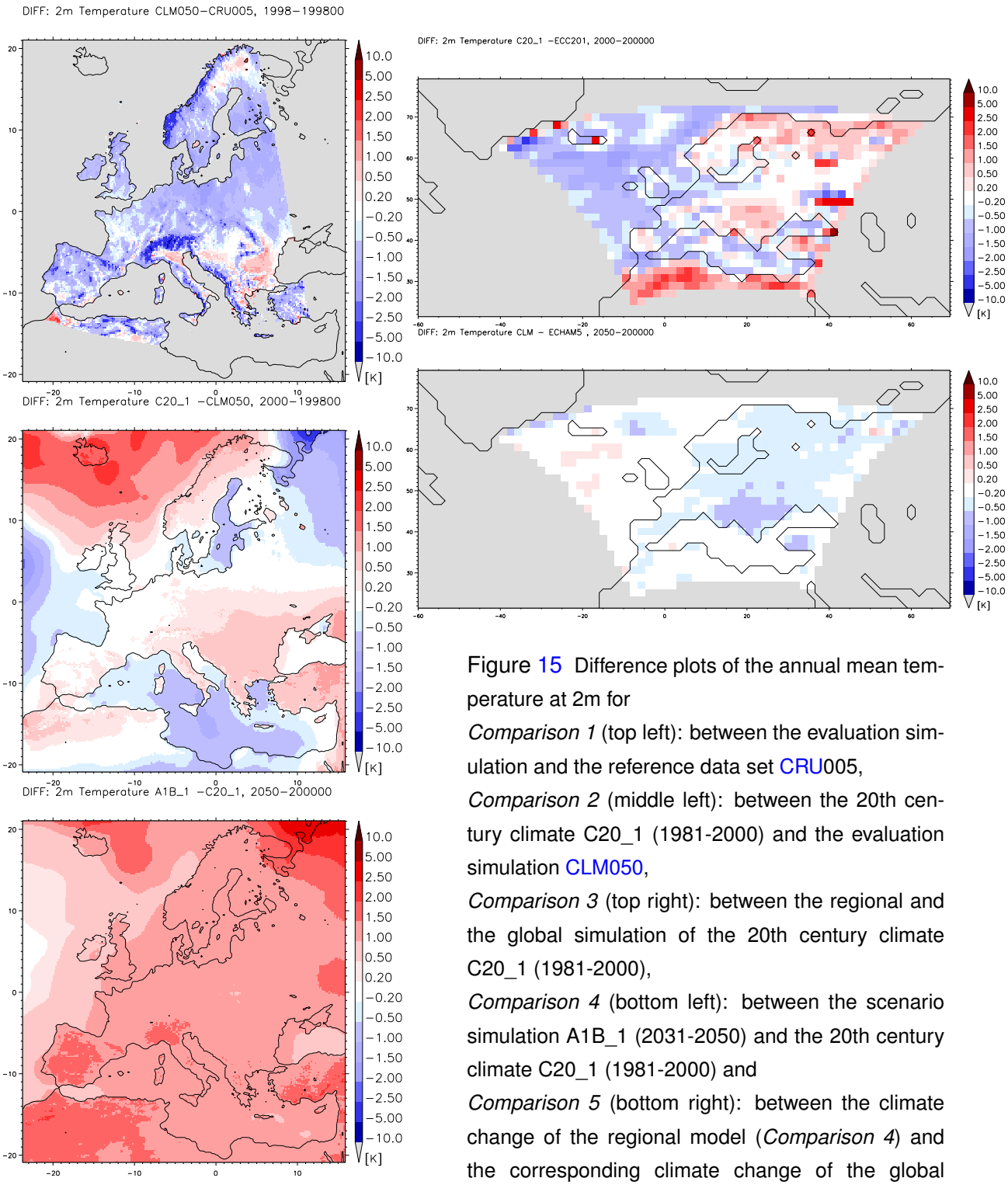

Figure 15 Difference plots of the annual mean temperature at 2m for

Comparison 1 (top left): between the evaluation simulation and the reference data set CRU005,

Comparison 2 (middle left): between the 20th century climate C20_1 (1981-2000) and the evaluation simulation CLM050,

Comparison 3 (top right): between the regional and the global simulation of the 20th century climate C20_1 (1981-2000),

Comparison 4 (bottom left): between the scenario simulation A1B_1 (2031-2050) and the 20th century climate C20_1 (1981-2000) and

Comparison 5 (bottom right): between the climate change of the regional model (*Comparison 4*) and the corresponding climate change of the global model (period 2031-2050 versus period 1981-2000).

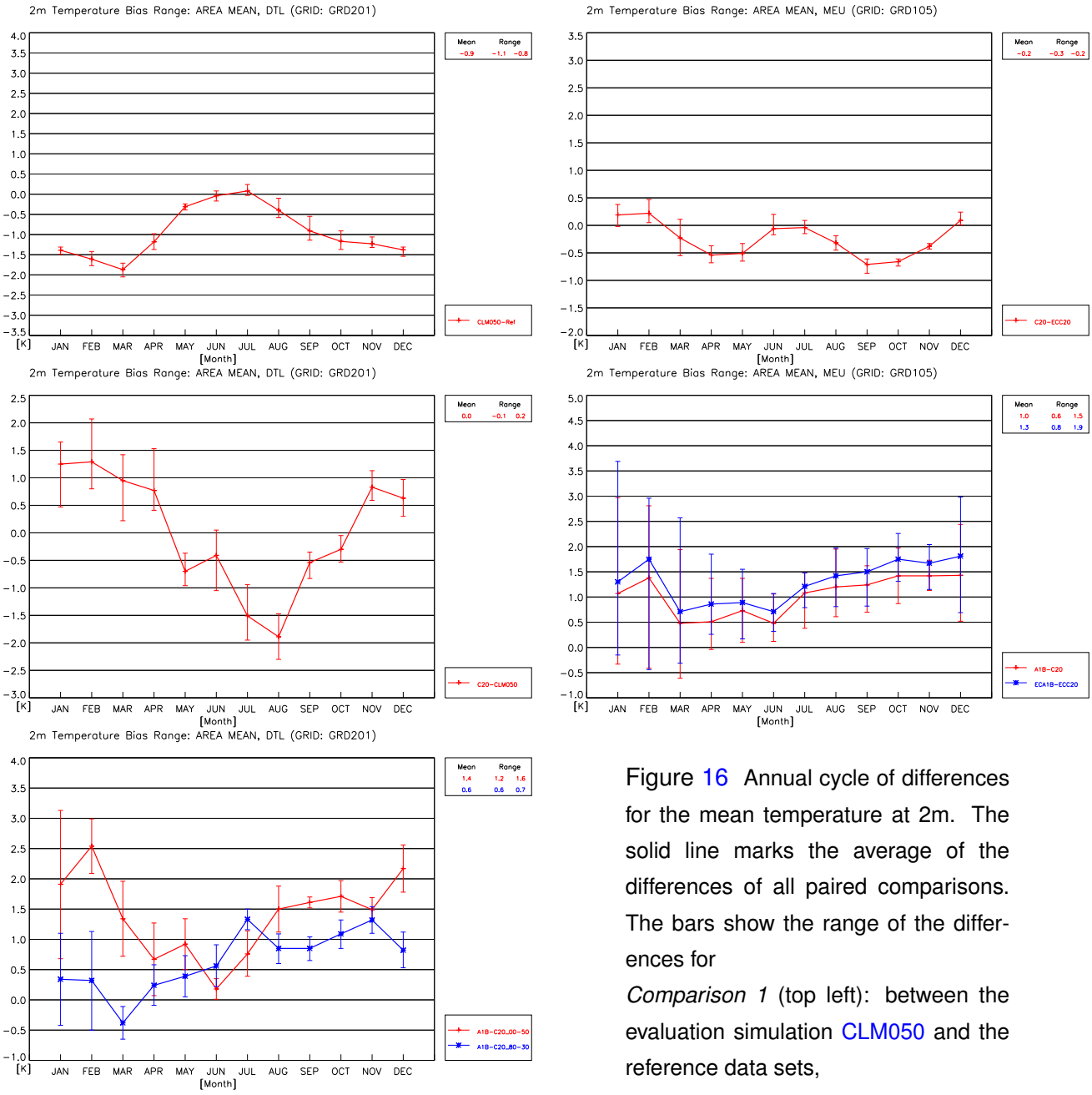

Figure 16 Annual cycle of differences for the mean temperature at 2m. The solid line marks the average of the differences of all paired comparisons. The bars show the range of the differences for

Comparison 1 (top left): between the evaluation simulation CLM050 and the reference data sets,

Comparison 2 (middle left): between the 20th century climates CLM-C20 and the evaluation simulation,
Comparison 3 (top right): between the regional and the global simulations of the 20th century climate,
Comparison 4 (bottom left): between the scenario simulations and the 20th century climates for the first time lag of 50 years (2011-2030 vs. 1961-1980: blue) and the second time lag of 50 years (2031-2050 vs. 1981-2000: red),
Comparison 5 (bottom right): between the scenario simulations and the 20th century climates for the regional model (red) and the global model (blue) comprising both 50 year time lags.

Table 15 Bias table for the climate change (*Comparison 4*) of the average temperature for all sub-regions (Figure 7, Table 8). The smallest and the largest difference of all comparisons between the scenario runs and the 20th century climates are given for annual values and for four monthly values. Positive deviations are highlighted in red, negative deviations in blue colour.

	Year		January		April		July		October	
Region	min.	max.	min.	max.	min.	max.	min.	max.	min.	max.
NEU	0,7	1,7	0,1	2,7	0,4	1,6	0,6	1,3	0,8	1,5
NEL	0,7	1,9	0,0	3,2	0,4	1,9	0,6	1,3	0,9	1,6
NEW	0,7	1,5	0,4	2,0	0,4	1,2	0,7	1,3	0,7	1,4
SEU	0,8	1,4	0,2	1,6	0,6	1,6	1,1	1,6	1,1	1,6
SEL	0,9	1,6	0,2	1,7	0,6	1,9	1,2	1,8	1,1	1,8
SEW	0,7	1,2	0,3	1,4	0,5	1,2	0,9	1,3	0,9	1,4
SCA	0,7	1,9	-0,1	3,1	0,1	1,3	0,2	1,4	0,4	1,7
NWE	0,6	1,2	-0,2	2,1	0,1	1,0	0,4	1,5	0,5	1,8
MEU	0,6	1,5	-0,4	3,0	-0,1	1,3	0,4	1,5	0,9	2,0
SWE	0,8	1,5	-0,1	1,6	-0,1	1,6	1,2	1,6	0,9	2,3
EEU	0,6	2,0	-0,1	3,3	0,3	2,3	0,6	1,2	1,0	1,8
SUE	0,8	1,7	0,1	2,2	0,4	2,0	0,6	1,7	0,9	2,0
NEE	0,6	2,3	-0,3	3,8	0,5	2,4	-0,2	2,0	0,8	1,7
RUS	0,8	2,2	0,4	3,5	0,9	3,4	0,6	1,8	0,9	1,8
VAS	0,8	1,6	0,1	1,2	0,9	2,2	1,3	2,3	0,5	1,7
NAF	0,9	1,6	0,1	1,6	0,6	1,9	1,0	2,1	0,9	1,8
MED	0,7	1,3	0,3	1,5	0,5	1,2	0,8	1,3	0,9	1,4
OSS	0,7	2,0	0,2	2,8	0,3	1,8	0,6	1,7	0,7	1,5
NOS	0,6	1,3	0,0	2,1	0,3	1,1	0,6	0,9	0,6	1,4
SWM	0,6	1,5	0,2	1,3	0,6	1,9	1,0	1,9	0,6	1,5
NOA	0,8	1,4	0,6	1,9	0,4	1,3	0,6	1,4	0,7	1,3
BIS	0,6	0,9	0,0	1,4	0,2	0,8	0,4	1,1	0,6	1,5
DTL	0,6	1,6	-0,4	3,1	-0,1	1,3	0,4	1,5	0,9	2,0
SLW	0,6	1,5	-0,5	3,0	0,0	1,1	0,6	1,3	0,7	1,7
ESS	0,6	1,4	-0,4	3,0	-0,1	1,1	0,4	1,8	0,8	2,0
LIN	0,5	1,6	-0,4	3,4	-0,1	1,3	0,5	1,4	0,9	2,0
MEI	0,6	1,6	-0,4	3,2	-0,1	1,3	0,3	1,7	0,8	2,0
STU	0,6	1,5	-0,6	2,9	-0,2	1,5	0,0	1,8	0,9	2,1
MUN	0,6	1,7	-0,6	3,1	-0,1	1,8	0,0	1,6	1,1	2,2
SAX	0,5	1,6	-0,5	3,3	-0,1	1,4	0,4	1,5	0,9	2,1
ALP	0,8	1,7	-0,4	2,8	0,1	2,0	0,3	1,8	1,1	2,3
POE	0,8	1,7	-0,1	2,6	-0,4	1,9	0,5	1,9	1,2	2,5
UNG	0,6	1,8	-0,1	2,6	-0,2	2,0	0,1	1,7	0,7	2,0
NSK	0,7	1,8	0,0	2,8	0,0	1,0	0,1	1,4	0,3	1,7
SSK	0,7	1,9	-0,1	3,2	0,1	1,4	0,2	1,4	0,5	1,8

6.2 Daily maximum of air temperature at 2m height

This variable indicates the monthly or annual average of the daily maximum of air temperature in 2 m above ground.

In COMPARISON 1 the evaluation run is compared to different reference data sets. Figure 17 (top left panel) presents the deviation of the evaluation simulation to the data set CRU007 for the annual averages of the daily maximum temperature. Near the coastline of the evaluation grid the CRU007 provides values over several sea grid points. The reason for this is the projection of the data set CRU007 from its original grid onto the evaluation grid, which may have differences in the land-sea distributions in coastal areas (see section 4.1.2). The simulation result is 0.3 to 1.1 K colder for Germany, depending on the reference data set considered. The deviations show a distinctive seasonal development (Figure 18, top left panel). The simulation is warmer from May to August (up to 1.9 K in July) and colder during the other months (up to 2.5 K in March). The averaged deviation of the model is larger than the variability of the reference data in the winter season (from October until March), and smaller from April to September.

COMPARISON 2 investigates the difference between the CLM-C20 runs and the evaluation run. Figure 17 (middle left panel) gives an example of the spatial deviation. The structures are similar for all paired comparisons (in Table 5). Furthermore, they are comparable to the spatial patterns in COMPARISON 2 of the daily mean temperature (see section 6.1). The annual averages of the maximum temperature of Germany are 0.2 to 0.5 K lower in the 20th century climates than in the evaluation run. The annual cycle of the deviations in Figure 18 (middle left panel) shows similarities to the behaviour of the daily mean temperature, too. The CLM-C20 runs are colder in summer and warmer in winter. Hence, the cold-bias in winter is damped down compared to the CLM050 run. In summer and in autumn the maximum temperatures in the CLM-C20 simulations are much colder than in the CLM050 run. Therefore, the 20th century runs feature a wider difference to the reference data than the evaluation run for the annual averages of the daily maximum temperature (about -1.25 K versus -0.86 K for CLM050). The variability of differences between the various 20th century climates and the evaluation climate for the different months vary between 0.34 and 1.64 K (the length of the bars in Figure 18, middle left panel). The least values occur during the last months of the year. For the winter season, the averaged deviation between the CLM-C20 runs and the evaluation run is smaller than the internal variability of the CLM-C20 runs. As a consequence, the winter maximum temperatures are better, summer values worse than in the CLM050 run.

COMPARISON 3 investigates the differences between the regional and the corresponding global sim-

ulation. The spatial patterns of the deviations are similar for all paired comparisons (see Table 6). Figure 17 (top right panel) presents an example. The CLM simulations are warmer over the land area (for Central Europe about 0.3 to 0.4 K over the whole year) and colder over the Atlantic Ocean. The contrary behaviour of the temperature differences over land and sea areas is probably resulting from the treatment of the coupling between the atmosphere and the surface below in both models. In the regional model it is basically different for land and sea grid cells. For land surfaces, the soil model included in CLM calculates the temperature at the ground interactively. For sea grid points, the values of the sea surface temperature (SST) are given by the global model. Figure 18 (top right panel) shows the annual cycle of the differences of the daily maximum of air temperature for Central Europe (MEU). From January to August the regional simulations are warmer, but colder from September to December. The difference between regional and global simulation (from April to November) is mostly larger than the variability of this difference.

COMPARISON 4 investigates the simulated climate change. Table 16 presents an overview for all sub-regions considered. The change of the maximum temperature shows remarkable similarities to the daily mean temperature. The annual averages of the daily maximum temperatures increase for all paired comparisons over the whole model domain (see the example in Figure 17, bottom left panel). Figure 18 (bottom left panel) presents the annual cycle of the climate change separately for the two intervals investigated. The warming is more intensive in the second interval (1.2 K to 1.5 K versus 0.5 K to 0.8 K in the first interval), mainly in autumn and winter. The internal variability of the simulated climate change signal is large, especially in winter. In January the simulated changes range from 0.35 K decrease up to 3.17 increase. Even a weak decrease of the maximum temperature can appear in winter and spring, primarily within the first interval. The amount of the simulated climate change (COMPARISON 4: 0.5 to 1.5 K) is larger than the uncertainty of the model (COMPARISON 1: -1.1 to -0.3 and COMPARISON 2: -0.5 K to -0.2 K). So, this can be stated as a reliable change.

COMPARISON 5 considers the differences of the climate change between regional and global model. The results of this comparison are similar to the behaviour of the daily mean temperature. Over the continent the CLM simulates a systematic lower warming than the global model (see Figure 17 (bottom right panel). This effect appears more intensive in the second interval (2031-2050 versus 1981-2000). Averaged over all paired comparisons, the increase of the daily maximum temperature simulated by the regional model is between 0.16 K (in January) and 0.5 K (in October) lower than the climate change signal of the global model (Figure 18, bottom right panel). But, the shape of the annual cycles is similar (same figure).

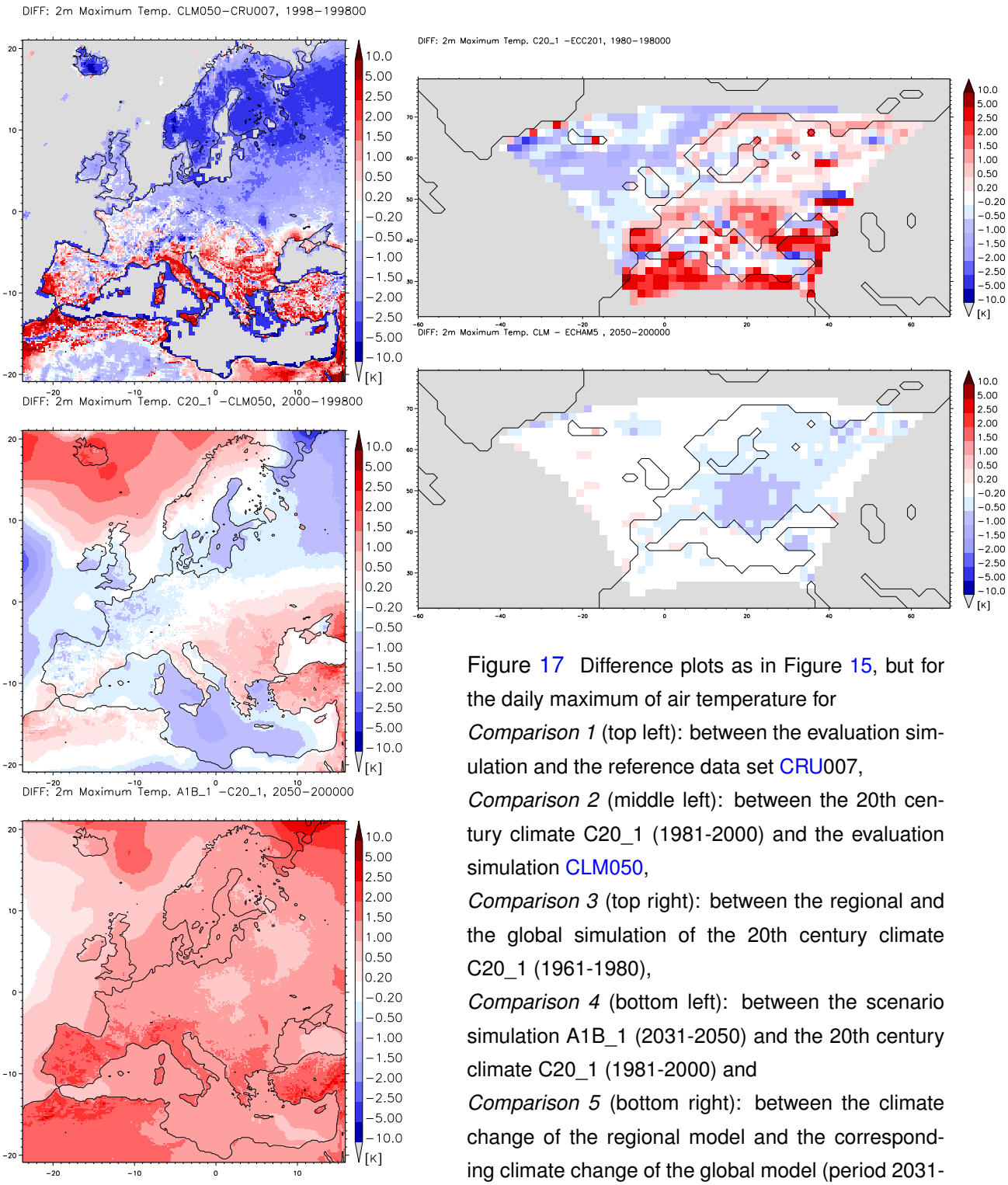

Figure 17 Difference plots as in Figure 15, but for the daily maximum of air temperature for

Comparison 1 (top left): between the evaluation simulation and the reference data set CRU007,

Comparison 2 (middle left): between the 20th century climate C20_1 (1981-2000) and the evaluation simulation CLM050,

Comparison 3 (top right): between the regional and the global simulation of the 20th century climate C20_1 (1961-1980),

Comparison 4 (bottom left): between the scenario simulation A1B_1 (2031-2050) and the 20th century climate C20_1 (1981-2000) and

Comparison 5 (bottom right): between the climate change of the regional model and the corresponding climate change of the global model (period 2031-2050 versus period 1981-2000).

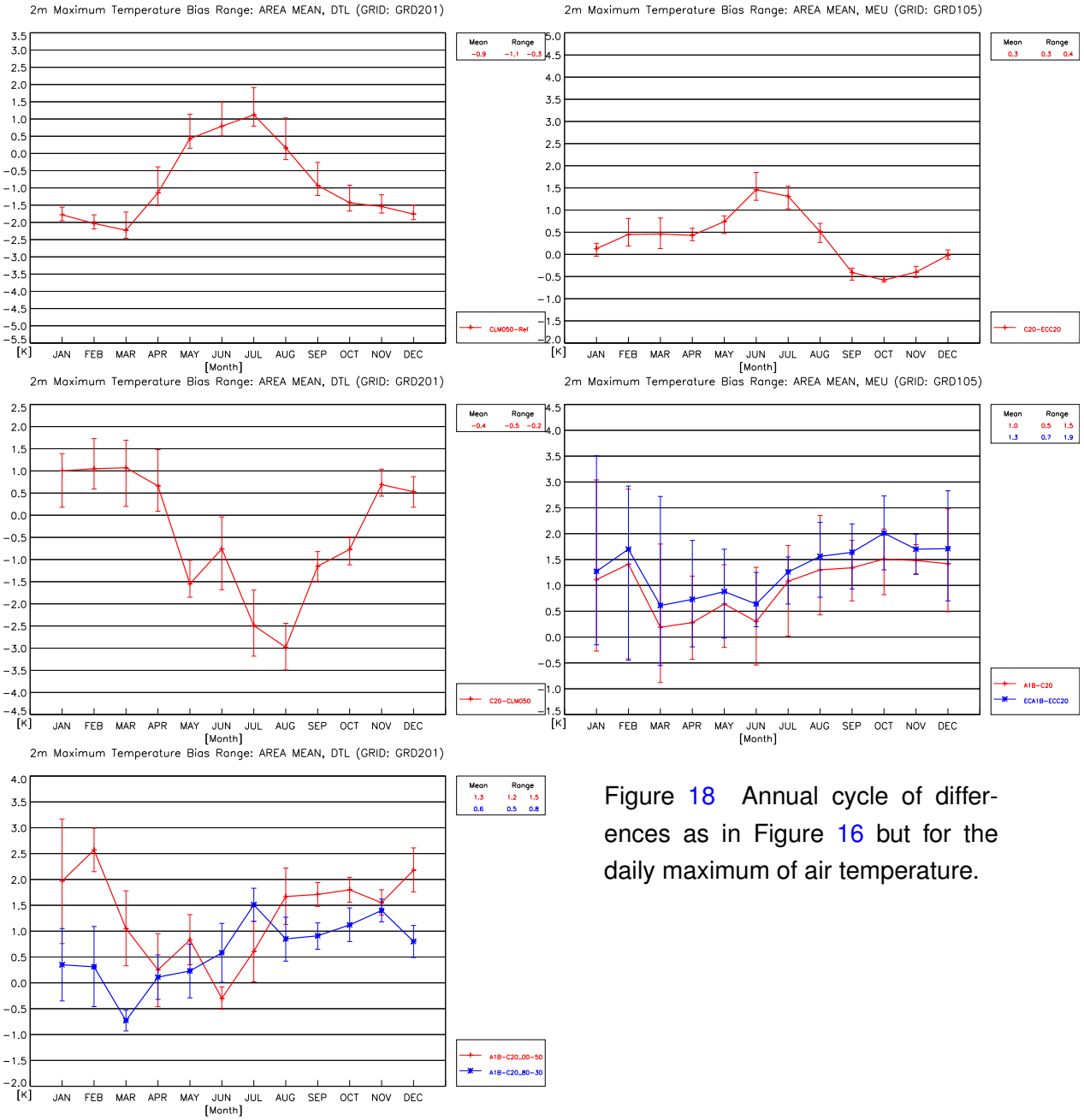

Figure 18 Annual cycle of differences as in Figure 16 but for the daily maximum of air temperature.

Table 16 Bias table for the climate change (*Comparison 4*) as in Table 15, but for the daily maximum of air temperature.

	Year		January		April		July		October	
Region	min.	max.	min.	max.	min.	max.	min.	max.	min.	max.
NEU	0,7	1,6	0,2	2,6	0,3	1,5	0,6	1,2	0,8	1,6
NEL	0,7	1,8	0,1	3,0	0,3	1,8	0,6	1,1	0,9	1,7
NEW	0,7	1,4	0,4	1,9	0,3	1,1	0,7	1,3	0,6	1,4
SEU	0,8	1,5	0,3	1,8	0,7	1,8	1,0	1,6	1,2	1,8
SEL	0,9	1,7	0,2	2,1	0,6	2,2	1,2	1,8	1,3	2,2
SEW	0,7	1,2	0,3	1,4	0,5	1,2	0,9	1,3	0,9	1,3
SCA	0,6	1,8	0,1	2,9	0,0	1,3	0,0	1,2	0,4	1,7
NWE	0,6	1,2	-0,3	2,2	-0,2	0,9	0,2	1,9	0,5	1,9
MEU	0,5	1,4	-0,3	3,0	-0,5	1,1	0,0	1,8	0,8	2,1
SWE	0,9	1,8	-0,2	2,2	-0,7	1,9	1,2	1,8	1,1	3,3
EEU	0,6	1,9	0,0	3,1	0,1	2,2	0,4	1,2	1,0	1,8
SUE	0,8	1,9	0,2	2,5	0,1	2,4	0,4	1,8	1,2	2,7
NEE	0,5	2,2	-0,1	3,5	0,5	2,4	-0,5	1,9	0,7	1,7
RUS	0,6	2,1	0,4	3,1	0,7	3,5	0,3	1,7	0,8	1,9
VAS	0,9	1,8	0,3	1,6	1,0	2,7	1,4	2,5	0,2	2,0
NAF	0,9	1,7	0,2	2,0	0,8	2,1	1,0	2,0	1,0	2,0
MED	0,7	1,3	0,3	1,4	0,5	1,2	0,8	1,3	0,9	1,3
OSS	0,7	1,9	0,3	2,8	0,3	1,7	0,7	1,7	0,7	1,5
NOS	0,6	1,2	0,1	2,1	0,2	1,1	0,6	0,9	0,6	1,5
SWM	0,6	1,5	0,3	1,2	0,6	1,9	0,9	1,9	0,6	1,5
NOA	0,8	1,4	0,6	1,7	0,4	1,2	0,6	1,4	0,6	1,3
BIS	0,6	0,9	0,0	1,3	0,2	0,7	0,3	1,1	0,6	1,5
DTL	0,5	1,5	-0,3	3,2	-0,5	0,9	0,0	1,8	0,8	2,0
SLW	0,5	1,4	-0,4	3,1	-0,4	0,7	0,3	1,7	0,7	1,7
ESS	0,5	1,3	-0,4	3,0	-0,4	0,7	0,1	2,2	0,8	2,1
LIN	0,4	1,5	-0,4	3,5	-0,5	0,6	0,2	1,5	0,8	1,8
MEI	0,4	1,5	-0,3	3,2	-0,7	0,9	-0,3	1,9	0,7	2,1
STU	0,5	1,7	-0,5	3,0	-0,9	1,5	-0,6	2,3	0,8	2,5
MUN	0,6	1,7	-0,6	3,1	-0,7	2,0	-0,5	2,0	1,0	2,4
SAX	0,4	1,5	-0,5	3,3	-0,5	0,9	0,0	1,5	0,9	2,1
ALP	0,7	1,9	-0,4	3,0	-0,3	2,4	0,1	2,1	1,1	2,8
POE	0,8	2,0	-0,1	3,1	-1,1	2,4	0,5	2,0	1,0	3,2
UNG	0,6	2,0	0,0	2,8	-0,7	2,2	0,0	1,8	0,9	2,5
NSK	0,6	1,7	0,2	2,7	0,0	1,2	-0,2	1,3	0,3	1,6
SSK	0,6	1,8	0,1	2,9	0,0	1,4	0,1	1,2	0,4	1,7

6.3 Daily minimum of air temperature at 2m height

This variable indicates the monthly or annual average of the daily minimum of air temperature in 2 m above ground.

COMPARISON 1 considers the deviation between the evaluation run and various reference data. Figure 19 (top left panel) shows the annual averaged deviation to the reference data set CRU007. The daily minimum temperature in the model is lower over large parts of Europe. For Germany, the simulation is 0.3 to 1.2 K colder than the observations. Figure 20 top left panel) shows the annual cycle of the deviations for Germany. The results of the simulation are mostly too cold. The annual cycle of deviations is less pronounced than for the maximum temperature (section 6.2). In winter, the error of the model is larger than the variability of the reference data. If the behaviour of the maximum temperature is taken into account, the simulated diurnal temperature range is too large in summer compared to the reference data. On the other hand, the diurnal temperature range is smaller from September to April.

COMPARISON 2 investigates the difference between the CLM-C20 runs and the evaluation run (see Figure 19, middle left panel). The behaviour of the minimum temperature over the sea is similar to the maximum temperature (Figure 17, middle left panel). But, there are some differences over the continent. The annual average of the minimum temperature is higher in the CLM-C20 runs than in the evaluation run (for Germany 0.3 to 0.5 K). The shape of the annual cycle is similar to that of the daily maximum temperature, but smaller in the amplitude. The 20th century runs are colder from June to October and warmer in winter (see Figure 20, middle left panel). The variability among the different CLM-C20 runs is relatively large and mostly larger than the difference to the evaluation run.

COMPARISON 3 investigates the differences between the regional and the corresponding global simulation. Figure 19 (top right panel) shows an example of the spatial pattern of the deviations. These are similar for all paired comparisons (see Table 6). In Central Europe the minimum temperature in the regional model is lower during most months (except in winter). The annual averaged difference amounts about 0.4 to 0.5 K. In contrast, the maximum temperature is higher in the regional model (section 6.2). The consequence is a stronger diurnal temperature variation in the regional simulation. During most months (except in winter) the differences between the models are larger than the variability of the paired comparison among each other (see Figure 20). Hence, the regional anomaly pattern is constant in time, except for the winter.

COMPARISON 4 investigates the simulated climate change. Table 17 gives an overview for all subregions. The annual averages increase for all paired comparisons. The increase is stronger in the

second interval (1.3 K to 1.6 versus 0.7 K to 0.8 K in the first interval). Figure 19 (bottom left panel) shows an example of the second interval. Figure 20 (bottom left panel) presents the annual cycle of climate change for both intervals. The internal variability of the simulated climate change signal is large, especially in winter. For example, the simulated climate change varies between -0.5 and +3.2 K in January. Within the first interval, even a weak cooling is possible. This behaviour shows great similarities to that of the daily mean temperature and the daily maximum temperature. The amount of the simulated climate change (COMPARISON 4: 0.5 to 1.7 K) is larger than the uncertainty of the model (COMPARISON 1: -1.2 to -0.3 and COMPARISON 2: 0.3 K to 0.5 K). So, the simulated increase of the minimum temperature is a reliable effect.

COMPARISON 5 investigates the differences between the climate change signals of the regional and global model. The patterns of the spatial differences are similar for all paired comparisons. Figure 19 (bottom panel) presents an example for the annual average. The regional model produces a lower warming than the global one for the land regions. The differences amount about 0.2 to 0.3 K per year. Figure 20 (bottom right panel) gives the annual cycles of the temperature change for both models. The CLM reduces the climate change of the forcing global model throughout the year. The effect is smaller in summer (in July: 0.07 K) than in winter (in January: 0.4 K). The shape of the annual cycle is nearly the same for both models.

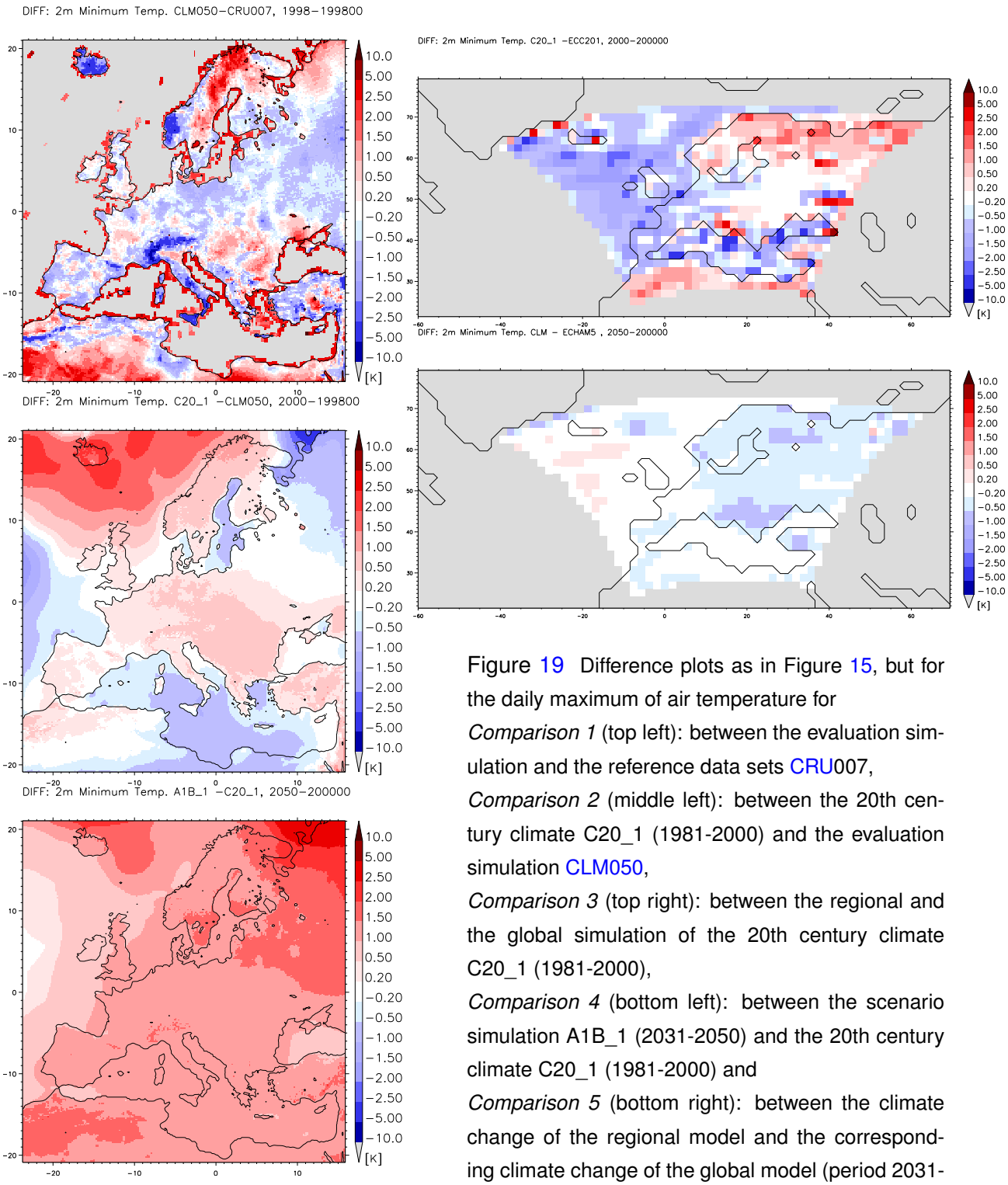

Figure 19 Difference plots as in Figure 15, but for the daily maximum of air temperature for

Comparison 1 (top left): between the evaluation simulation and the reference data sets CRU007,

Comparison 2 (middle left): between the 20th century climate C20_1 (1981-2000) and the evaluation simulation CLM050,

Comparison 3 (top right): between the regional and the global simulation of the 20th century climate C20_1 (1981-2000),

Comparison 4 (bottom left): between the scenario simulation A1B_1 (2031-2050) and the 20th century climate C20_1 (1981-2000) and

Comparison 5 (bottom right): between the climate change of the regional model and the corresponding climate change of the global model (period 2031-2050 versus period 1981-2000).

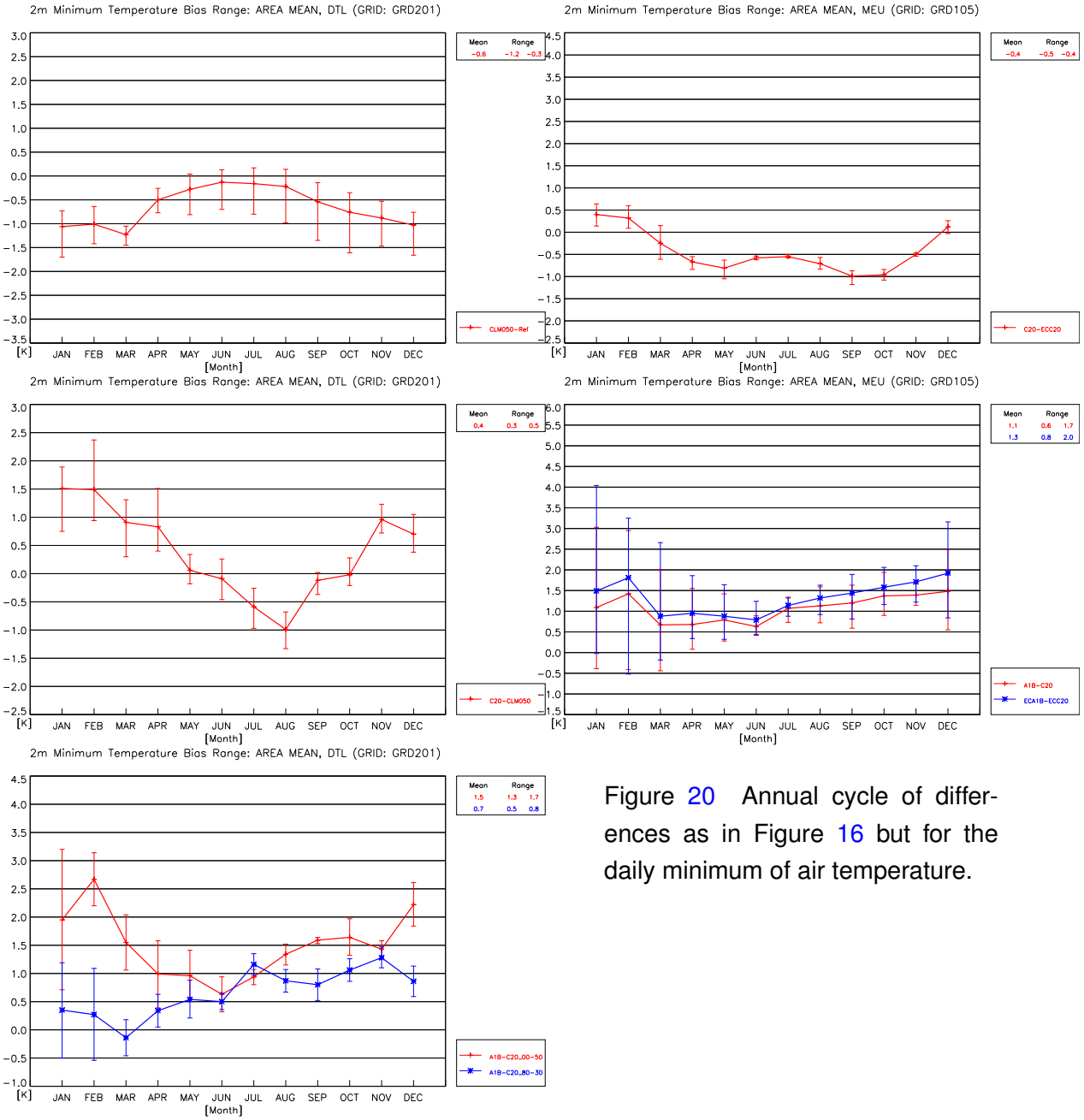

Figure 20 Annual cycle of differences as in Figure 16 but for the daily minimum of air temperature.

Table 17 Bias table for the climate change (*Comparison 4*) as in Table 15, but for the daily minimum of air temperature.

	Year		January		April		July		October	
Region	min.	max.	min.	max.	min.	max.	min.	max.	min.	max.
NEU	0,7	1,8	0,1	2,8	0,5	1,7	0,6	1,4	0,8	1,5
NEL	0,7	2,0	-0,1	3,4	0,6	2,1	0,6	1,4	0,9	1,6
NEW	0,7	1,5	0,3	2,0	0,4	1,2	0,7	1,3	0,7	1,4
SEU	0,8	1,4	0,2	1,5	0,5	1,4	1,1	1,6	1,0	1,5
SEL	0,8	1,5	0,2	1,6	0,5	1,6	1,3	1,9	1,0	1,5
SEW	0,7	1,3	0,3	1,5	0,5	1,2	0,9	1,3	1,0	1,4
SCA	0,7	2,0	-0,2	3,3	0,2	1,6	0,3	1,6	0,4	1,8
NWE	0,6	1,1	-0,2	2,0	0,3	1,1	0,6	1,2	0,5	1,7
MEU	0,6	1,6	-0,4	3,1	0,1	1,5	0,7	1,4	0,9	2,0
SWE	0,8	1,3	-0,1	1,5	0,2	1,3	1,1	1,7	0,7	1,8
EEU	0,6	2,1	-0,1	3,7	0,5	2,3	0,6	1,3	1,0	1,7
SUE	0,8	1,6	0,0	2,1	0,4	1,6	0,7	1,7	0,7	1,6
NEE	0,7	2,5	-0,6	4,1	0,7	2,7	0,2	2,2	0,8	1,8
RUS	0,9	2,3	0,5	3,8	1,0	3,3	0,4	1,7	0,9	1,9
VAS	0,7	1,5	0,0	1,1	0,8	1,9	1,3	2,3	0,6	1,5
NAF	0,8	1,5	0,1	1,5	0,4	1,7	1,0	2,2	0,9	1,6
MED	0,7	1,3	0,3	1,6	0,5	1,3	0,8	1,3	0,9	1,4
OSS	0,7	2,0	0,1	2,8	0,4	1,9	0,6	1,7	0,6	1,5
NOS	0,6	1,3	0,0	2,1	0,3	1,1	0,6	1,0	0,6	1,4
SWM	0,6	1,5	0,1	1,3	0,6	1,9	0,9	1,8	0,6	1,5
NOA	0,8	1,5	0,6	2,0	0,4	1,4	0,6	1,4	0,8	1,3
BIS	0,6	0,9	0,1	1,4	0,2	0,8	0,4	1,1	0,5	1,5
DTL	0,5	1,7	-0,5	3,2	0,1	1,6	0,8	1,4	0,9	2,0
SLW	0,5	1,7	-0,6	3,0	0,2	1,5	0,6	1,0	0,8	1,8
ESS	0,6	1,6	-0,5	3,0	0,1	1,4	0,8	1,4	0,8	2,0
LIN	0,4	1,8	-0,5	3,5	0,1	1,8	0,5	1,3	0,9	2,0
MEI	0,5	1,8	-0,5	3,4	0,0	1,6	0,8	1,5	0,8	2,0
STU	0,6	1,6	-0,6	3,0	0,1	1,6	0,6	1,5	0,8	2,1
MUN	0,6	1,8	-0,6	3,3	0,0	1,6	0,5	1,5	1,1	2,0
SAX	0,5	1,8	-0,5	3,4	0,0	1,8	0,7	1,4	0,9	2,0
ALP	0,8	1,7	-0,4	3,0	0,1	1,7	0,5	1,6	1,1	2,0
POE	0,8	1,6	-0,1	2,4	0,3	1,5	0,6	1,8	1,1	2,2
UNG	0,7	1,8	-0,2	2,6	0,2	1,8	0,3	1,5	0,5	1,7
NSK	0,7	1,8	-0,1	2,9	0,1	1,1	0,3	1,6	0,4	1,8
SSK	0,7	2,1	-0,2	3,4	0,2	1,7	0,3	1,6	0,4	1,8

6.4 Precipitation sum

This variable indicates the accumulated precipitation amount per month or year.

In COMPARISON 1 the evaluation simulation is compared to different reference data sets. Figure 21 (top left panel) shows as an example the difference of the annual sum of precipitation between the model and GPC003. The patterns of the deviations are strongly heterogeneous. Overestimation of precipitation on the windward side and underestimation in lee of the mountains occur in mountainous areas. The annual cycle of the difference for Germany is shown in Figure 22 (top left panel). Depending on the reference data set the model overestimates the precipitation for Germany by about 12 to 96 mm per year. The simulated amount of precipitation is higher in winter and spring (up to 21.2 mm in January), but lower in the summer (up to 10.9 mm in July). The differences of the various reference data sets among themselves are higher in winter (up to 13.6 mm in December) than in summer (4 to 6 mm). The uncertainty of the reference data for the monthly averages is slightly smaller than the error of the model concerning this reference data. The various observations differ by 85 mm over the complete year. But, the model result is merely about 48 mm too much precipitation averaged over all reference data. It must be taken into account that all observation data used here are not corrected with regard to the collective losses. A correction would lead especially in winter to higher precipitation values of an unknown amount.

COMPARISON 2 presents the influence of the forcing data (the results of the global model simulations) on the regional simulation. Figure 21 (middle left panel) gives an example. The annual sum of precipitation in the CLM-C20 simulations is higher over large parts of Europe than in the evaluation simulation. The patterns of these spatial differences are similar for all four considered paired comparisons (in Table 5). For Germany, 127 to 178 mm more precipitation is simulated in the CLM-C20 runs over the whole year. Figure 22 (middle left panel) shows the annual cycle. The precipitation is higher during nearly all months in the CLM-C20 runs. Exceptions occur primarily in spring and early summer. Thus, the error of the model with regard to the observation data used here has become larger in the 20th century simulations. This effect already occurs in the forcing data. The global EC-C20 runs (the forcing data of CLM-C20) produce more than 200 mm more precipitation in Central Europe than the ERA40 data (the forcing data of CLM050). The CLM-C20 simulations show an internal variability of the annual sum of about 50 mm. So, they vary less than the reference data among each other or the 20th century simulation compared to the evaluation run. Both CLM-C20 runs differ only marginally (0.5 mm for the first period 1961-1980 and 2.5 mm for the second period 1981-2000), and much less than the two 20-year periods itself (for both runs about 50 mm).

COMPARISON 3 identifies the features of the regional 20th century climate caused by the global model. Figure 21 (top right panel) exemplarily shows the spatial difference between the regional and the global model run. The considerable differences close to the lateral boundaries are an effect of the coupling between both models. Because, the global model only prescribes cloud water content and water vapour content in the boundary zone, but no precipitation values are given. The precipitation must be completely developed by the CLM. This leads, in particular in case of inflow, to a precipitation deficit at the boundary. For this reason the precipitation in the "sponge"-zone is generally underestimated. The "sponge"-zone is not included in the data streams D2 and D3. In Central Europe the annual precipitation sum is 129 to 145 mm higher in the CLM than in the corresponding ECHAM5 simulation. The differences for each month are given in Figure 22 (top right panel). The deviations in winter are weak (up to 5 mm). The main differences appear in summer time (up to 33 mm per month). These differences are clearly larger than the variability of the investigated paired comparisons (indicated by the bars in Figure 22, top right panel). Therefore, the regional model generates a more realistic annual cycle of precipitation in Central Europe, with two maxima in summer and winter. In contrast the global simulation produces only one maximum in winter and a minimum in summer. This concerns all CLM-C20 runs.

COMPARISON 4 investigates the simulated climate change. Table 18 summarises the paired precipitation changes for all sub-regions. The change over an interval of 50 years shows a high variability. The intensity and the pattern of the change vary strongly for the paired comparisons, for monthly sums as well as for annual sums. For the first considered interval (2011-2030 versus 1961-1980) decrease as well as increase can occur for Central Europe. For the second interval (2031-2050 versus 1981-2000) the difference pattern (see Figure 21, bottom left panel) becomes stabilised. For this interval an increase of 42 to 82 mm is simulated for Germany. Figure 22 (bottom left panel) shows the annual cycle of the climate change signal separately for both intervals. The model tends to an increase of precipitation in spring and autumn. In summer, no reliable trend can be recognised. But for every month, paired comparisons can be found which produce either an increase or a decrease of precipitation. The ranges of the simulated changes are very large for the whole year. They vary between -26 to 82 mm per year. On the other hand the uncertainty of the model is of the same order of magnitude or even larger (COMPARISON 1: 12 to 96 mm and COMPARISON 2: 127 to 178 mm). In this case no stable and reliable precipitation signal on time scales of 20-year averages over 50-year intervals can be detected for Germany until the middle of this century and for the A1B scenario.

COMPARISON 5 investigates the deviation of the regional climate change signal from the global one. Figure 21 (bottom right panel) gives an example. Clear spatial patterns are not to be recognised. The

differences amount from -6 to 22 mm for Central Europe. Hence, it is smaller than the change itself (in the regional model: -31 to 69 mm; in the global model: -35 to 60 mm). The consideration of the monthly sums in Figure 22 (bottom right panel) indicates a slight tendency towards a more positive (or less negative) trend in the regional model. However, the uncertainties are very large. The stable spatial structure of the precipitation change for the second interval is present in the global model, too.

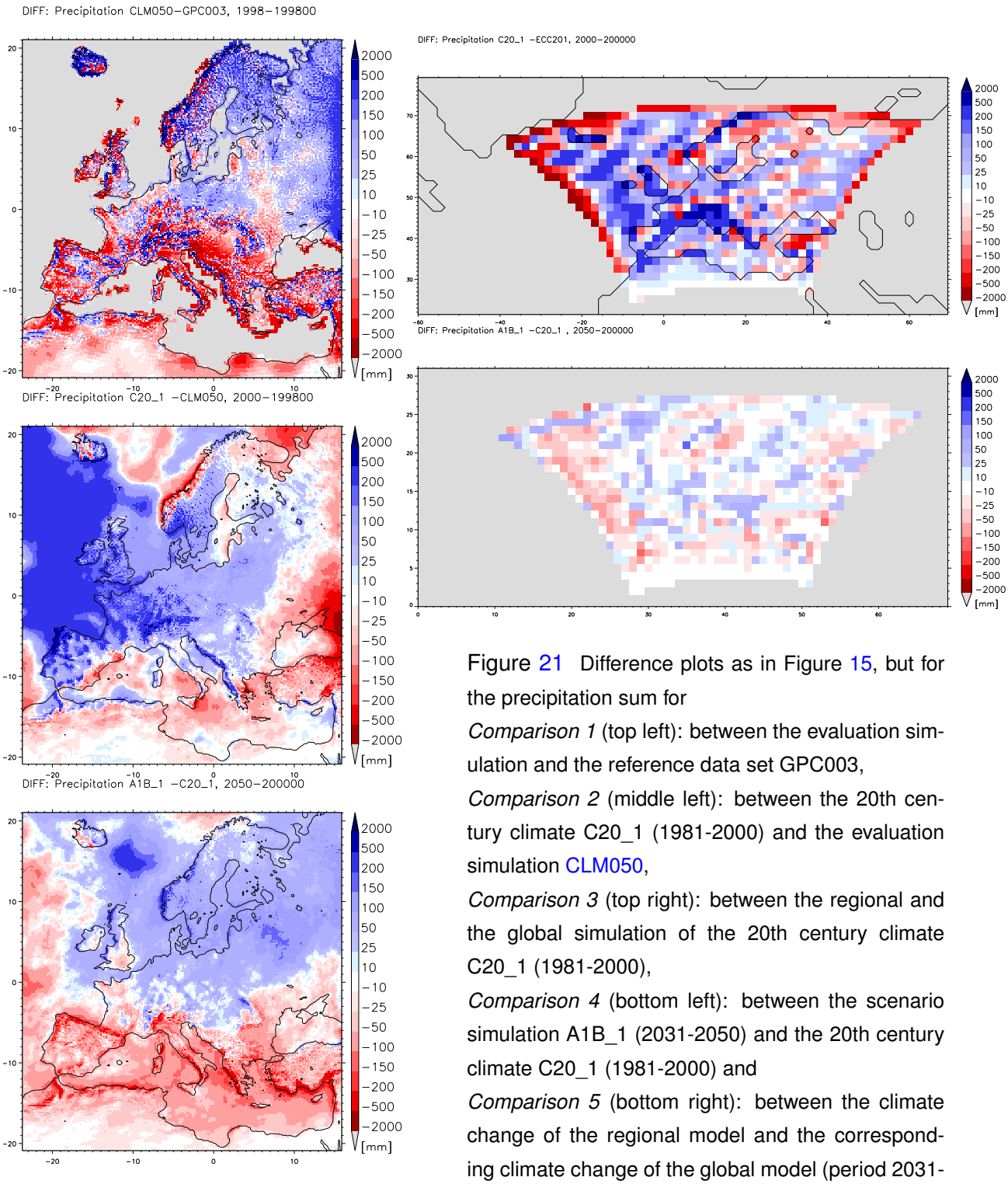

Figure 21 Difference plots as in Figure 15, but for the precipitation sum for

Comparison 1 (top left): between the evaluation simulation and the reference data set GPC003,

Comparison 2 (middle left): between the 20th century climate C20_1 (1981-2000) and the evaluation simulation CLM050,

Comparison 3 (top right): between the regional and the global simulation of the 20th century climate C20_1 (1981-2000),

Comparison 4 (bottom left): between the scenario simulation A1B_1 (2031-2050) and the 20th century climate C20_1 (1981-2000) and

Comparison 5 (bottom right): between the climate change of the regional model and the corresponding climate change of the global model (period 2031-2050 versus period 1981-2000).

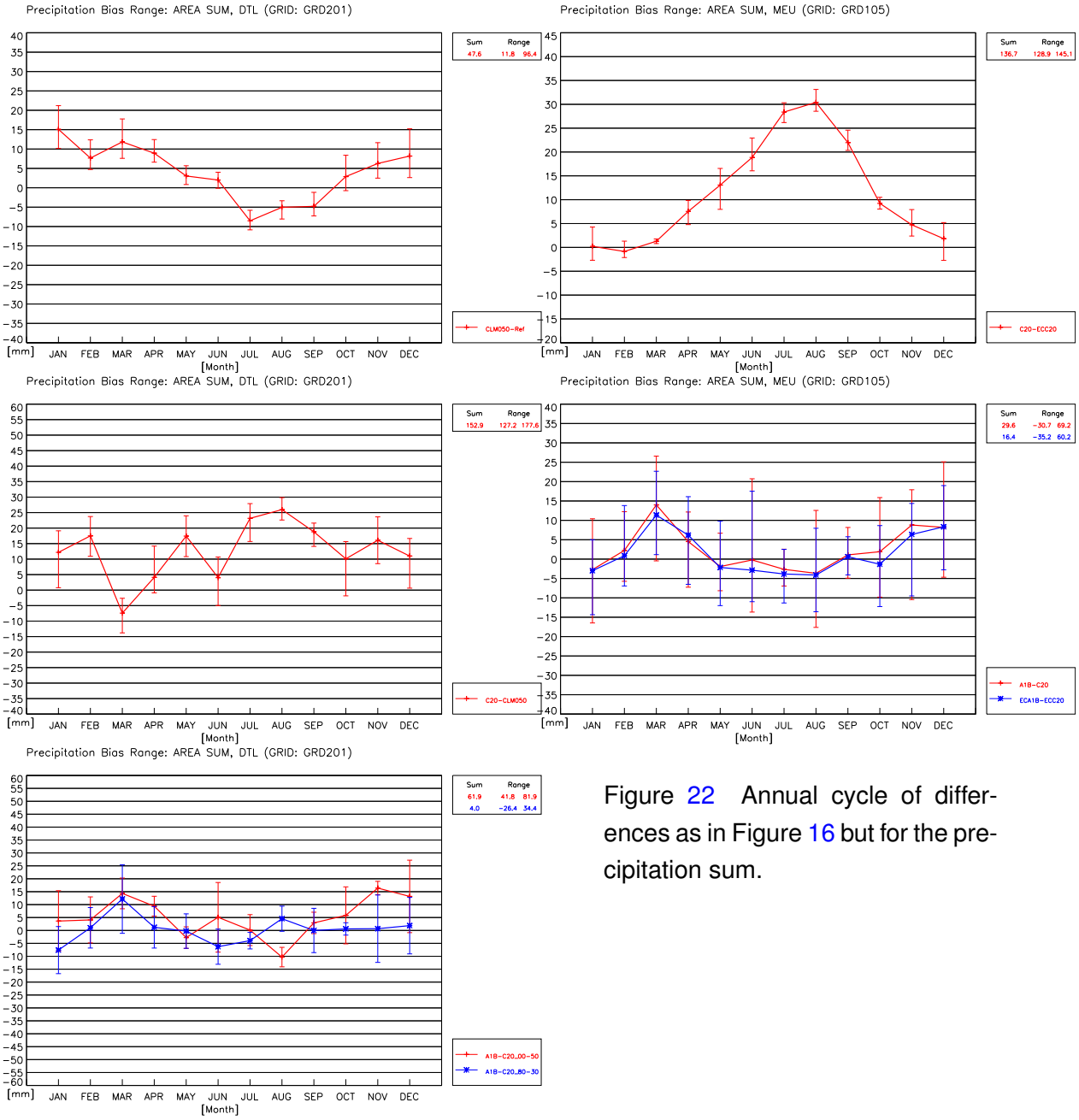

Figure 22 Annual cycle of differences as in Figure 16 but for the precipitation sum.

Table 18 Bias table for the climate change (*Comparison 4*) as in Table 15, but for the precipitation sum.

	Year		January		April		July		October	
Region	min.	max.	min.	max.	min.	max.	min.	max.	min.	max.
NEU	20	73	-4	12	0	6	-5	5	6	15
NEL	15	67	-3	11	2	7	-7	4	4	14
NEW	15	96	-6	14	-3	5	-5	6	8	17
SEU	-70	-5	-20	3	-9	5	-2	0	-15	-3
SEL	-73	-9	-19	3	-11	7	-3	0	-15	-1
SEW	-67	-1	-22	2	-6	4	-1	0	-16	-5
SCA	32	92	-3	19	-5	7	-9	15	6	13
NWE	-30	94	-19	9	-5	4	-16	0	4	23
MEU	-28	71	-16	11	-7	11	-6	3	-9	16
SWE	-111	2	-43	10	-16	17	-4	4	-30	9
EEU	6	61	-2	10	5	9	-6	0	-2	12
SUE	-105	22	-23	6	-15	16	-8	4	-22	6
NEE	26	95	3	15	-5	9	-7	12	6	18
RUS	9	64	1	9	3	11	-14	0	-1	16
VAS	-72	-10	-14	2	-9	0	-5	0	-11	1
NAF	-42	-14	-8	0	-6	-1	0	0	-8	-1
MED	-78	1	-23	1	-6	3	-1	0	-18	-5
OSS	14	93	-4	12	-1	12	-5	8	2	22
NOS	-4	90	-15	13	-6	7	-13	3	6	23
SWM	-24	1	0	8	-2	4	-6	2	-15	9
NOA	34	124	-3	24	-10	8	0	10	5	29
BIS	-21	74	-14	11	-2	6	-10	1	-17	23
DTL	-26	82	-17	15	-7	13	-7	6	-5	17
SLW	-31	115	-23	20	-3	16	-18	0	0	25
ESS	-44	126	-20	21	-11	17	-19	12	-5	22
LIN	-45	76	-18	20	-5	15	-14	5	-6	12
MEI	-18	105	-17	15	-8	16	-18	13	-6	15
STU	-24	80	-6	6	-8	17	-8	18	-12	18
MUN	-30	58	-21	6	-14	22	-14	16	-18	16
SAX	-48	94	-24	24	-12	16	-11	17	-16	12
ALP	-65	51	-19	-2	-15	37	-19	2	-42	12
POE	-167	27	-15	14	-31	50	-6	1	-55	15
UNG	-43	28	-8	0	-10	13	-13	6	-15	5
NSK	22	139	-2	45	-21	9	-6	23	3	35
SSK	20	79	-4	11	-2	8	-10	14	1	11

6.5 Wind speed at 10m height

The wind speed 10 m above ground is the scalar wind speed 10 m above the model ground.

Detailed descriptions of the comparisons discussed below can be found in sections 4.1 and in section 6.1. The reference data sets used are described in Table 10.

In COMPARISON 1 the evaluation simulation is compared with different reference data sets. Figure 23 (top left panel) shows the deviation of the simulation from the MARS01 data set for the 20 year annual average wind speed 10 m above ground. It exhibits regional and large scale positive biases with a peak of up to +2 m/s in Eastern Europe and regional scale negative biases of up to -1.5 m/s at the west coast of Scandinavia, in France, parts of the Iberian Peninsula and parts of North Africa. These patterns can also be found in the comparisons of the 20 year monthly averages (not shown here). The high deviations along the coast lines are caused by different resolutions of the data sets and different classification of coastal areas as land or sea.
Since the MARS01 data are the only reference data based on observations which cover most of the model domain, it could not be determined whether these bias patterns, especially constant positive biases over Eastern Europe, originate from the MARS01 data or from CLM. The MARS data set, which is used for model evaluation on climatological time scales for the first time, was created for agricultural seasonal prediction. Only few observations in mountainous regions are taken into account. The only other reference data set available is provided by DWD and covers the region of Germany only. Both data sets show a positive bias for the 10 year annual average and all 10 year monthly averages for Germany (Figure 24, top left panel).

COMPARISON 2 presents the influence of the forcing data (the results of the global model simulations) on the regional simulation. As shown in Figure 23 (middle left panel) there are only minor differences between both models. For most land sites the differences are below ± 0.5 m/s. Over sea some regions exhibit deviations of up to ± 1.0 m/s. The same is true for the two 20th century runs (C20_1 and C20_2) and time periods (1961-1980 and 1981-2000) investigated (not shown here). For Germany the 20 yr monthly average deviations vary from about -0.5 to +0.5 m/s (Figure 24, middle left panel) and show even smaller differences between the two 20th century runs and time periods.

COMPARISON 3 investigates the differences between the regional and the corresponding global simulation. Patterns of positive bias occur mostly over land sites of the global model and negative bias is found over water sites near the coast lines (Figure 23, top right panel). The higher wind speeds in the regional model occur in regions influenced by orography. This can be explained by the lower resolution of the global model and its flatter orography. The most striking smaller wind speeds of

the regional model occur over the region of Italy. This is also an effect of the lower resolution of the global model. It labels the region of Italy as sea and not as land. The same patterns as in Figure 23 (top right panel) can be found in all annual average differences (both runs and both time periods). Similar patterns are visible in the monthly average differences (not shown here). The monthly deviations for Central Europe (Figure 24, top right panel) show a positive bias, which varies between +0.2 and +0.6 m/s. It is significant for all months, since the variability of the difference (2 simulations and 2 periods) is much smaller than the deviation.

The mean wind speed 10 m above ground exhibits a strong land-sea contrast for the evaluation simulation and for the 20th century simulations. The absolute values are much higher over sea than over land (see Figure 33, bottom panel). However, there are no climatological observations of the wind speed at 10 m over sea. In section 6.13 the results are compared with the mean wind speed at higher altitudes.

COMPARISON 4 investigates the simulated climate change of the regional model. For the wind speed 10 m above ground the 50 yr climate change signal of 20 yr annual averages is below ± 0.5 m/s for all regions (Figure 23, bottom left panel). The corresponding monthly average climate change signal for the area of Germany is small (± 0.2 m/s) for the change between 1961-1980 and 2011-2030. The climate change signal is higher for the comparison of the periods 1981-2000 and 2031-2050 (-0.2 to +0.7 m/s). The variability of the 20 yr averages is significantly higher in the winter months (Figure 24, bottom left panel). For most of the months, the climate change signal is smaller than the variability of the climate change signals for the different pair comparisons. Thus, the climate change signal is not significant. The other regions exhibit similar behaviour (see Table 19 for details).

COMPARISON 5 investigates the consistency of and the differences between the climate change signals of the regional and of the global model. The differences between the climate change signals of the regional and of the global model have regional scales and are below ± 0.2 m/s for 20 yr annual average differences (Figure 23, bottom right panel). Figure 24 shows the annual cycle of the average climate change signals of the regional (red curve) and of the global (blue curve) model and their variabilities for the region of Central Europe (MEU). For MEU the differences between the climate change signals investigated are smaller than 0.1 m/s for all months. No significant differences have been identified between the climate change signals at the scale of the global model resolution for all 20 yr monthly averages and regions considered.

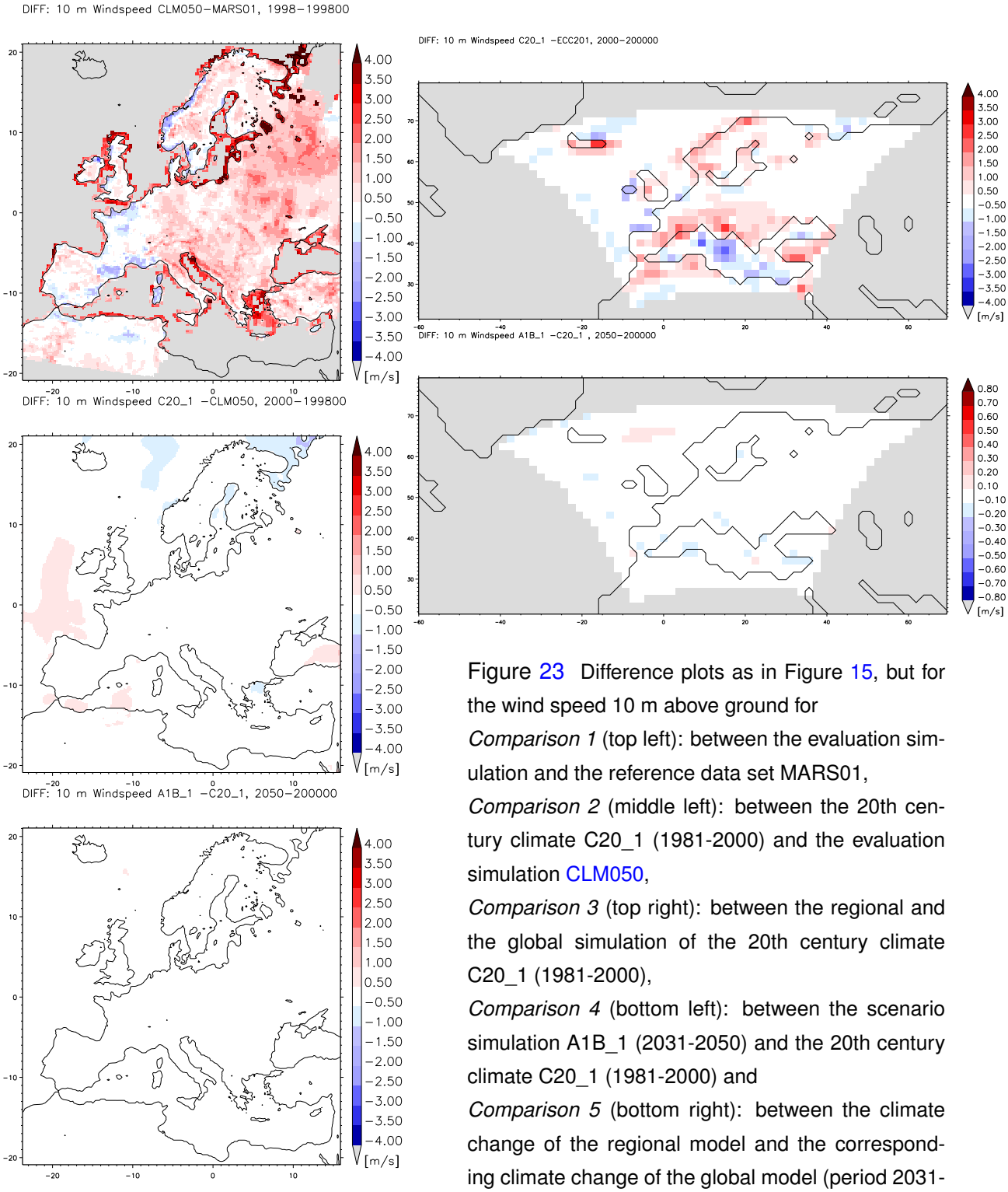

Figure 23 Difference plots as in Figure 15, but for the wind speed 10 m above ground for

Comparison 1 (top left): between the evaluation simulation and the reference data set MARS01,

Comparison 2 (middle left): between the 20th century climate C20_1 (1981-2000) and the evaluation simulation CLM050,

Comparison 3 (top right): between the regional and the global simulation of the 20th century climate C20_1 (1981-2000),

Comparison 4 (bottom left): between the scenario simulation A1B_1 (2031-2050) and the 20th century climate C20_1 (1981-2000) and

Comparison 5 (bottom right): between the climate change of the regional model and the corresponding climate change of the global model (period 2031-2050 versus period 1981-2000).

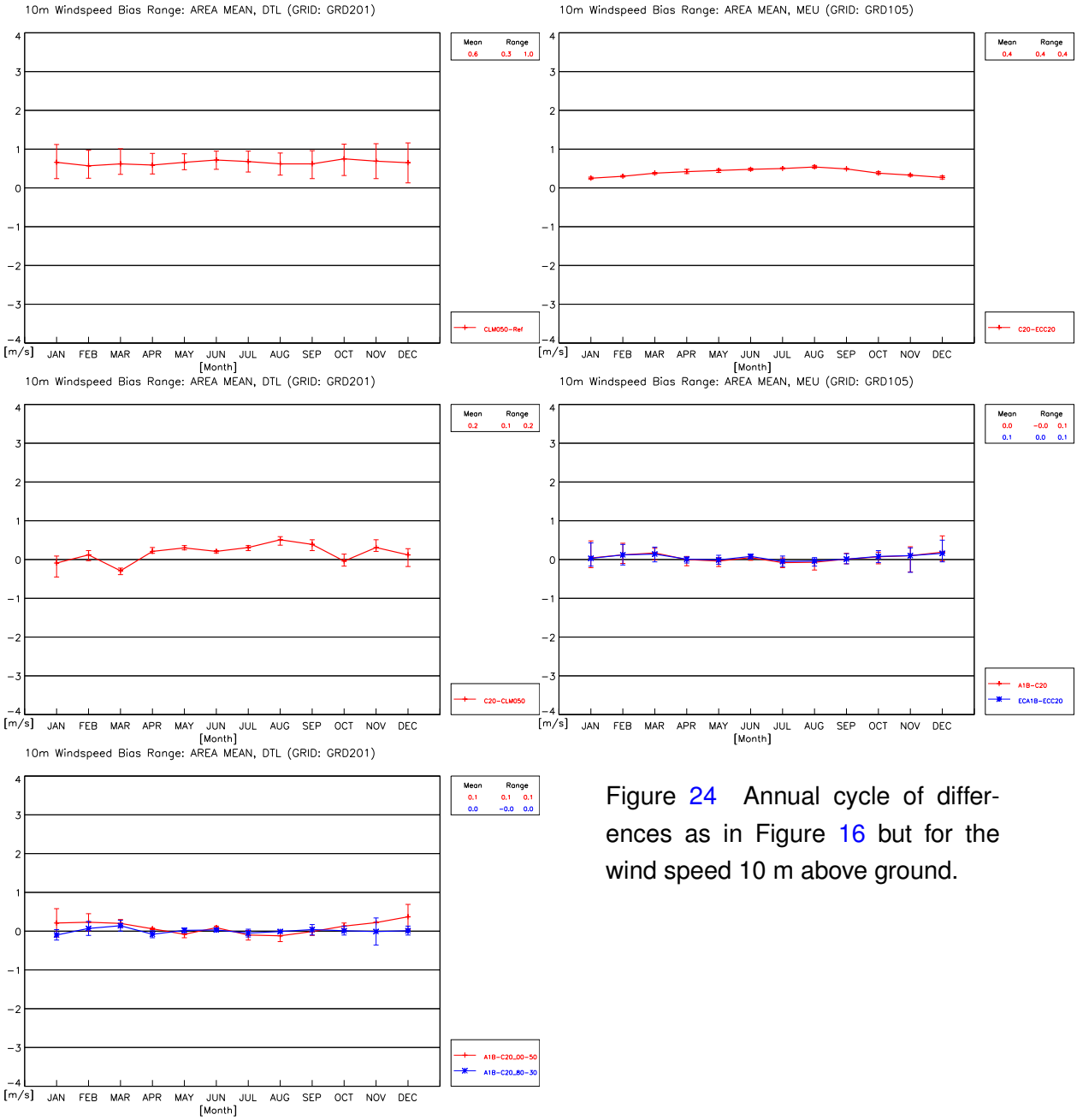

Figure 24 Annual cycle of differences as in Figure 16 but for the wind speed 10 m above ground.

Table 19 Bias table for the climate change (*Comparison 4*) as in Table 15, but for the wind speed 10 m above ground.

	Year		January		April		July		October	
Region	min.	max.	min.	max.	min.	max.	min.	max.	min.	max.
NEU	0.0	0.1	0.0	0.4	-0.2	0.0	-0.1	0.1	0.1	0.3
NEL	0.0	0.1	0.0	0.3	-0.1	0.1	-0.1	0.1	0.0	0.1
NEW	0.0	0.1	-0.1	0.4	-0.4	-0.1	-0.2	0.2	0.1	0.5
SEU	-0.1	0.0	-0.5	0.1	-0.1	0.1	0.0	0.1	-0.1	0.0
SEL	-0.1	0.0	-0.3	0.0	-0.1	0.1	0.0	0.0	-0.1	0.0
SEW	-0.1	0.0	-0.8	0.2	-0.2	0.2	-0.1	0.1	-0.2	0.0
SCA	0.0	0.0	0.0	0.2	-0.2	0.0	-0.1	0.1	0.0	0.2
NWE	0.0	0.1	-0.2	0.4	-0.2	-0.1	-0.2	0.0	0.0	0.3
MEU	0.0	0.1	-0.2	0.5	-0.2	0.1	-0.2	0.0	-0.1	0.2
SWE	-0.1	0.0	-0.6	0.1	-0.2	0.2	-0.1	0.1	-0.3	0.1
EEU	0.0	0.1	-0.1	0.4	0.0	0.2	-0.2	0.1	-0.1	0.2
SUE	-0.1	0.0	-0.1	0.0	-0.1	0.1	0.0	0.1	-0.1	0.0
NEE	0.0	0.0	0.0	0.3	-0.1	0.1	0.0	0.1	-0.1	0.3
RUS	0.0	0.1	0.2	0.4	0.0	0.1	-0.1	0.1	0.1	0.2
VAS	0.0	0.0	-0.1	0.1	-0.1	0.1	0.0	0.0	0.0	0.1
NAF	-0.1	0.0	-0.4	0.0	-0.1	0.0	0.0	0.1	-0.1	0.0
MED	-0.1	0.0	-0.8	0.2	-0.3	0.2	-0.1	0.1	-0.2	0.0
OSS	0.1	0.2	0.0	0.6	0.0	0.3	-0.3	0.3	0.1	0.6
NOS	0.0	0.1	-0.5	0.9	-0.4	0.0	-0.6	0.3	0.1	0.6
SWM	-0.1	0.1	0.0	0.2	-0.2	0.2	0.0	0.3	-0.2	0.2
NOA	-0.1	0.1	-0.2	0.5	-0.7	0.0	-0.3	0.2	0.0	0.8
BIS	-0.1	0.1	-0.3	0.2	-0.4	0.0	-0.3	0.0	-0.2	0.3
DTL	0.0	0.1	-0.2	0.6	-0.2	0.1	-0.2	0.1	-0.1	0.2
SLW	0.0	0.1	-0.2	0.7	-0.2	0.1	-0.4	0.3	-0.2	0.4
ESS	0.0	0.1	-0.2	0.6	-0.2	0.1	-0.2	0.1	0.0	0.2
LIN	0.0	0.1	-0.2	0.6	-0.1	0.2	-0.3	0.1	-0.2	0.3
MEI	0.0	0.1	-0.2	0.6	-0.2	0.1	-0.2	0.0	-0.1	0.1
STU	0.0	0.1	-0.2	0.4	-0.2	0.1	-0.1	0.0	0.0	0.1
MUN	-0.1	0.1	-0.3	0.6	-0.2	0.1	-0.1	0.0	-0.1	0.1
SAX	0.0	0.1	-0.3	0.8	-0.2	0.2	-0.3	0.1	-0.2	0.2
ALP	0.0	0.0	-0.2	0.1	-0.1	0.1	-0.2	0.0	-0.1	0.0
POE	-0.1	0.0	-0.1	0.0	-0.1	0.1	-0.1	0.1	-0.3	0.1
UNG	0.0	0.0	-0.1	0.2	-0.2	0.1	0.0	0.1	-0.2	0.0
NSK	0.0	0.1	-0.1	0.2	-0.4	0.0	0.0	0.1	-0.1	0.3
SSK	0.0	0.0	0.0	0.2	-0.2	0.1	-0.1	0.1	0.0	0.2

6.6 Mean sea level pressure

The mean sea level pressure is the pressure extrapolated to the altitude of the sea level.

Detailed descriptions of the comparisons discussed below can be found in sections 4.1 and in section 6.1. The reference data sets are described in Table 10.

In COMPARISON 1 the evaluation simulation is compared with different reference data sets. The only reference data set available for the whole model domain is ERA040. For Germany also DWD001 data are used. Figure 25 (top left panel) shows the deviation from ERA040. The 20 year annual average difference exhibits a positive bias between +1 and +5 hPa for most of the regions. The "wave" structure in Figure 25 (top left panel) is caused by different resolutions of the CLM050 and ERA040 data sets. Figure 26 (top left panel) also shows a general positive bias for Germany for the monthly averages (except in June, where it is nearly 0). It has two peaks, in February with nearly +2 hPa and October with about +2.5 hPa. The deviations of the monthly averages are significant, because the differences between the reference data are small in comparison with the deviation CLM050-ERA040. The pressure deviations are uncorrelated in time with the deviations of the 2 m temperature from ERA40 2 m temperature in time. Furthermore, the positive mean pressure deviation is inconsistent with the cold bias of the 2 m temperature. It should be noted, that the mean sea level pressure and the 2 m temperature are diagnostic variables. The consistency of the deviations has to be investigated using the dynamical variables temperature and pressure on model levels, which has not been done yet.

COMPARISON 2 presents the influence of the forcing data (the results of the global model simulations) on the regional simulation. All comparisons show a negative deviation over north-west Europe with a maximum of up to -5 hPa north-west of the British Islands and a slight positive deviation of up to +2 hPa over Northern Scandinavia for the annual average (Figure 25, middle left panel). In January (not shown here) the region with negative deviation is located over the British Isles with up to -8 hPa and a region of positive deviation over Northern Scandinavia with up to + 9 hPa. In July (not shown here) there is a negative deviation of up to -5 hPa all over Northern Europe. The monthly deviation for the region of Germany (Figure 26, middle left panel) shows significant negative deviations in January and February of -4 to -7 hPa and deviations between +2 and -4 hPa for the rest of the year.
Localised differences in the mean sea level pressure higher than 1 hPa are associated with differences in the wind field of 0.5 m/s and more between 300 to 500 hPa. However, the effect on the wind speed near the ground is more than one order of magnitude weaker. Therefore, the differences between the 10m-wind speeds are small and significant.

COMPARISON 3 investigates the differences between the regional and the corresponding global simulation. The differences between the 20 yr annual averages of the models (Figure 25, top right panel) are much weaker than the results of COMPARISON 2. Only in January (not shown here) there is a positive bias of +1 to +3 hPa over south Eastern Europe which is uncorrelated with the differences between the regional model runs. The monthly averages (Figure 26, top right panel) in Central Europe (region MEU) show a slight positive bias of 0 to +1 hPa. The small differences between the regional and global simulation indicate that the substantial part of the strong deviations shown in COMPARISON 2 are caused by the global model.

COMPARISON 4 investigates the simulated climate change. There is a change of the annual average over Northern Europe of up to -2 hPa between 1981-2000 and 2031-2050 (Figure 25, bottom left panel). The monthly averages (not shown here) show different deviation patterns for different model runs and time periods with higher deviations in winter and for the climate change between 1981-2000 and 2031-2050. This variability is shown for Germany (DTL) in Figure 26 (bottom left panel) as vertical bars for each month in the year. Table 20 summarises the results for each region. It exhibits strong negative deviations of up to -4.8 hPa over Northern Europe (regions NOA, SCA and NEE) and strong positive deviations over Southern Europe (regions SWE and SUE) with a maximum over the Alpine region (regions STU, MUN, ALP, POE and UNG) with up to +6.1 hPa. This indicates a change in the general circulation with lower pressure over Northern Europe and higher over the Alpine region in January. In October the highest negative pressure changes occur over the North Atlantic (NOA), Scandinavia (SCA) and the Baltic Sea (OSS) with up to -4.0 hPa and the highest positive over Southeast Europe (SWE) and the Alps (ALP) with up to +3.0 hPa.

COMPARISON 5 investigates the consistency of and the differences between the climate change signals in the regional and the global model. Figure 25 (bottom right panel) shows deviations between both climate change signals of less than ± 0.2 hPa, but over the alpine region, where the difference reaches +0.4 hPa. Please note that the scale is only 1/5th of that of the panel above. In Figure 26 the annual cycles of the monthly average climate change signals of the regional model (red curve) and of the global model (blue curve) are compared. The differences between the curves are negligible compared to their variabilities (derived from different model runs and time periods). This indicates that on the spatial scale of the MEU region the mean sea level pressure climate change signals of the regional and of the global model (COMPARISON 4) are consistent.

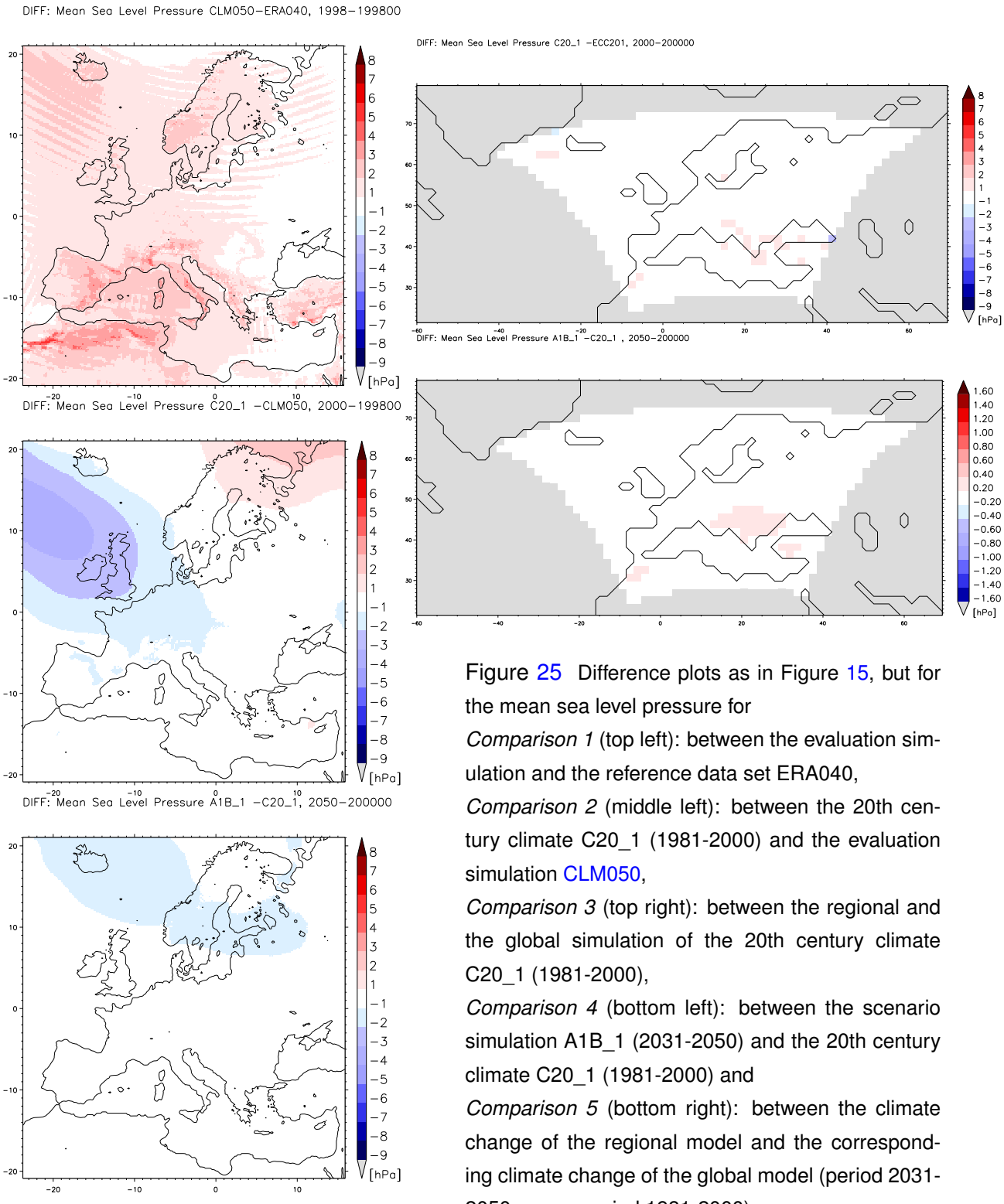

Figure 25 Difference plots as in Figure 15, but for the mean sea level pressure for

Comparison 1 (top left): between the evaluation simulation and the reference data set ERA040,

Comparison 2 (middle left): between the 20th century climate C20_1 (1981-2000) and the evaluation simulation CLM050,

Comparison 3 (top right): between the regional and the global simulation of the 20th century climate C20_1 (1981-2000),

Comparison 4 (bottom left): between the scenario simulation A1B_1 (2031-2050) and the 20th century climate C20_1 (1981-2000) and

Comparison 5 (bottom right): between the climate change of the regional model and the corresponding climate change of the global model (period 2031-2050 versus period 1981-2000).

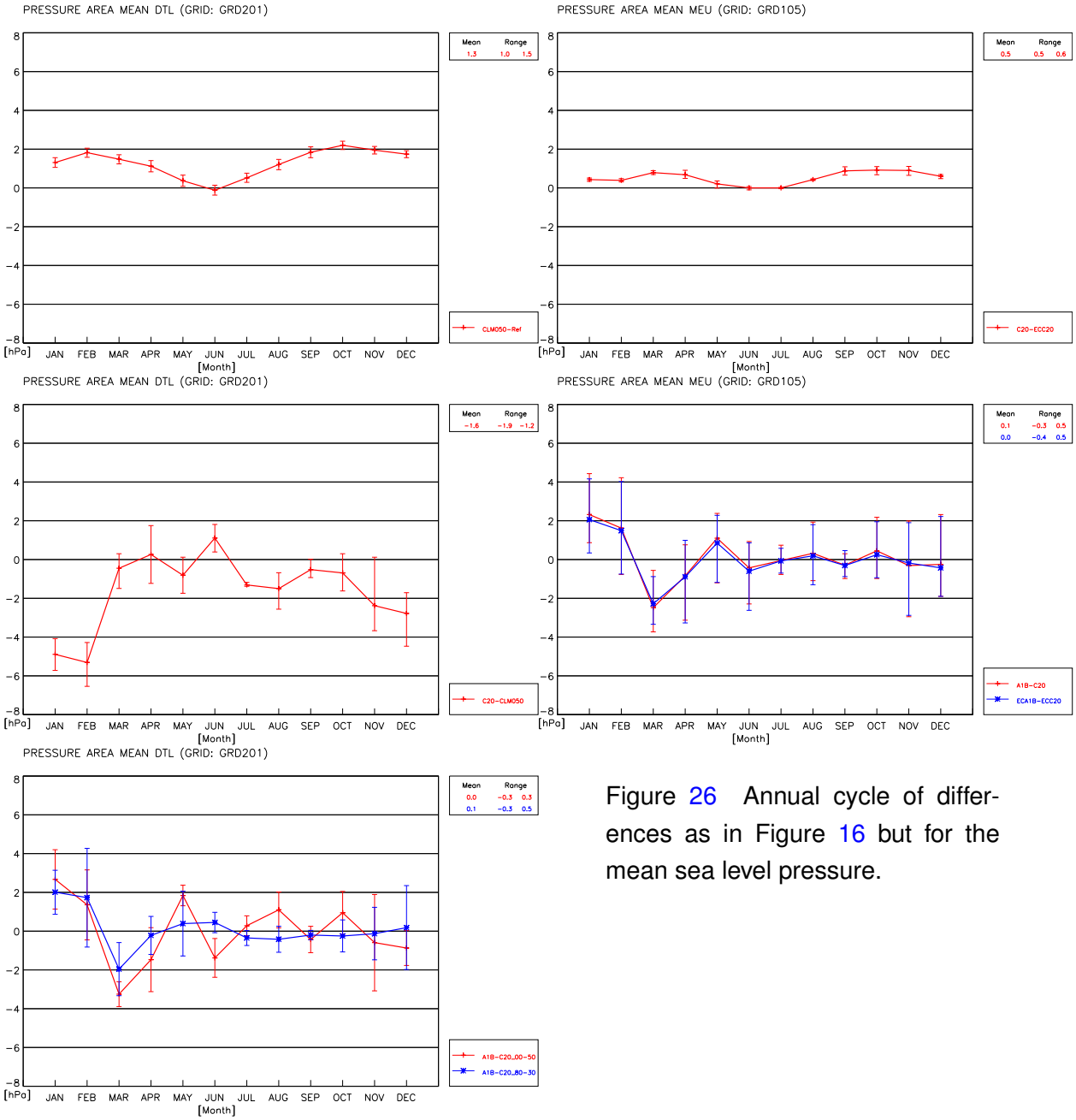

Figure 26 Annual cycle of differences as in Figure 16 but for the mean sea level pressure.

Table 20 Bias table for the climate change (*Comparison 4*) as in Table 15, but for the mean sea level pressure.

	Year		January		April		July		October	
Region	min.	max.	min.	max.	min.	max.	min.	max.	min.	max.
NEU	-1.0	-0.1	-1.5	1.4	-1.4	0.7	-0.8	1.5	-2.2	0.0
NEL	-0.9	-0.1	-0.9	1.4	-1.6	0.4	-0.5	1.2	-2.0	0.2
NEW	-1.3	0.1	-2.5	1.9	-0.9	1.1	-1.2	2.0	-2.5	-0.3
SEU	-0.1	0.7	0.4	4.0	-1.7	0.8	-0.9	-0.1	0.0	1.5
SEL	0.0	0.7	0.4	3.8	-1.7	0.8	-0.9	-0.1	0.0	1.5
SEW	-0.1	0.7	0.3	4.1	-1.8	0.8	-1.0	-0.2	0.1	1.4
SCA	-1.5	-0.2	-3.8	1.6	-1.6	1.3	-1.7	2.4	-3.8	0.1
NWE	-0.4	0.6	-0.8	4.0	-2.4	1.0	-0.5	1.5	-1.5	2.2
MEU	-0.3	0.5	0.9	4.5	-3.2	0.8	-0.8	0.7	-1.0	2.2
SWE	0.1	0.7	-0.4	4.6	-2.2	1.2	-1.2	-0.2	-0.1	3.0
EEU	-0.6	0.0	0.2	2.5	-2.1	0.2	-0.5	0.8	-2.0	0.7
SUE	-0.3	0.9	1.0	5.4	-2.6	1.0	-0.9	0.2	-0.2	1.7
NEE	-1.5	0.1	-4.8	-0.2	-2.1	1.6	-2.0	1.6	-3.5	-0.2
RUS	-0.7	0.2	-2.0	1.7	-1.8	0.1	-0.2	0.4	-2.8	0.7
VAS	-0.1	0.5	0.3	2.5	-1.1	0.5	-1.1	0.1	-0.3	0.6
NAF	0.0	0.5	0.2	2.9	-1.1	0.8	-0.8	-0.3	0.0	1.8
MED	-0.2	0.8	0.4	4.3	-1.7	0.9	-1.0	-0.2	0.1	1.5
OSS	-1.3	0.0	-1.7	1.7	-2.3	0.9	-1.2	2.0	-3.7	0.1
NOS	-1.0	0.4	-0.1	3.4	-1.7	1.3	-1.1	2.3	-2.3	0.6
SWM	-0.1	0.6	0.2	3.1	-1.9	0.5	-1.1	0.1	-0.5	1.3
NOA	-1.7	0.0	-4.4	2.3	-0.3	2.0	-1.6	2.3	-4.0	-0.2
BIS	-0.2	0.5	-1.2	4.1	-2.2	1.2	-0.4	1.1	-1.0	2.5
DTL	-0.3	0.5	0.9	4.2	-3.1	0.8	-0.7	0.8	-1.1	2.0
SLW	-0.8	0.4	0.6	3.4	-2.6	0.8	-0.7	1.5	-1.7	1.1
ESS	-0.3	0.6	0.7	4.7	-3.2	0.9	-0.8	0.8	-1.3	2.3
LIN	-0.5	0.4	0.8	3.2	-2.9	0.5	-0.6	1.0	-1.0	1.5
MEI	-0.3	0.6	0.9	4.6	-3.2	0.9	-0.9	0.7	-1.0	2.3
STU	-0.3	0.7	0.7	5.6	-3.4	1.0	-1.1	0.4	-0.7	2.7
MUN	-0.3	0.7	0.8	5.6	-3.4	1.0	-1.1	0.5	-0.6	2.8
SAX	-0.3	0.5	0.9	3.8	-3.2	0.7	-0.8	0.9	-0.9	1.9
ALP	-0.3	0.9	0.7	5.9	-3.4	0.9	-0.9	0.6	-0.4	2.8
POE	-0.4	0.9	1.0	6.1	-3.2	1.1	-1.1	0.2	-0.4	2.5
UNG	-0.4	0.8	0.9	5.0	-3.0	0.9	-1.0	0.4	-0.5	1.8
NSK	-1.6	-0.2	-3.9	2.2	-1.2	1.5	-1.9	2.6	-3.7	0.1
SSK	-1.5	-0.2	-3.8	1.4	-1.7	1.3	-1.6	2.4	-3.9	0.1

6.7 Number of summer days

The number of summer days indicates the area averaged number of days per year with a daily maximum temperature above 25 °C.

COMPARISON 1 considers the deviation between the evaluation run and the reference data. Figure 27 (top left panel) presents the difference to the MARS05 data set. The simulated number of summer days is higher than observed over large parts of the continent. The reason is the overestimation of the daily maximum temperature in summer (see section 6.2). For Germany, the observed number of summer days per year amounts from 28 days (DWD001) to 30 days (MARS05). About 37 summer days occur nn the evaluation run.

COMPARISON 2 investigates the difference between the 20th century runs and the evaluation run. Figure 27 (middle left panel) presents exemplarily the yearly average of one comparison. The spatial patterns are similar for all paired comparisons. The differences are negligible over the Atlantic Ocean, but in this area summer days occur only very rarely. Over Central Europe the CLM-C20 runs feature a smaller number of summer days than the CLM050 run. This is caused by the lower maximum temperatures in summer time in the CLM-C20 runs (see section 6.2). For the region of Germany the difference amounts to 11 to 16 days. Thus, in contrast to the evaluation run, the number of summer days in the CLM-C20 runs is lower than in the reference data. The difference between the 20th century climates and the evaluation climate is larger than the variability between the various 20th century climates CLM-C20.

COMPARISON 3 investigates the differences between the regional and the global simulation. In central and southern parts of the model domain, where summer days frequently occur, the regional model mostly simulates more summer days than the global model (see Figure 27, top right panel). The structures are stable for all paired comparisons. In Central Europe the difference amounts about 12 and 14 days. The difference between both models is larger than the variability of the paired comparisons. In COMPARISON 2 (Figure 27, middle left panel) a deviation between the CLM-C20 runs and the CLM050 run is conspicuous over the Mediterranean. As COMPARISON 3 shows no systematic deviations between the regional and the global simulation in this area, the deviation between the two regional simulations in COMPARISON 2 must be caused by the different forcing data.

COMPARISON 4 investigates the simulated climate change. Table 21 gives an overview for all subregions. Figure 27 (bottom left panel) shows an example for the second interval (2031-2050 versus 1981-2000). The patterns are similar for all paired comparisons. The number of summer days increases over large parts of Central and Southern Europe. A decrease seems possible too in parts of

north-east Europe, mainly within the first interval (2011-2030 versus 1961-1980). The increase of the number of summer days is more intensive within the second interval, consistent to the different temperature variables (see section 6.1 to 6.3). For Germany, the number of summer days increases by 2 to 8 days. Therefore, the amount of climate change (COMPARISON 4: 2.4 to 8.0 days) is smaller than the uncertainty of the model (COMPARISON 1: 6.8 to 9.6 days and COMPARISON 2: -16.5 to -11.1 days). So, the uncertainty of the simulated climate change is large.

COMPARISON 5 considers the differences of the climate change between regional and global simulation. Consistent to the lower increase of the simulated maximum temperatures in the regional simulation (section 6.2), the increase of the number of summer days is lower in CLM than in the global model (see Figure 27). In the regional simulation, the increase amounts about 2.5 to 8.1 days (Central Europe), compared to 5.5 to 12.0 days in the global one. Because the number of summer days are only considered as annual frequencies a monthly variability cannot be presented here.

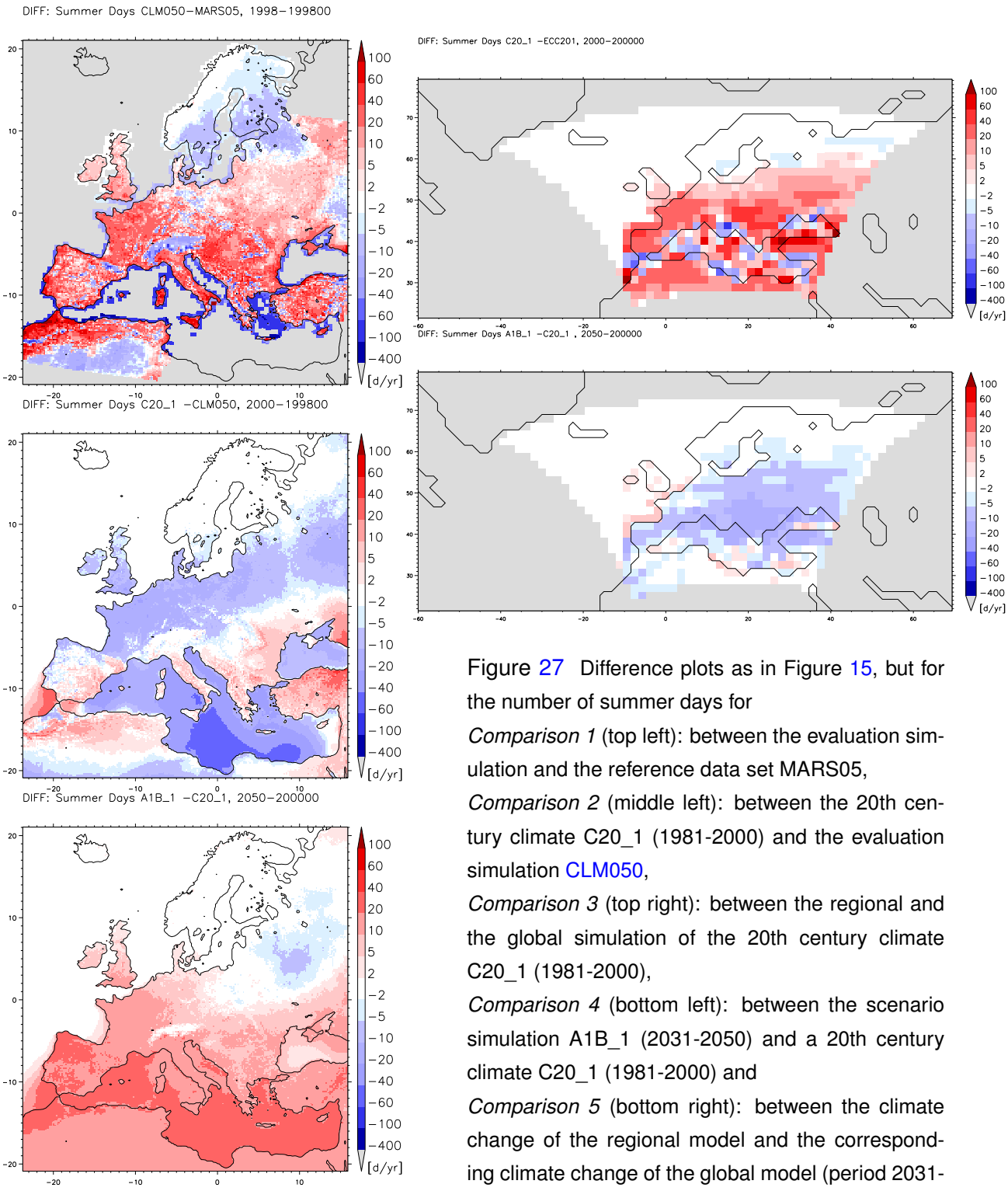

Figure 27 Difference plots as in Figure 15, but for the number of summer days for

Comparison 1 (top left): between the evaluation simulation and the reference data set MARS05,

Comparison 2 (middle left): between the 20th century climate C20_1 (1981-2000) and the evaluation simulation CLM050,

Comparison 3 (top right): between the regional and the global simulation of the 20th century climate C20_1 (1981-2000),

Comparison 4 (bottom left): between the scenario simulation A1B_1 (2031-2050) and a 20th century climate C20_1 (1981-2000) and

Comparison 5 (bottom right): between the climate change of the regional model and the corresponding climate change of the global model (period 2031-2050 versus period 1981-2000).

Table 21 Bias table for the climate change (*Comparison 4*) of the number of summer days. The smallest and the largest difference of all comparisons between the scenario runs and the 20th century climates are given for annual values. Positive deviations are highlighted in red, negative deviations in blue colour.

	Year	
Region	min.	max.
NEU	0,6	3,1
NEL	0,9	5,1
NEW	0,1	0,1
SEU	11,6	20,2
SEL	9,3	17,3
SEW	14,6	24,4
SCA	-0,1	0,6
NWE	2,0	9,7
MEU	2,7	8,4
SWE	8,4	19,1
EEU	0,4	9,1
SUE	7,5	16,7
NEE	-0,5	0,9
RUS	-0,2	10,4
VAS	8,9	15,1
NAF	8,6	18,1
MED	17,1	29,5
OSS	0,0	0,1
NOS	0,0	0,2
SWM	5,7	14,6
NOA	0,0	0,0
BIS	0,2	0,8
DTL	2,4	8,0
SLW	0,5	4,4
ESS	1,5	8,4
LIN	0,2	6,6
MEI	1,8	9,4
STU	1,8	12,9
MUN	2,3	10,8
SAX	1,4	7,5
ALP	3,7	9,6
POE	5,2	19,1
UNG	4,6	18,6
NSK	0,0	0,6
SSK	-0,1	0,6

6.8 Number of frost days

The number of frost days indicates the area averaged number of days per year with a daily minimum temperature below 0 °C.

In COMPARISON 1 the evaluation simulation is compared to reference data sets. Figure 28 (top left panel) shows the difference between the CLM050 simulation and the MARS05 data. The red coloured grid cells along the coastline demonstrate an effect of the projection between the various grids (see section 4.1.2). The model produces more frost days than observed nearly everywhere. For Germany, the CLM differs about 18 to 21 days per year to the various reference data. The reason of the overestimation is the underestimation of the minimum temperatures during the winter (see section 6.3).

COMPARISON 2 investigates the difference between the CLM-C20 runs and the evaluation run. Figure 28 (middle left panel) presents exemplarily one of the comparisons. The spatial patterns are similar for all paired comparisons. The number of frost days in the 20th century runs is lower than in the evaluation run almost everywhere over the land area. For Germany, this difference amounts about 17 to 22 days. This fact compensates the underestimation of the CLM050 run for the number of frost days (CLM050 simulates about 100 days per year compared to 79 to 82 days in the reference data). As described in section 6.3 the underestimation of the minimum temperature in winter is less in the CLM-C20 runs. The difference between the 20th century climates and the evaluation climate is larger than the variability of the various realisations of the 20th century climate.

COMPARISON 3 investigates the differences between the regional and the global simulation, where Figure 28 (top right panel) just illustrates one example of the spatial distribution. The patterns of the differences are similar for all paired comparisons considered here. Within Central Europe, the regional model provides about 1 to 4 frost days more than the global one. Thus, the deviation among both models is, compared to the differences in the comparisons 1 and 2, relatively small.

COMPARISON 4 investigates the simulated climate change. Table 22 gives an overview for all sub-regions. Figure 28 (bottom left panel) shows an example for the second interval (2031-2050 versus 1981-2000). The number of frost days decreases in all paired comparisons. The decline is stronger in the second period. The number of frost days is reduced by about 10 to 35 days for Germany. Hence, the amount of climate change (COMPARISON 4: 10 to 35 days) has a similar order of magnitude as the uncertainty of the model (COMPARISON 1: 18 to 21 days and COMPARISON 2: 17 to 22 days). The simulated climate change signal may be reliable. The regional model tends to an overestimation of frost days due the cold bias in winter, if 'perfect' boundary conditions from ECMWF ERA40 Re-

analyses are taken to drive the model (evaluation run CLM050). By using global climate simulations (ECHAM5) of the 20th century as 'non perfect' boundary conditions, this feature of the regional model is nearly compensated by a complex but probably faulty influence of the global model. This leads, in contrast to the evaluation run, to a proper reproduction of the number of frost days in the 20th century runs. So, the basis of the climate change detection seems to be correct, but just due to an coincidental superposition of two erroneous influences.

COMPARISON 5 considers the differences of the climate change between regional and global model. Figure 28 gives an example of a difference plot. In Central Europe, the regional model tends to a slightly lower decrease of the number of frost days of -9.3 to -32.7 days compared to -11.3 to -34.1 days in the global model. A monthly variability cannot be presented here, because the number of frost days is only considered as annual frequency.

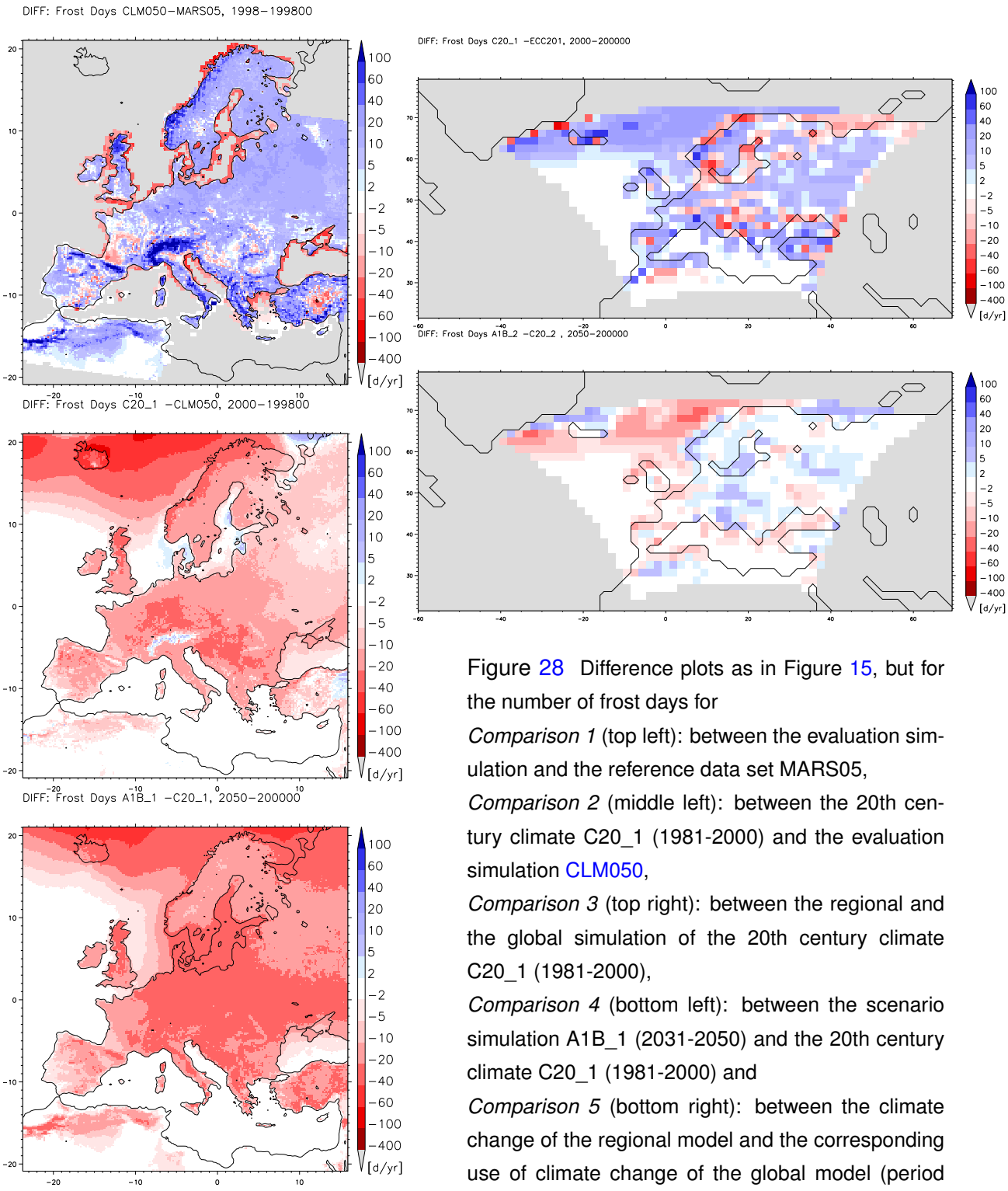

Figure 28 Difference plots as in Figure 15, but for the number of frost days for

Comparison 1 (top left): between the evaluation simulation and the reference data set MARS05,

Comparison 2 (middle left): between the 20th century climate C20_1 (1981-2000) and the evaluation simulation CLM050,

Comparison 3 (top right): between the regional and the global simulation of the 20th century climate C20_1 (1981-2000),

Comparison 4 (bottom left): between the scenario simulation A1B_1 (2031-2050) and the 20th century climate C20_1 (1981-2000) and

Comparison 5 (bottom right): between the climate change of the regional model and the corresponding use of climate change of the global model (period 2031-2050 versus period 1981-2000).

Table 22 Bias table for the climate change (*Comparison 4*) as in Table 21, but for the number of frost days.

	Year	
Region	min.	max.
NEU	-25,6	-10,4
NEL	-28,1	-10,6
NEW	-21,7	-9,3
SEU	-7,6	-2,6
SEL	-12,7	-4,5
SEW	-1,2	0,1
SCA	-24,3	-8,7
NWE	-19,8	-8,3
MEU	-32,7	-9,2
SWE	-13,0	-4,0
EEU	-34,5	-13,8
SUE	-21,3	-7,8
NEE	-22,2	-7,2
RUS	-27,7	-10,4
VAS	-16,5	-4,7
NAF	-5,1	-1,8
MED	-0,3	0,1
OSS	-39,9	-11,3
NOS	-11,1	-1,3
SWM	-8,6	-0,4
NOA	-21,4	-11,4
BIS	-1,1	0,1
DTL	-34,7	-9,6
SLW	-38,2	-8,8
ESS	-30,7	-5,9
LIN	-37,7	-9,9
MEI	-36,6	-10,9
STU	-32,8	-8,2
MUN	-33,6	-9,1
SAX	-35,8	-10,2
ALP	-30,2	-13,5
POE	-24,3	-3,2
UNG	-26,5	-8,8
NSK	-26,2	-10,5
SSK	-23,8	-8,2

6.9 Number of days with intensive precipitation

This variable indicates the area averaged number of days per year with diurnal precipitation amounts larger than 10 mm.

In COMPARISON 1 the evaluation simulation is compared to the reference data sets DWD003 and MARS05. The spatial deviations between model and observation show a very heterogeneous structure (see Figure 29, top left panel), as for the precipitation sum, too (see section 6.4). For Germany, 18.5 days with intensive precipitation are recorded in the evaluation run. So, the simulation is within the range of the reference data (MARS05: 17.3 days, DWD003: 23.0 days).

COMPARISON 2 investigates the difference between the 20th century runs and the evaluation run. The spatial pattern of deviations between CLM-C20 runs and evaluation run is similar for all considered paired comparisons (see Figure 29, middle left panel). The 20th century climates tend to a higher number of days with intensive precipitation. The CLM-C20 runs exhibit 3.8 to 5.6 more days per year for Germany than the CLM050 run. This is consistent with higher annual precipitation sums in the 20th century runs (see Section 6.4). With values between 22.3 and 24.1 days per year the CLM-C20 runs tend to slightly higher numbers than the reference data. The deviation to the evaluation run is larger than the variability of the 20th century climates among each other

COMPARISON 3 investigates the differences between the regional and the global simulation. Figure 29 (top right panel) illustrates an example for the comparison. All paired comparisons feature similar spatial structures of the deviations. In the CLM the number of days with intensive precipitation is about 3.7 to 4.4 days higher than in the corresponding global simulation for the region of Central Europe, which corresponds to the higher precipitation sum in the regional simulation than in the global one (see section 6.4). Furthermore, a higher resolution model is able to simulate more intense precipitation events. The deviation between the regional and the global model is larger than the variability of the paired comparisons between both models.

COMPARISON 4 investigates the simulated climate change. Within the first interval no steady spatial patterns for the deviations can be recognised. In the second interval the structures are stabilised with a reduction in the number of days with intensive precipitation in Southern Europe and an increase in Central and Northern Europe (Figure 29, bottom left panel). For Germany the climate change signal ranges from -0.9 to 3.2 days per year. Thus, the number of days with intensive precipitation tends to increase. The amount of climate change (COMPARISON 4: -0.9 to 3.2 days) is somewhat smaller than the uncertainty of the model (COMPARISON 1: -4.5 to 1.2 days, COMPARISON 2: 3.8 to 5.6 days). The climate change signal for the days with intensive precipitation is therefore only hardly reliable on

time scales of 20-year averages over 50-year intervals for Germany until the middle of this century and for the A1B scenario. Table 23 gives an overview over the climate change for all sub-regions.

COMPARISON 5 considers the differences of the climate change between the regional and global model. The differences between both models for the climate change show no clear spatial pattern. Figure 29 presents an example. For Central Europe, the regional climate change signal (-1.0 to 2.7 days per year) differs only slightly from the global one (-0.1 to 2.8 days per year). Hence, the deviation of the climate change signal between both models is only small, while the difference of the simulated absolute values between the models is larger (COMPARISON 3: 3.7 to 4.4 days).

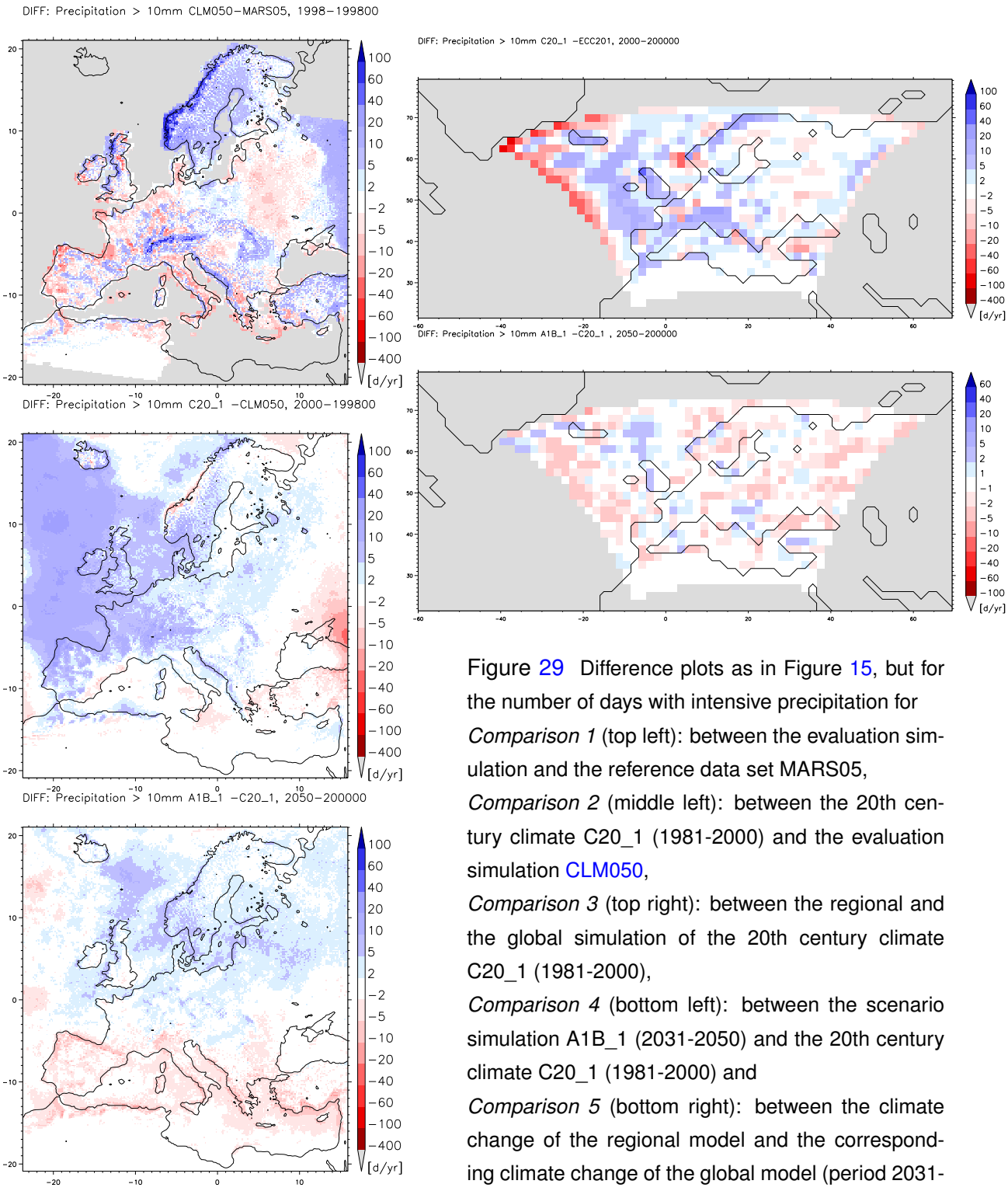

Figure 29 Difference plots as in Figure 15, but for the number of days with intensive precipitation for *Comparison 1* (top left): between the evaluation simulation and the reference data set MARS05,
Comparison 2 (middle left): between the 20th century climate C20_1 (1981-2000) and the evaluation simulation CLM050,
Comparison 3 (top right): between the regional and the global simulation of the 20th century climate C20_1 (1981-2000),
Comparison 4 (bottom left): between the scenario simulation A1B_1 (2031-2050) and the 20th century climate C20_1 (1981-2000) and
Comparison 5 (bottom right): between the climate change of the regional model and the corresponding climate change of the global model (period 2031-2050 versus period 1981-2000).

Table 23 Bias table for the climate change (*Comparison 4*) as in Table 21, but for the number of days with intensive precipitation (> 10 mm/day).

	YEAR	
Region	min.	max.
NEU	0,8	2,9
NEL	0,7	2,4
NEW	0,9	4,1
SEU	-1,9	-0,1
SEL	-2,0	-0,2
SEW	-1,9	0,0
SCA	1,4	3,7
NWE	-0,9	3,7
MEU	-0,9	2,7
SWE	-3,4	0,2
EEU	0,4	2,0
SUE	-2,9	0,7
NEE	0,6	3,2
RUS	0,8	2,2
VAS	-1,8	-0,1
NAF	-1,0	-0,4
MED	-2,2	0,0
OSS	0,9	4,0
NOS	0,4	3,7
SWM	-0,4	0,4
NOA	1,7	5,3
BIS	-0,3	3,5
DTL	-0,9	3,2
SLW	-0,9	4,1
ESS	-1,8	5,0
LIN	-1,5	2,9
MEI	-0,6	4,9
STU	-0,7	3,9
MUN	-1,2	2,6
SAX	-1,8	3,5
ALP	-1,9	1,6
POE	-5,3	0,7
UNG	-0,7	1,5
NSK	1,1	5,4
SSK	0,8	3,2

6.10 Frequency distribution of daily precipitation

The frequency distribution of daily precipitation indicates the area averaged number of days per year with more precipitation amount than specified thresholds.

In COMPARISON 1 the evaluation simulation is compared to reference data sets. Figure 30 (top left panel) presents the comparison for the frequency distribution of daily precipitation for the region of Germany. Compared to the reference data, the model overestimates the total number of days with a daily precipitation of more than 3 mm (CLM050: 107.5 days per year, MARS05: 90.6 days per year). This was found primarily for the classes with low amounts of precipitation. Within the medium range, the model (e.g. exceeding 13 mm: 9.27 days) is close to the reference data (9.01 days). For the higher classes, the CLM result differs again more from the observation.

COMPARISON 2 investigates the difference between the CLM-C20 runs and the evaluation run. The CLM-C20 runs are characterised by a larger number of days with precipitation (> 3 mm). For Germany (see Figure 30, middle left panel), the 20th century climates feature about 19.2 days more than the evaluation run. The higher values in the 20th century climates affect all classes up to 20 mm. Thus, the overestimation of days with precipitation compared to the reference data is still increased by using the global climate runs to drive the model.

COMPARISON 3 investigates the differences between the regional and the corresponding global simulation. Figure 30 (top right panel) shows the frequency distribution of daily precipitation for the regional and the global simulations of the climate of the 20th Century. The differences are mainly striking in the higher classes. For example, in the CLM-C20 climates an exceeding of 20 mm occurs on 0.88 days per year, but the EC-C20 climates on only 0.08 days per year. A regional model should provide higher numbers of days with intense precipitation, because a higher resolution model is able to simulate intense precipitation events with a higher accuracy. The deviation of the regional model to the corresponding global model is stable for all paired comparisons. The CLM simulates 7.4 days per year more with precipitation > 3 mm than the global model (class > 3 mm for Central Europe: MARS05: 90.4 days, CLM050: 108.0 days, CLM-C20: 126.7 days, EC-C20: 119.3 days). So, the EC-C20 simulations for the total number of days are closer to the observations than the CLM-C20 simulations. Within the higher classes the 20th century runs overestimate the number of days more than the evaluation run (class > 18 mm for Central Europe: MARS05: 1.18 days, CLM050: 1.59 days, CLM-C20: 2.09 days, EC-C20: 0.44 days). On the other hand the global model provides too low frequencies in this range.

COMPARISON 4 investigates the simulated climate change. Figure 30 (bottom left panel) presents

the change in the frequency distribution separately for the first and the second interval. The different development of the total precipitation for the two periods has already been described in section 6.4. The number of days with precipitation increases primarily in the second period (red curve in figure 30, bottom left panel) similar to the annual precipitation sums. In the first interval (blue curve) the total number of precipitation days decreases. The numbers within the middle classes increase slightly (less than 0.5 days/year). Therefore, the climate change signal varies in time. When considering the average over both intervals, the number of days with more than 3 mm increases about 2.14 days per year. For strong precipitation, the number of days with more than 18 mm increases about 0.17 days per year. The amount of the simulated climate change (> 3 mm, COMPARISON 4: 2.14 days) is much smaller than the uncertainty of the model mainly for the lower classes (> 3 mm, COMPARISON 1: 16.9 days and COMPARISON 2: 19.2 days) and comparable for the higher classes (> 18 mm: COMPARISON 4: 0.18 days; COMPARISON 1: 0.17 days and COMPARISON 2: 0.15 days).

COMPARISON 5 investigates the differences of the climate change between regional and global model. Figure 30 gives the climate change signals of both models for Central Europe. The CLM simulates an increase in the total number of days with precipitation for each class. In the global simulation the increase in almost all classes is compensated by a decrease in the lowest class. Therefore, the total number of days with precipitation decreases slightly. Thus, the difference for the climate change signal between the models is large in the lower classes.

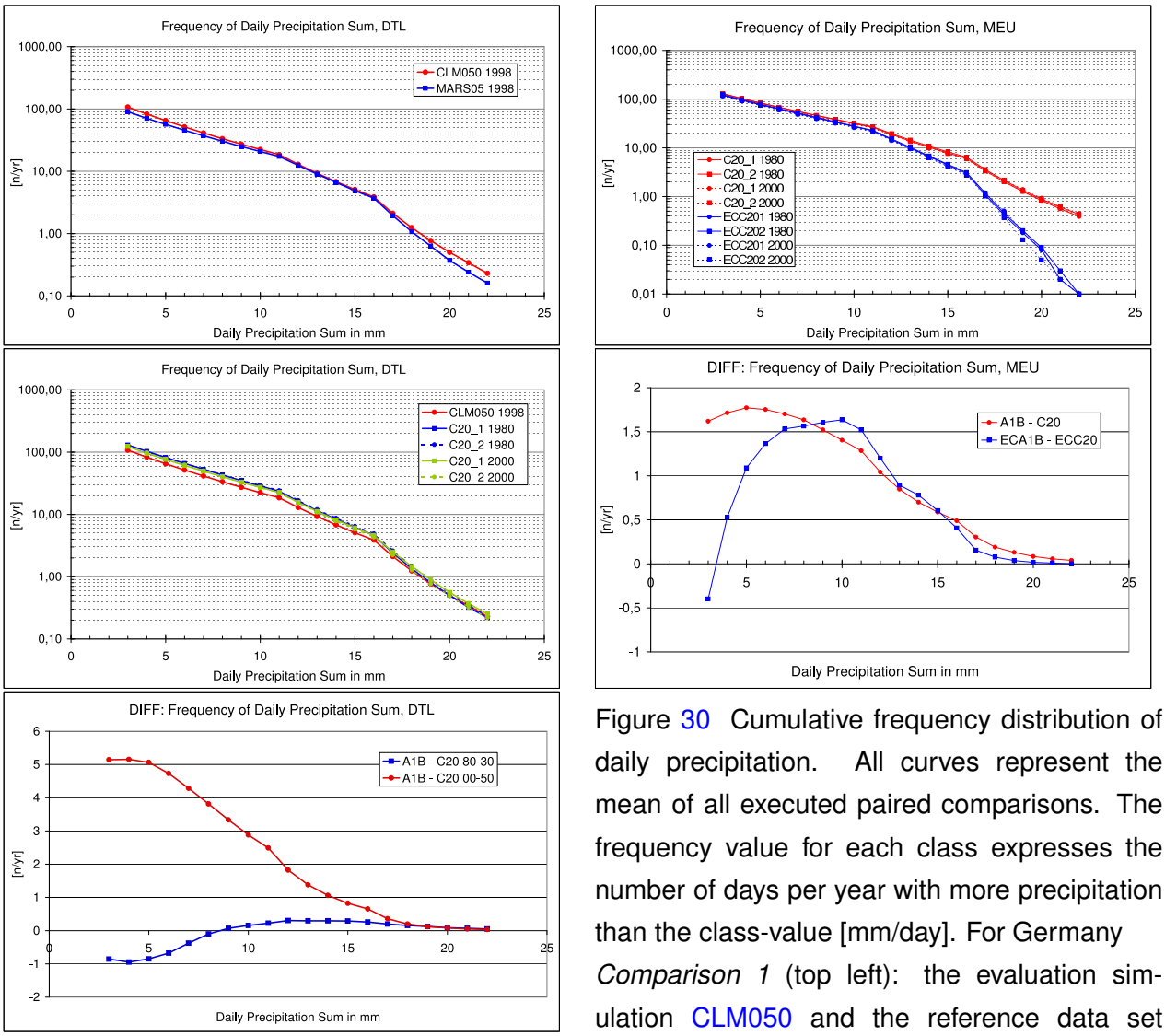

Figure 30 Cumulative frequency distribution of daily precipitation. All curves represent the mean of all executed paired comparisons. The frequency value for each class expresses the number of days per year with more precipitation than the class-value [mm/day]. For Germany *Comparison 1* (top left): the evaluation simulation CLM050 and the reference data set MARS05, *Comparison 2* (middle left): the 20th century climates CLM-C20 and the evaluation simulation , *Comparison 3* (top right): the regional and the global simulations of the 20th century climate, *Comparison 4* (bottom left): the difference between the scenario simulations and the 20th century climates averaged for the first 50-year interval (2011-2030 vs. 1961-1980: blue) and the second 50-year interval (2031-2050 vs. 1981-2000: red), *Comparison 5* (bottom right): the difference between the scenario simulations and the 20th century climates for the regional model (red) and the global model (blue) for both 50-year intervals for Central Europe.

6.11 Persistence of dry days

The persistence of dry days indicates the frequency of continuous periods without precipitation, which are as long as the specified threshold or longer.

In COMPARISON 1 the evaluation simulation is compared to the reference data sets. Figure 31 (top left panel) shows the frequency of dry periods, depending on their minimum length for Germany. The model underestimates the number of dry spells from a minimum length of 5 days. Dry periods of a minimum length of 15 days occur only 0.49 times per year in the simulation (about 5 times in 10 years) and 0.79 times/year in the reference data set MARS05 (about 8 times in 10 years). This fact is linked to the slightly higher precipitation sums in the simulation (see section 6.4) and in particular to the overestimation of the number of days with precipitation (see section 6.10).

COMPARISON 2 investigates the difference between the 20th century runs and the evaluation run. The CLM-C20 runs feature a smaller number of dry periods in all classes (see Figure 31, middle left panel). Thus, the underestimation compared to the reference data is more pronounced. Dry spells with a minimum length of 15 days only occur about 2 times in 10 years (MARS05: about 8 events, CLM050: about 5 events). The further decrease of the number of dry periods in the CLM-C20 runs is consistent to the increase of the number of precipitation days (section 6.10).

COMPARISON 3 investigates the differences between the regional and the corresponding global simulation. Figure 31 (top right panel) gives the frequencies of dry periods for the regional and the global simulations for Central Europe. Both models range similarly. The values of the regional model, averaged over all realisations, differ only slightly from those of the global model (not shown here). The CLM simulates for a minimum duration of 3 days 14.88 events per year (for 10 days: 1.12 events), the global model produces 14.58 events (1.15 events). The differences between the CLM-C20 simulations and the corresponding global simulations (absolute values for Central Europe and a minimum length of 15 days: CLM-C20: 0.218 events per year, EC-C20: 0.220 events per year) are clearly smaller than the differences between CLM-C20 runs and CLM050 run (CLM050: 0.510 events per year).

COMPARISON 4 investigates the simulated climate change. Figure 31 (bottom left) illustrates the change for both intervals for Germany. The simulation tends to a decrease in the number of dry spells with a length of 3 days and more (about 0.3 events per year). This is mainly found for the second interval. Consistently, the precipitation sum and the number of days with precipitation in this interval are higher, too (see sections 6.4 and 6.10). The simulated climate change signal (minimum length

of 3 days: COMPARISON 4: -0.3 events per year) is much smaller than the uncertainty of the model (COMPARISON 1: 4.14 events per year and COMPARISON 2: -13.05 events per year).

COMPARISON 5 considers the consitency of and the differences between the climate change signals in the regional and the global model. Figure 31 (bottom right) gives the climate change signals of both models for Central Europe. The global model produces in almost all classes an increase of the number of dry periods. In contrast, the CLM simulates for the classes with shorter duration (up to the class of 7 days) a decrease in the number and for the classes with a duration of 8 to 14 days a slight increase. So, this curve indicates a slight shift of the duration of dry periods towards larger durations. For the number of all dry spells (with a minimum length of 3 days) the CLM provides a decrease of 0.15 events per year, the ECHAM5 computes an increase of 0.79 events. Hence, the climate change signals in both models differ. The differences are small compared to the uncertainty ranges of the regional simulation, as discussed above, but larger than the absolute differences between the global and the regional model (COMPARISON 3).

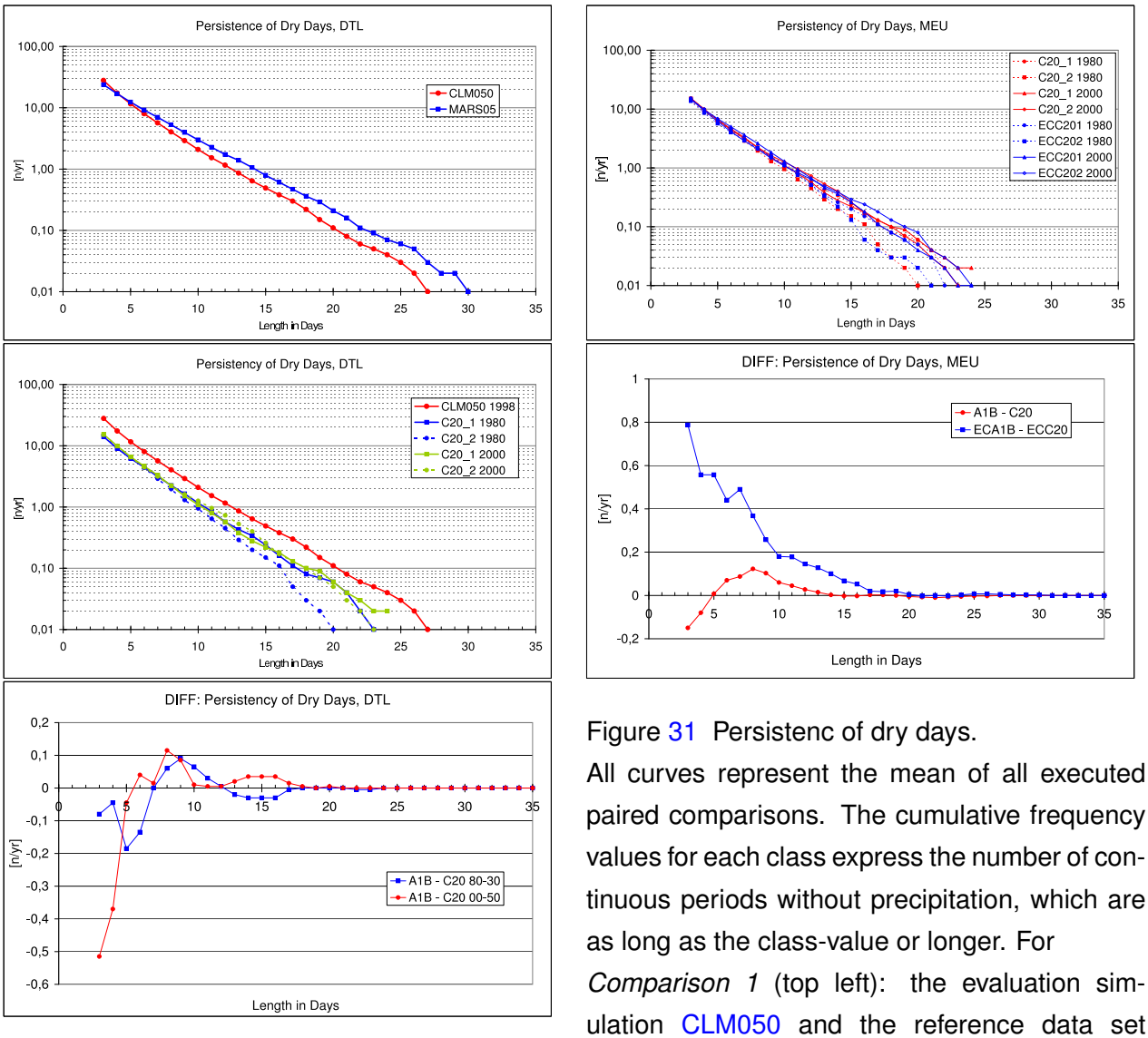

Figure 31 Persistenc of dry days.
All curves represent the mean of all executed paired comparisons. The cumulative frequency values for each class express the number of continuous periods without precipitation, which are as long as the class-value or longer. For *Comparison 1* (top left): the evaluation simulation CLM050 and the reference data set MARS05,
Comparison 2 (middle left): the 20th century climates CLM-C20 and the evaluation simulation,
Comparison 3 (top right): the regional and the global simulations of the 20th century climate,
Comparison 4 (bottom left): the difference between the scenario simulations and the 20th century climates averaged for the first 50-year interval (2011-2030 vs. 1961-1980: blue) and the second 50-year interval (2031-2050 vs. 1981-2000: red),
Comparison 5 (bottom right): the difference between the scenario simulations and the 20th century climates for the regional model (red) and the global model (blue) for both 50-year intervals.

6.12 Humidity

The humidity is represented by two variables: the relative humidity and the water vapour pressure. The water vapour pressure is the atmospheric pressure of water vapour. The relative humidity is the ratio of the partial pressure of water vapour in an air-water mixture and the maximal water vapour pressure at a given temperature. Figure 32 (top left panel) shows the annual average of the relative humidity from the 20th century run C20_1 for the time period 1981-2000. It varies between 80 and 90 % for all land regions north of the Alps and between 90 and 100% for Scandinavia. Over land of Northern Europe the relative humidity is higher than 80% for all monthly averages (not shown here). These values seem to be too high.

Figure 32 (top right panel) shows the relative humidity difference of the 20 yr annual averages 1981-2000 between the results of the C20_1 regional model and the driving ECC201 global model run. Substantial differences occur near the coasts, where the land-sea-masks are different. In most other regions the deviations are smaller than $\pm 6\%$. This indicates that the problem of too high humidity is present in the global model and could not be overcome by the regional model.

Climatological observations of near surface atmospheric humidity are available for water vapour pressure only. They are described in Table 10. Since the water vapour pressure can not be calculated from the output variables of the CLM050 evaluation simulation, the reference data sets could only be compared with the C20_1 20th century run results. Figure 32 (middle and bottom left panel) shows the differences of water vapour pressure from C20_1 and MARS001 as well as from C20_1 and CRU005 data. There is a positive bias over Central Europe and Scandinavia and a negative bias over Southern Europe and North Africa. However, substantial differences between the MARS001 and the CRU005 comparisons occur for Northern Scandinavia. Figure 32 (bottom right panel) shows the 20 yr monthly average deviations of the C20_1 20th century climate from the reference data sets MARS001, CRU005 and CRU007 for all months for Germany (notice that the unit of this panel is Pa). A clear maximum deviation of up to +1.5 hPa occurs in spring and a minimum of up to -0.3 hPa in winter.

The relative humidity can be estimated from the water vapour pressure and the air temperature. Taking the deviations shown in COMPARISON 1 for these variables (see also section 6.1) the resulting deviation for the mean relative humidity can be estimated.
For Germany, the 20 year annual average of the relative humidity decreases by roughly 10%, if the temperature is increased by 1 K and the water vapour pressure is decreased by 0.5 hPa. This calculation shows that the evaluation results for temperature and water vapour pressure may explain the high

values of relative humidity. However, a more detailed analysis is needed for both temperature and the relative humidity before using the humidity data of the model runs.

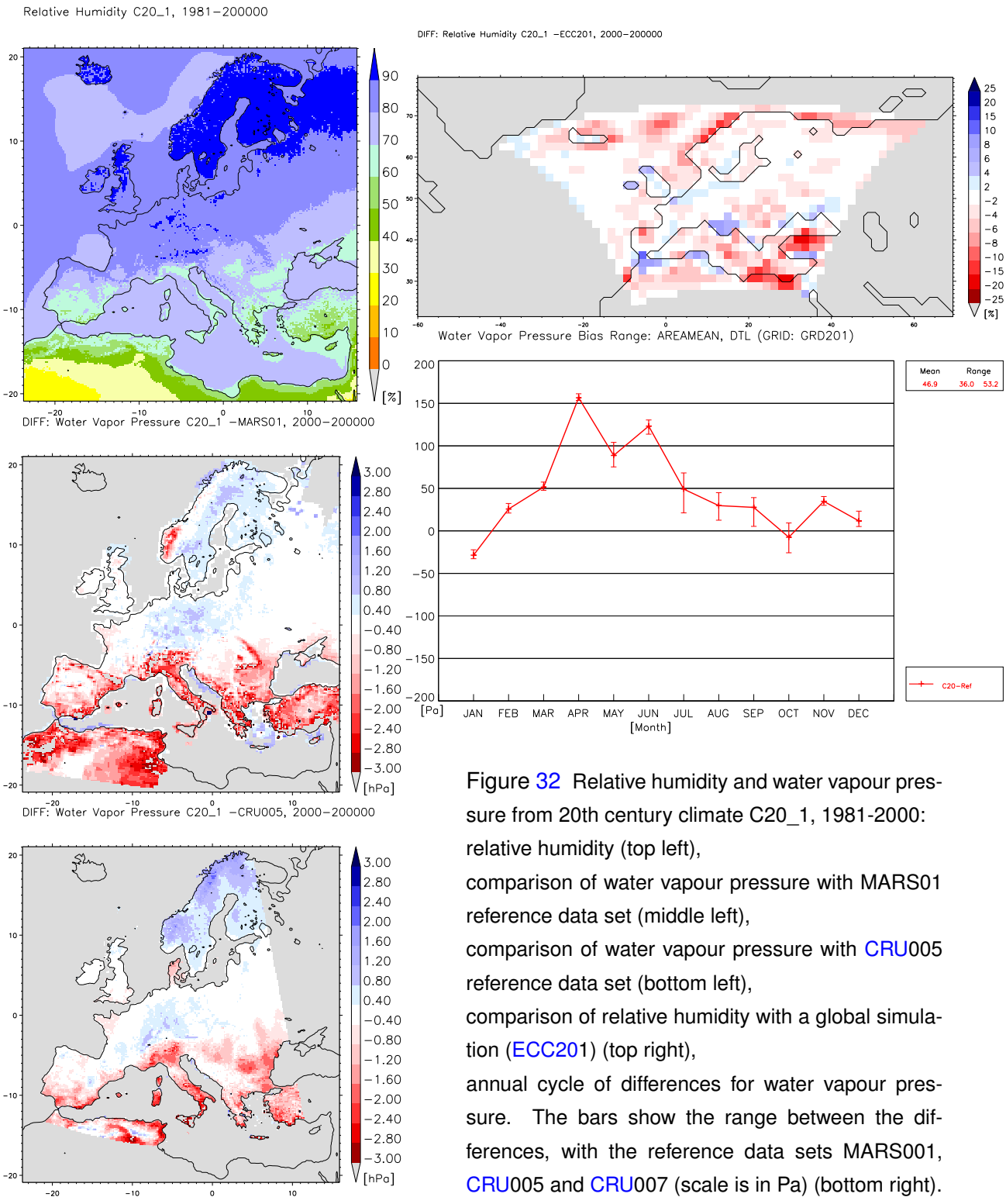

Figure 32 Relative humidity and water vapour pressure from 20th century climate C20_1, 1981-2000:
relative humidity (top left),
comparison of water vapour pressure with MARS01 reference data set (middle left),
comparison of water vapour pressure with CRU005 reference data set (bottom left),
comparison of relative humidity with a global simulation (ECC201) (top right),
annual cycle of differences for water vapour pressure. The bars show the range between the differences, with the reference data sets MARS001, CRU005 and CRU007 (scale is in Pa) (bottom right).

6.13 Coastal wind variability

This comparison investigates, whether the strong change of the wind speed 10 m above ground at the coast lines can also be detected in the wind speeds at higher altitudes of the lowest model levels (level 32 and 31).

Figure 33 shows the January 2000 mean wind speed 10 m above ground (bottom) and the wind speed on the lowest model levels 32 and 31 of the C20_1 model run. Level 32 (middle) is 33.85 m above ground over sea and level 31 (top) 110.3 m over sea. Over land areas, the height above ground may be much lower or much higher on the second lowest model level (level 31) due to the terrain following coordinates, which are not necessarily parallel to the ground, especially in mountainous regions.

The 10 m wind decreases strongly at the coast lines by more than 5 m/s coming from the open sea. This effect is weaker in Figure (33, middle) showing the mean wind speed at level 32 and degrades even more in the top panel showing the mean wind speed at level 31. The interpretation of these results is difficult, since the wind speeds are averaged with different methods from the u and v wind components. The mean wind speed 10 m above ground is calculated as

$$\overline{\sqrt{u^2 + v^2}}$$

whereas the mean wind speeds at levels 32 and 31 are calculated as

$$\sqrt{\overline{u}^2 + \overline{v}^2}$$

and contain only the stationary component of the wind.

The wind speed near the coasts has to be investigated in more detail in order to derive its quality.

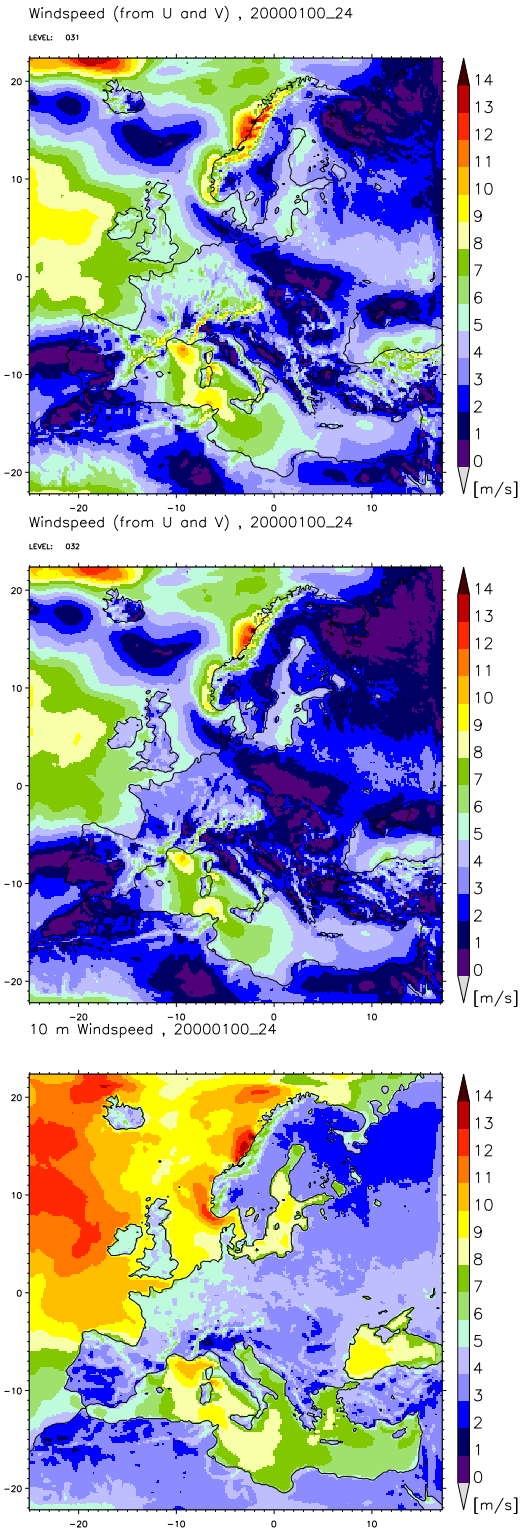

Figure 33 Wind speed from 20th century climate C20_1 for January 2000:
calculated on the second lowest model level (level 31) from the monthly average of wind vectors u and v (top)
on the lowest model level (level 32) calculated from the monthly average of wind vectors u and v (middle),
10 meter above ground (bottom).

7 Summary

The national Earth system research service group "Model and Data" conducted climate simulations for Europe with the regional climate model CLM developed by the CLM Community and with the model configuration provided by the CLM Community members from BTU, GKSS and PIK. CLM was forced with the output of the global climate model ECHAM5/MPIOM developed by the Max Planck Institute for Meteorology. The global climate change projections for the A1B and B1 scenarios of the 21st century as well as the reconstruction of the last four decades of the 20th century, which had been calculated by ECHAM5/MPIOM as contribution to the IPCC AR4 report, were applied by the regional model CLM in order to assess projections for the grid size of 0.165° (area of about 18×18 km^2) in Europe.

It is the first time that several realisations of different climate scenarios and present day climate conditions are produced with the same configuration of a non-hydrostatic regional climate model at a high horizontal resolution. Thus, with this contribution the idea of ensemble simulations has further advanced to the regional scale.

An extended quality control has been performed by the Department of Environmental Meteorology at the Brandenburg University of Technology in Cottbus. A specific strategy was developed and applied to the global and regional simulation results and to an additionally conducted evaluation simulation to check and ensure the quality of the produced climate data. This quality control strategy aims at the determination of the consistency of the provided data sets, on a quantification of model inherent uncertainties, and on conclusions about the reliability of detected climate change signals. The required investigations are based on 5 different types of comparisons to examine the conformance with observational data, the consistency and deviation between regional and global model results, and the modification of present-day conditions in a potential future climate scenario.

The analysis confirms that the provided data are of satisfying high quality and in accordance with today's state of science in climate research. All fields investigated are physically consistent. The analysis exhibits that the relevance or reliability of the simulated climate changes depends on the considered model variable, statistical quantitiy, time period, and region. The gain of resolution in the regional simulations compared to the global ones, the so-called added value, is exemplified and differs between parameters and regions, too. The analysis of selected results, which represent only a small fraction of the entire data volume, gives an idea of the overall potential of the generated data.

The strategy of analysis and the systematic discussion of results introduced in this report provides a

framework to investigate and assess the quality and suitability of the generated data for diverse applications. All discussions and analyses are restricted here to a previously selected set of parameters, regions, and the A1B scenario. The conclusions drawn in this report for a particular variable in a specific region cannot generally be assigned to other variables and regions. Each applications of the model data therefore requires an indispensable own careful investigation of quality and uncertainty for which this report can be used as an adequate guideline. In addition, a large set of figures and tables are provided as a supplement to this report to support these own investigations in advance of further applications of the data.

The state of quality control ensures that standard climatological parameters can now officially be released. They are accessible from the WDCC/CERA database at M&D. The access to the data is free of charge and researchers as well as non-scientific users are encouraged to contact the Service Group Adaptation (SGA) at M&D for access to the data or for assistance in using the data. Therefore, this paper marks the beginning of the exploration of this in many aspects overwhelming regional climate model data set. For instance, specific humidity was found to increase in the 200 hPa level. Does this represent a change at the tropopause?

8 Acknowledgement

The work is a contribution to the funding priority "klima*zwei*: Research for Climate Protection and Protection from Climate Impacts" of the German Federal Ministry of Education and Research (BMBF). The simulations were run on NEC SX–6 machines of the DKRZ (German Climate Computer Centre) and of the HLRS (Univ. Stuttgart). We are grateful for support from the staffs and from NEC. SGA-Offenbach provided access to data of the observational network of the DWD. The support from the people running the WDCC is much appreciated. The work was done in close cooperation with the CLM community, in particular the Brandenburgische Technische Universität Cottbus (BTU), the GKSS-Forschungszentrum Geesthacht, and the Potsdam Institute for Climate Impact Research (PIK).

9 References

Auer, I., R. Böhm, A. Jurković, A. Orlik, R. Potzmann, W. Schöner, M. Ungersböck, M. Brunetti, T. Nanni, M. Maugeri, K. Briffa, P. Jones, D. Efthymiadis, O. Mestre, J.-M. Moisselin, M. Begert, R. Brazdil, O. Bochnicek, T. Cegnar, M. Gajić-Čapka, K. Zaninović, Ž. Majstorovic, S. Szalai, T. Szentimery, L. Mercalli, L., 2005. A new instrumental precipitation dataset for the Greater Alpine Region for the period 1800-2002. Int. J. Climatol., **25**, 139–166.

Beck, C., J. Grieser, B. Rudolf, 2005. A new monthly precipitation climatology for the global land areas for the period 1951 to 2000. Klimastatusbericht, Deutscher Wetterdienst, Offenbach, 181 – 190.

Böhm, U., M. Kücken, W. Ahrens, A. Block, D. Hauffe, K. Keuler, B. Rockel, A. Will, 2006. CLM – The climate version of LM: Brief description and long-term application. Proceedings from the COSMO General Meeting 2005. COSMO Newsletter, *http://www.cosmo-model.org*, **6**, 225 – 235.

Damrath, U., G. Doms, D. Frühwald, E. Heise, B. Richter, J. Steppeler, 2000. Operational quantitative precipitation forecasting at the German weather service. J. Hydrol., **239**, 260–285.

Doms, G., and U. Schättler, 2003 . A Description of the nonhydrostatic regional model LM, Part II: Physical Parameterization. Consortium for Small Scall Modelling (COSMO), *http://www.cosmo-model.org*.

Frei, C., C. Schär, 1998 . A precipitation climatology of the Alps from high-resolution rain-gauge observations. Int. J. Climatol., **18**, 873–900.

Fuchs, T., U. Schneider, B. Rudolf, 2007. Global precipitation analysis products of the GPCC. *http://www.dwd.de/en/FundE/Klima/KLIS/int/GPCC/Reports_Publications/... .../QR/GPCC_intro_products_2007.pdf*, Deutscher Wetterdienst , Offenbach.

Gayler, V., S. Legutke, 2005 . The PRISM Standard Running Environment, PRISM Report Series, *http://www.prism.enes.org/Publications/Documentation/index.php*, **5**, 40 pp.

Giorgi, F., B. Hewitson, J. Christensen, M. Hulme, H. von Storch, P. Whetton, R. Jones, L. Mearns, C. Fu, 2001. Regional climate information - Evaluation and projections. In Climate Change 2001. The Scientific Basis, Contribution of Working Group I to the Third Assessment Report of the Intergovernmental Panel on Climate Change, J. T. Houghton, Y. Ding, D. J.

Griggs, M. Noguer, P. J. van der Linden, X. Dai, K. Maskell, C. A. Johnson (Eds.). Cambridge University Press, Cambridge, UK, 583–638.

Goot, E. v.d., S. Orlandi, 2003 . Technical description of interpolation and processing of meteorological data in CGMS. Technical Report, Joint Research Centre, Ispra. *http://mars.jrc.it/marsstat/Crop_Yield_Forecasting/cgms.htm*, .

Heise, E., B. Ritter, R. Schrodin, 2006. Operational implementation of the multi-layer soil model. COSMO Technical Report, *http://www.cosmo-model.org*, **9**, 19 pp.

IPCC, 2007 . Climate Change 2007. The Physical Science Basis. Contribution of Working Group I to the Fourth Assessment Report of the Intergovernmental Panel on Climate Change [Solomon, S., D. Qin, M. Manning, Z. Chen, M. Marquis, K. B. Averyt, M. Tignor, H. L. Miller (Eds.)]. Cambridge University Press, Cambridge, United Kingdom and New York, NY, USA, 996 pp.

Jungclaus J., N. Keenlyside, M. Botzet, H. Haak, J.-J. Luo, M. Latif, J. Marotzke, U. Mikolajewicz, and E. Roeckner, 2006. Ocean Circulation and Tropical Variability in the Coupled Model ECHAM5/MPIOM, in "SPECIAL SECTION: CLIMATE MODELS AT THE MAX PLANCK INSTITUTE FOR METEOROLOGY (MPI-M)", J. Climate, 19, No. 16.

Keuler, K., A. Will, and K. Radtke, 2008. Quality of Regional Climate Simulations with the CLM, Meteorol. Z., in preparation.

Legutke, S., I. Fast, V. Gayler, 2007. The PRISM Standard Compile Environment, PRISM Report Series **4**, 83 pp, *http://www.prism.enes.org/Publications/Documentation/index.php*.

Leung, L. R., L. O. Mearns, F. Giorgi, R. L. Wilby, 2003. Workshop on Regional Climate Research: Needs and Opportunities. Bull. Amer. Met. Soc. **84**, 89–95.

Mearns, L. O., F. Giorgi, P. Whetton, D. Pabon, M. Hulme, M. Lal, 2003. Guidelines for Use of Climate Scenarios Developed from Regional Climate Model Experiments. In the frame of IPCC 2007, DDC of IPCC TGCIA, Final Version – 10/30/03.

Mitchell, T. D. and P. D. Jones, 2005 . An improved method of constructing a database of monthly climate observations and associated high resolution grids. Int. J. Climatol., **25**, 693–712.

Nakićenović, N., R. Swart (Eds.), 2000. Special Report on Emissions Scenarios. A Special Report of Working Group 3 of the Intergovernmental Panel on Climate Change. Cambridge, University Press, Cambridge, United Kingdom and New York, NY, USA, 599 pp.

New, M., D. Lister, M. Hulme, I. Markin, 2002. A high-resolution data set of surface climate over land areas. Climate Research, **21**, 1–25.

Roeckner E., G. P. Brasseur, M. Giorgetta, D. Jacob, J. Jungclaus, C. Reick, J. Sillmann, 2006. Climate Predictions for the 21th Century, Max Planck Institute for Meteorology, Hamburg, Germany, October 2006.

Rodriguez-Puebla C., A. H. Encinas, S. Nieto, J. Garmendia, 1998. Spatial and temporal patterns of annual precipitation variability over the Iberian Peninsula. Int. J. Climatol., **18**, 299–316.

Smerdon, J. E., and M. Stieglitz, 2006 . Simulating heat transport of harmonic temperature signals in the Earth's shallow subsurface: Lower-boundary sensitivities. Geophys. Res. Lett., **33**, doi:10.1029/2006GL026816.

Schrodin, R., E. Heise, 2001 . The multi-layer version of the DWD soil model TERRA_LM. COSMO Technical Report, *http://www.cosmo-model.org*, **2**, 18 pp.

Schulz, J. P. and E. Heise, 2003 . A new scheme for diagnosing near-surface convective gusts, COSMO Newsletter, *http://www.cosmo-model.org*, **3**, 221-225.

Steppeler, J., G. Doms, U. Schättler, H. W. Bitzer, A. Gassmann, U. Damrath, G. Gregoric, 2003. Meso-gamma scale forecasts using the non-hydrostatic model LM. Meteorol. Atmos. Phys. **82**, 75–96.

Troen, I. and E.L. Petersen, 1989 . European Wind Atlas. ISBN 87-550-1482-8. Risø National Laboratory, Roskilde, 656 pp.

Uppala, S. M., P. W. Kallberg, A. J. Simmons, U. Andrae, V. da Costa Bechtold,M. Fiorino, J. K. Gibson, J. Haseler, A. Hernandez, G. A. Kelly, C. Li, K. Onogi, S. Saarinen, N. Sokka, R. P. Allan,E. Andersson, K. Arpe, M. Q. Balmaseda, A. C. M. Beljaars, L. van de Berg, J. Bidlot, N. Bormann, S. Caires, F. Chevallier, A. Dethof, M. Dragosavac, M. Fisher, M. Fuentes, S. Hagemann, E. Holm, B. J. Hoskins, L. Isaksen, P. A. E. M. Janssen, R. Jenne, A. P. McNally, J.-F. Mahfouf, J.-J. Morcrette, N. A. Rayner, R. W. Saunders, P. Simon, A. Sterl, K. E. Trenberth, A. Untch, D. Vasiljevic, P. Viterbo, J. Woollen, 2005. The ERA-40 Re-Analysis. Quart. J. R. Meteorol. Soc., 131, 2961-3012, doi:10.1256/qj.04.176.

Walter, A., K. Keuler, D. Jacob, R. Knoche, A. Block, S. Kotlarski, G. Müller-Westermeier, D. Rechid, W. Ahrens, 2006. A high resolution reference data set of German wind velocity 1951-2001 and comparison with regional climate model results. Meteorol. Z., 15, 585–596.

Will, A., 2008. Physics and Dynamics of the CLM. in preparation for Meteorol. Z..

10 Acronyms

AR4	IPCC fourth assessment report
BMBF	German Federal Ministry of Education and Research
BTU	Brandenburgische Technische Universität
CDO	Climate Data Operator software package
CLM	Climate version of the regional 'Lokal-Modell' of the DWD
CLM050	CLM run with ERA40 forcing
CLM-C20	CLM run with ECHAM5/MPIOM 20C3M forcing
CLM-CCS	20 yr-period CLM runs with ECHAM5/MPIOM forcing for the SRES A1B projection
COSMO	Consortium of national weather services for small scale modelling
CRU	Climate Research UNIT
DKRZ	German Climate Computing Centre
DWD	German Meteorological Service
ECC20*n*	EC-C20 simulations of four periods of 20 years (n=1,2)
ECHAM5	European Centre Hamburg Model (global climate model)
ECMWF	European Centre of Medium-Range Weather Forecasts
ECOCLIMAP	Global database of land surface parameters
EC-C20	ECHAM5/MPIOM simulation of the 20C3M scenario
EC-CCS	20-yr periods out of the ECHAM5/MPIOM SRES A1B scenario
ENSEMBLES	European Commission's 6th Framework Programme funded project of an ensemble prediction system for climate change
ERA-40	ECMWF re-analysis project
GCM	Global Climate Model
GKSS	GKSS Research Centre Geesthacht
GRIB	(GRIdded Binary) file format
IPCC	Intergovernmental Panel on Climate Change
klima*zwei*	BMBF funding priority "Research for Climate Protection and the Protection from Climate Impacts"
LM	Lokal-Modell of the DWD
MPIOM	Max-Planck-Institute Ocean Model
M&D	Model and Data Group
NetCDF	Network Common Data Format for exchanging scientific data

PIK	Potsdam Institute for Climate Impact Research
PRISM	Project for Integrated Earth System Modelling
RCM	Regional Climate Model
SGA	Service Group Adaptation at Model&Data
SRES	IPCC Special Report on Emissions Scenarios
SST	Sea-surface temperature
SVN	Subversion; open-source-software version control system
UTC	Universal Time Code
WDCC	World Data Centre for Climate
20C3M	IPCC AR4 20th century climate reconstruction experiments

11 Appendix

Brief description about each parameter provided on the model (D2) and geographical (D3) grid, respectively.

AEVAP_S
Evaporation. AEVAP_S = ALHFL_S $\times$ 10800 / (2.501 * 10^6)

ALB and **ALB_NN**
Surface albedo. ALB was derived by bi-linear interpolation and ALB_NN by the nearest neighbour assignment.

Surface albedo is set to a maximum of 0.7 (snow cover and sea ice) and to a minimum of 0.07 (water). Sea ice is derived from the SST of the MPIOM with the results being transformed to the horizontal resolution of ECHAM5, i.e. approximately 200 km. Thus, Baltic Sea basins are poorly resolved, partly by one grid box, and total melting can be observed via the albedo only over such large areas.

The figures show the melting of sea ice in the Bothnian Bay of two consecutive output fields for ALB_NN.

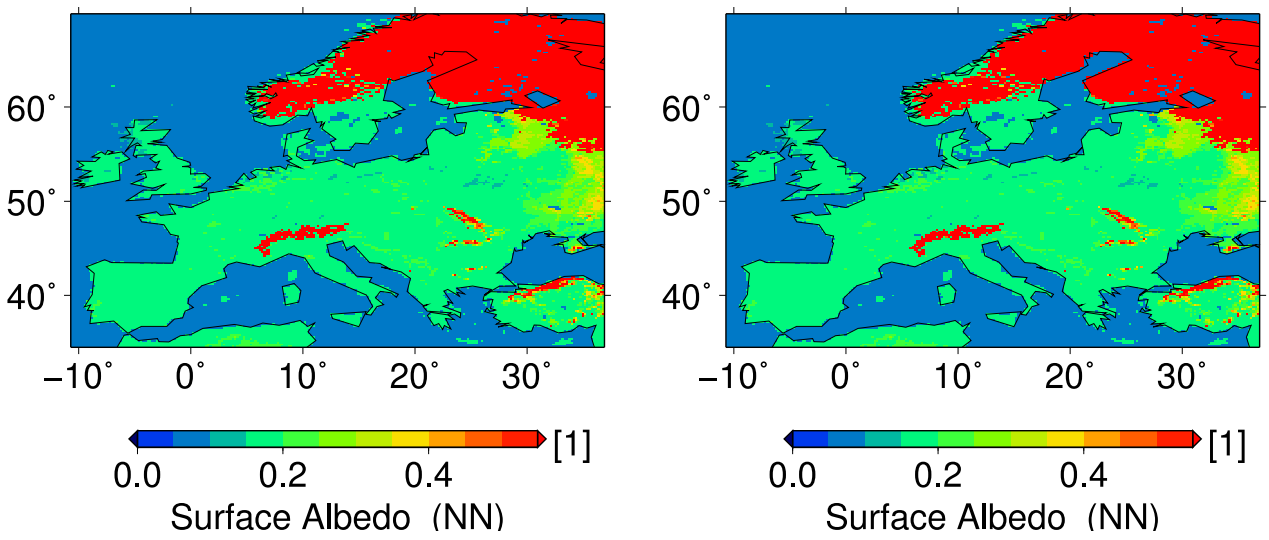

Figure 34 Surface albedo according the nearest-neighbour assignment at two successive times with lag of 3 hours. Scenario: CLM_C20_2_3h_ALB_NN (D3), Model Date: 1964-04-01.
Left: Time is 15 UTC *Right:* Time is 18 UTC.

ALHFL_S
Surface latent heat flux. The surface latent heat flux density is the exchange of heat between the surface and the air on account of evaporation (including sublimation). Downward defines positive.

APAB_S
Surface photosynthetic active radiation. Radiative flux density is the sum of shortwave and longwave radiative flux densities and "photosynthetic" radiation is the part of the spectrum which is used in photosynthesis, i.e. 300-700 nm.

ASHFL_S
Surface sensible heat flux, i.e. the exchange of heat between the surface and the air by motion of air. Downward defines positive.

ASOB_S
Surface net downward shortwave radiation, i.e. the difference between radiation from above (downwards) and radiation from below (upwards). Downward defines positive.

The shortwave radiation balance is strongly influenced by atmospheric pollutants - gases or aerosols. For the CLM runs the aerosol content in the atmosphere is prescribed for rural, urban, desert or sea regions and constant with time.

ASOB_T
Net downward shortwave radiation (at model top), i.e. the difference between radiation from above (downwards) and radiation from below (upwards). Downward defines positive.

ATHB_S
Surface net downward longwave radiation. Net downward radiation is the difference between downward directed radiation and radiation from the surface. Downward defines positive.

ATHB_T
Outgoing longwave radiation (at model top). Net downward radiation is the difference between downward directed radiation and radiation from below. Downward defines positive.

BOX_AREA
Area of gridboxes.

CAPE_CON
Specific convectively available potential energy. Represents the amount of buoyant energy available to accelerate a parcel vertically. Potential energy is the sum of the gravitational potential energy relative to the geoid and the centripetal potential energy. (The geopotential is the specific potential energy.)

CLCH
High cloud cover. Fraction of grid-cell area. High clouds are all clouds at pressure levels < 400 hPa.

CLCL
Low cloud cover. Fraction of grid-cell area. Low clouds are all clouds at pressure levels > 800 hPa.

CLCM
Medium cloud cover. Fraction of grid-cell area. Medium clouds are all clouds at pressure levels between 800 hPa and 400 hPa.

CLCT
Total cloud cover.

CON_TOT
Convective precipitation. Sum of convective liquid and convective snow precipitation over the time interval.

DURSUN
Sunshine duration. Defined as instantaneous 1-hourly value of direct shortwave radiation (normal to the surafce) exceeding 120 W/m^2. Rounded to full hours expressed in seconds.

FD
Number of frost days, i.e. with $T_{min}(2m) < 0$ °C.

FR_LAND
Land-sea fraction by bi-linear interpolation.

FR_LAND_NN
Land-sea fraction, assigned from nearest-neighbour.

GPH
Geopotential, i.e. the sum of the specific gravitational potential energy relative to the geoid and the specific centripetal potential energy. GPH is availablen on each pressure level. Due to high orography in the model region, the 1000 hPa, 925 hPa level, and partly also the 850 hPa level are often below the orographic height. Thus, the geopotential of such levels is a fictive value (see also PMSL).

GSP_TOT
Large scale precipitation, sum of grid scale liquid and grid scale snow precipitation.

GZ0
Surface roughness length. Constant or slowly varying fields. Note: this is different to GZ0 in the original model output, where GZ0 is given in units of [m^2/s^2] with the scaling factor $1/g$ as netCDF attribute.

HBAS_CON
Height of convective cloud base.

HHL
Height. Geometric height on half levels. 3D-field on 33 model half levels.

HMO3
Air pressure at ozone maximum. Constant or slowly varying fields.

HSURF
Surface height by bi-linear interpolation.

HSURF_NN
Surface height, assigned from nearest-neighbour.

HTOP_CON
Height of convective cloud top.

HZEROCL
Height of freezing level. Height of a freezing level in meter above sea level. Gives the height of the lowest 0 °C. A missing value is set, when the temperature of the lowest atmospheric layer is below 0 °C.

ID
Number of ice days, i.e. with $T_{max}(2m) < 0$ °C.

IDIV_HUM
Atmosphere water divergence.

IWATER
Cloud condensed water content.

IWV
Precipitable water.

LAI

The leaf area index (fractional vegetation coverage) is prescribed for each land use type by an annual course with the maximum (representing the vegetation period) and minimum (representing the resting period) value of LAI fixed for the given land use type. The function, which describes the annual course, depends on latitude and surface height determining the onset and the duration of the vegetation period.

LAT
Latitude. Value at the centre of the grid-box.

LAT_BNDS
Latitude of the bounds. Values at the 4 corners of the grid-box.

LON
Longitude. Value at the centre of the grid-box.

LON_BNDS
Longitude of the bounds. Values at the 4 corners of the grid-box.

MFLX_CON
Convective mass flux density.

OMEGA
Omega (dp/dt). Lagrangian tendency of air pressure, often called "omega", plays the role of the upward component of air velocity when air pressure is being used as the vertical coordinate. If the vertical air velocity is upwards, it is negative when expressed as a tendency of air pressure; downwards is positive. On each pressure level.

PLCOV
Vegetation area fraction (see also LAI).

PMSL

Mean sea level pressure.

Sea level pressure is determined in elevated orographic heights by extrapolating the surface pressure using fictive temperature and humidity values. The error increases with increasing orographic height of the grid box. Therefore, the orography is often reflected in maps of sea level pressure (see also GPH). The figure shows the 20-years average of PMSL from 1979 to 1998.

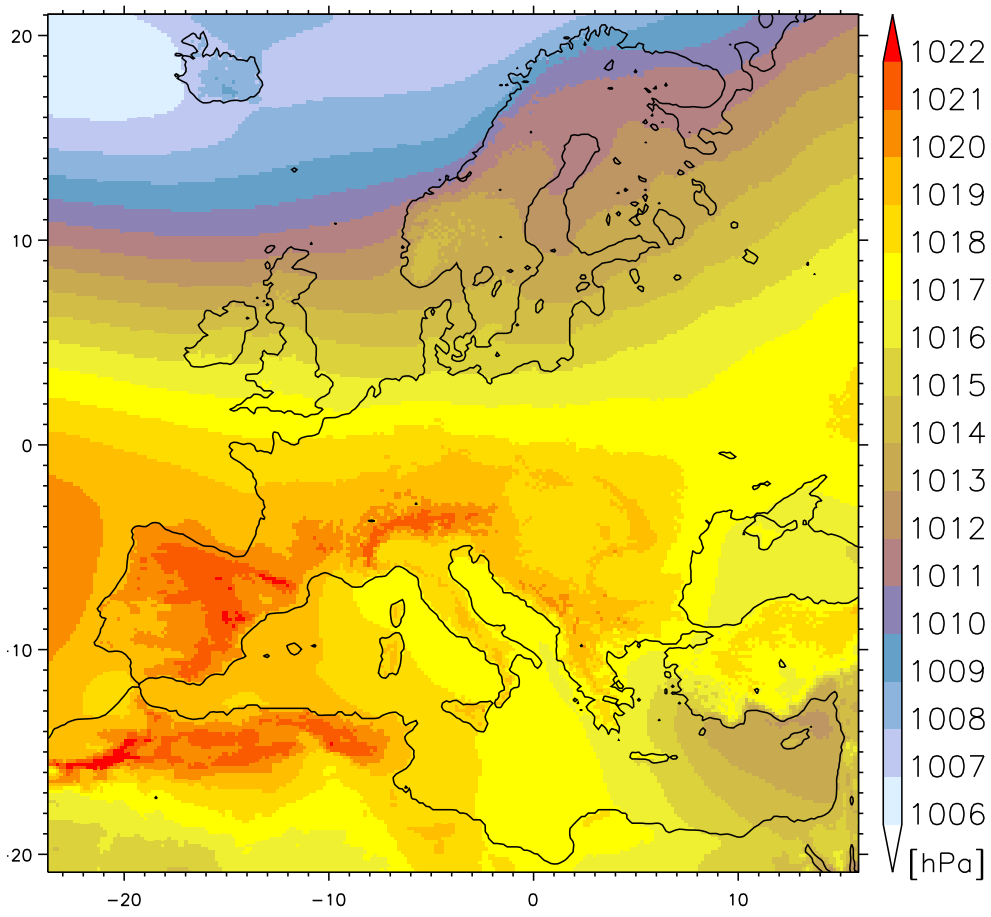

Figure 35 20-year average of mean sea level air pressure from year 1979 to 1998. Scenario: CLM C50, i.e. forced by ERA40 (details on page 35).

PRECIP_TOT

Total precipitation. Sum of all precipitation types: PRECIP_TOT=RAIN_CON + SNOW_CON + RAIN_GSP + SNOW_GSP.

The annual sum of precipitation over the coastal areas appears to be too large, particularly over northern Portugal / northwestern Spain where a mean annual sum of more than 2500 mm between 1961 and 1990 is simulated

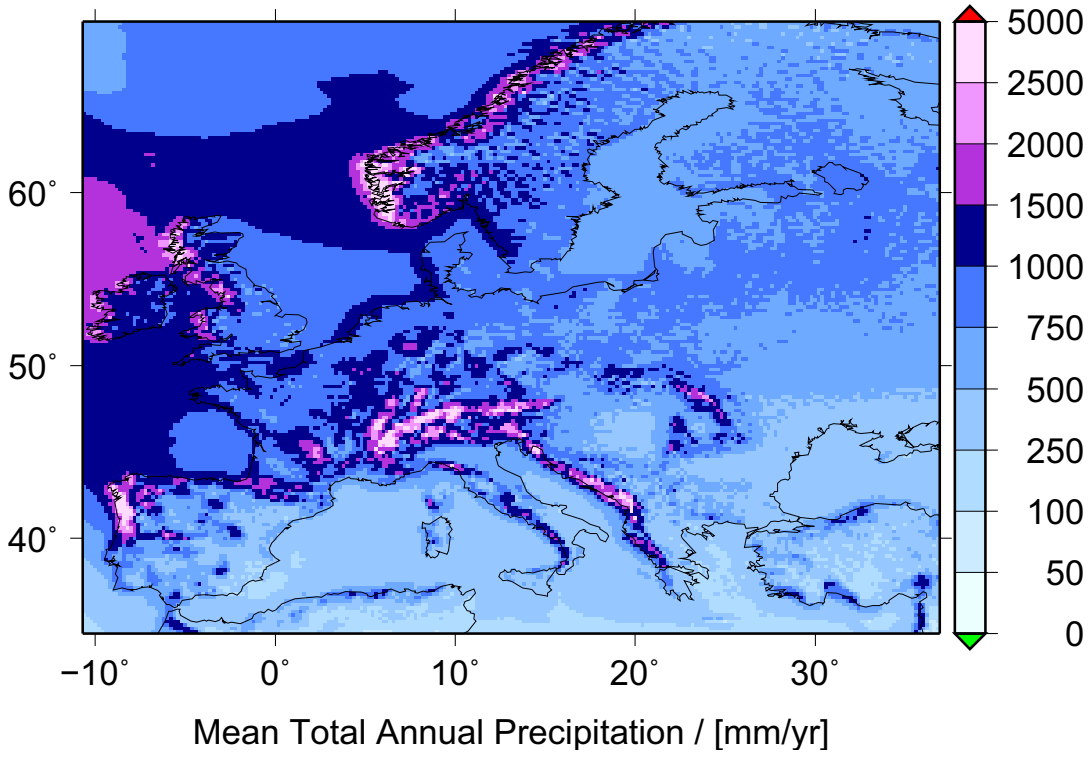

Figure 36 Mean annual total precipitation for the period 1961 – 1990. Scenario: CLM C20_1 (D3).

Measured annual precipitation in this region slightly exceeds 1200 mm for the period 1949 to 1995 (Rodriguez-Puebla et al., 1998).

The largest daily sum of PRECIP_TOT in the C20_1-run is 479 mm and occurs in the Mediterranean Sea between Sicily and Tunisia. There, the precipitation maximum is related to a small cyclonic structure.

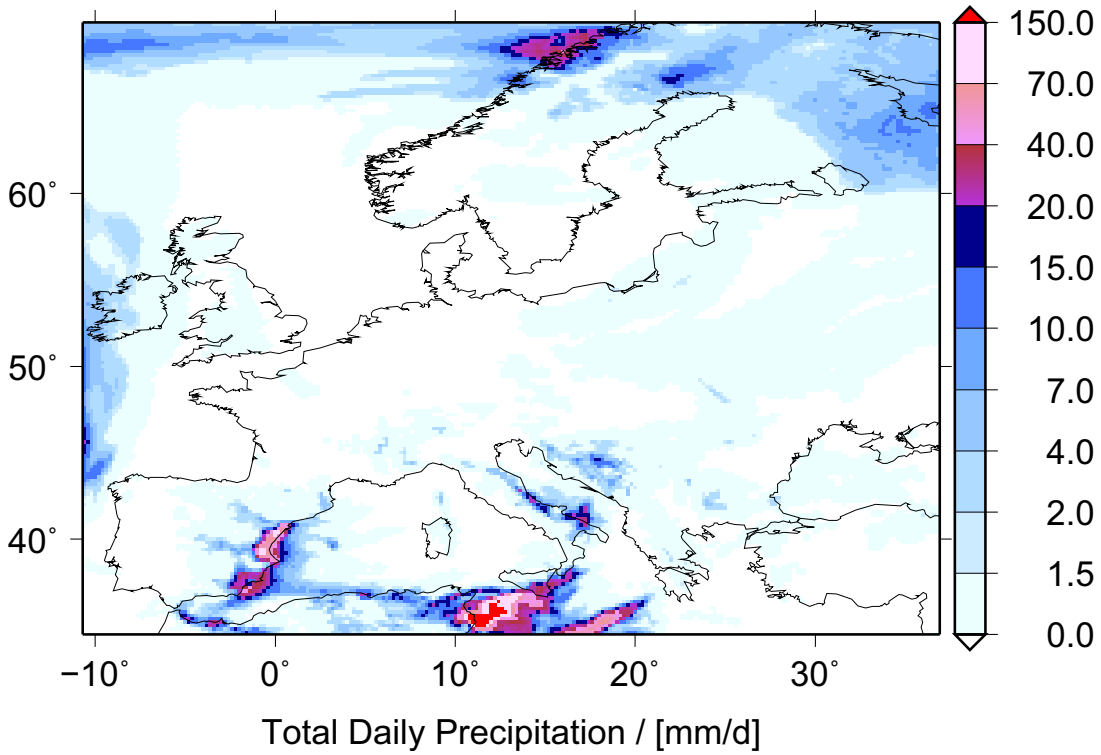

Figure 37 Daily total precipitation of the scenario CLM_C20_1_D3 at the model date 1981-10-08.

PS

Surface pressure.

QV

Specific humidity on each pressure level.

Very small negative values of QV may occur at higher atmospheric pressure levels (upper troposphere / lower stratosphere). The reason is the interpolation of small humidity values from model levels to pressure levels. The interpolation routine may occasionally produce negative or near-zero values.

One of the most distinct changes in the scenario runs can be found in high level specific humidity, namely in QV200. The values at the end of the 21. century in the A1B scenario rise to the double of those at the beginning of the century.

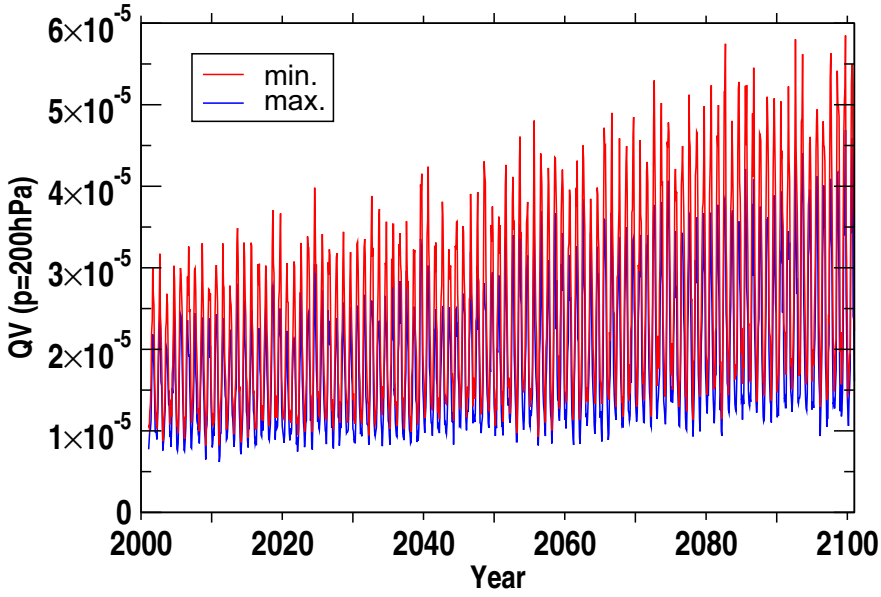

Figure 38 Minimum (blue) and maximum (red) of monthly mean specific humidity QV on the 200 hPa pressure level. CLM A1B_2 (D3) scenario for the region 45.9 to 55.1° N and 3.9 to 17.1° E.

The figure shows the minimum and maximum values of specific humidity on the 200 hPa level in the region of Germany, Swiss and Austria. The increase of summer values with time is possibly due to a rise of the tropopause and thus an upward mixing of humidity up to 200 hPa.

QV_S
Surface specific humidity.

R10MM
Number of days with total precipitation $>$10 mm.

R20MM
Number of days with total precipitation $>$20 mm.

RAIN_CON
Amount of convective rainfall.

RAIN_GSP
Amount of large scale rainfall.

RAIN_TOT
Amount of total rainfall. Sum of convective (RAIN_CON) and large scale (RAIN_GSP) rainfall

REL_HUM
Relative humidity.

ROOTDP
Root depths is prescribed and constant for each grid box.

RR1MM
Number of days with total precipitation.

RUNOFF_G
Subsurface runoff.

RUNOFF_S
Surface runoff.

SNOWFREQ
Relative frequency of potential snowfall at surface.

SNOWLMT
Height of the snowfall limit above sea level. This value gives the height in the atmosphere above which possible precipitation would be frozen. Below this height, possible precipitation would be liquid. A missing value is set, when the height of this virtual limit would be lower than the topography in the responding grid box. Thus, missing values state that all possible precipitation in this gridbox would fall as snow.

SNOW_CON
Amount of convective snowfall.

SNOW_COV
Number of days with snowcover. Days with W_SNOW > 0.01 kg/m^2 are counted. This parameter gives the ensemble size for the averaging of T_SNOW (see also T_SNOW, W_SNOW).

SNOW_DAYS
Number of days with snowfall. Note that this number is important for the assessment of the monthly and yearly value of T_SNOW (see T_SNOW). Only with a sufficiently high number of snowdays the value of T_SNOW is reliable.

SNOW_GSP
Large scale snowfall. Amount of grid scale snow fall.

SNOW_TOT
Amount of snowfall. Sum of convective and grid scale snow precipitation: SNOW_TOT=SNOW_CON + SNOW_GSP.

SOILTYP_NN
Soil type.

SU
Number of summer days, i.e. with $T_{max}(2m) > 25$ °C.

T
Air temperature on each pressure level.

TD_2M
Dew point temperature at 2 m height.

TD_2M_AV
Dew point temperature at 2 m height. Average.

TMAX_2M

Maximum air temperature at 2 m height.

Extraordinary high values have been reported for TMAX_2M. Such an event was found for France in the A1B_1 scenario of July 2062. The panel on the left shows the spatial distribution for the July 12. Notice that the area of high temperatures extends into the valley of the Rhine river. The figure on the right contrasts the time series of the daily maximum of TMAX_2M by CLM and the corresponding forcing field by ECHAM/MPIOM, respectively, occurring in a grid-cell anywhere in France.

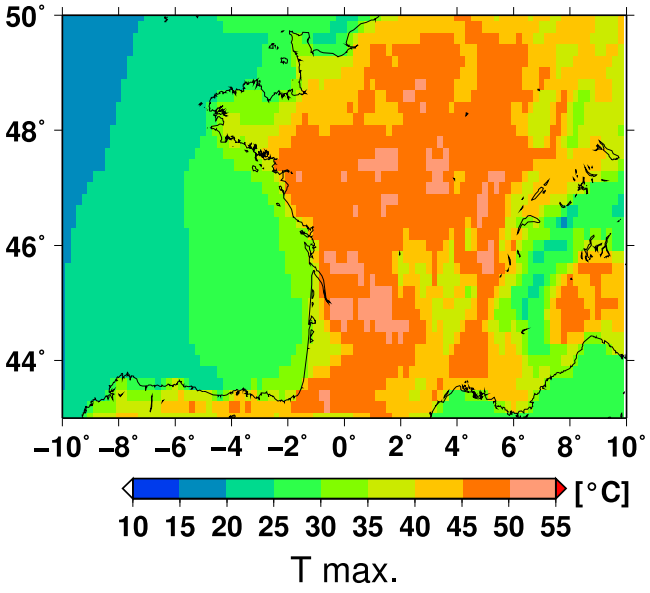

Figure 39 a Maximum temperature at 2m (TMAX_2M) of CLM_A1B_1 for July 12 in model year 2062.

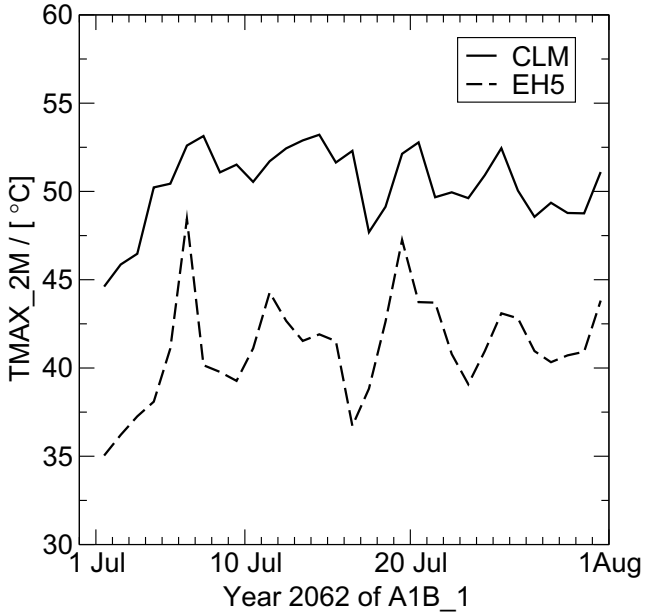

Figure 39 b Time series of the maximum temperature out of the TMAX_2M field for France in the model month of July 2062 of the A1B_1 scenario from CLM and ECHAM/MPIOM.

TMIN_2M

Minimum air temperature at 2 m height.

TR

Number of tropical nights, i.e. days with $T_{min}(2m) > 20$ °C.

T_2M

Air temperature at 2 m height. The histogram of 3 h-values of T_2M in moderate climate regions like Germany exhibits a peak at 0 °C, which is presumably due to longer periods of melting snow. Nevertheless, the question remains whether a parameter, which is interpolated from values between the surface and the lowest model level by the application of a temperature profile, is so close to the temperature of the melting surface.

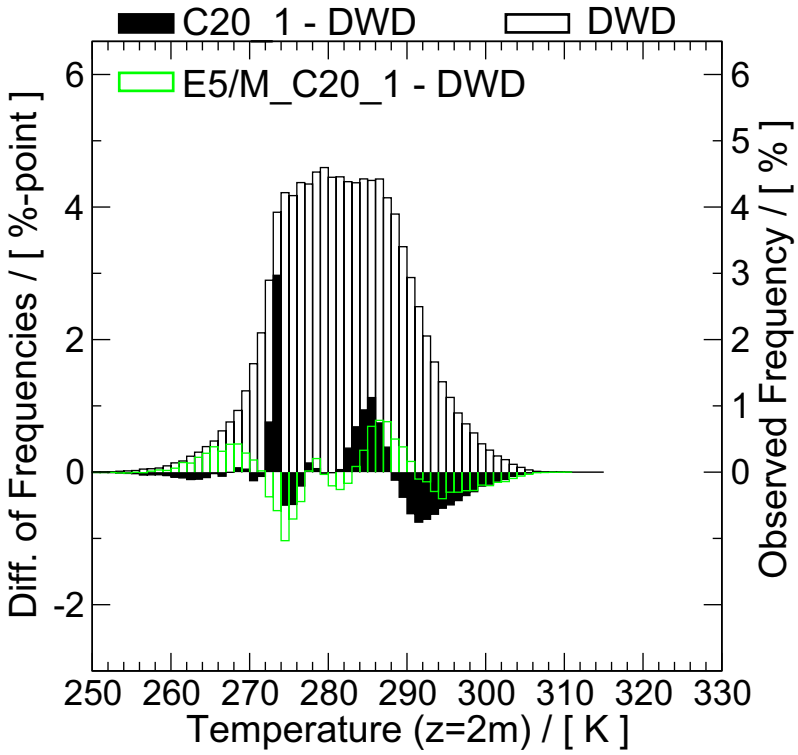

Figure 40 Frequency distribution of temperature at 2 m height for the region Lüchow, Northern Germany, for the period 1960 to 2000. Right hand side: the distribution from hourly observations by the DWD. Left hand side: the difference of the distribution of modelled temperature from the oberservations. The CLM C20_1 (D3) scenario in solid black for the region of size 1°× 1°. Open green bars for ECHAM5/MPIOM for the grid box around Lüchow.

T_2M_AV
Air temperature at 2 m height. Daily average given at the end of the day.

T_G
Grid mean surface temperature. Calculated as weighted mean of the fractions with and without snow in the gridbox.

T_S
Soil surface temperature.

T_SNOW
Snow surface temperature; set to missing value if W_SNOW < 0.01 kg/m^2.

A mean value is only taken over days with snow in time interval. The number of days with snow is provided by the parameter SNOW_COV which gives the ensemble size for the averaging of T_SNOW. Mean values of T_SNOW should be neglected where the ensemble size is too small.

Occasionally a snow temperature of >0 °C occurs in isolated grid boxes, which can in the worst case also present a monthly or yearly mean value. The reason for a snow temperature higher than the melting point is that while a water equivalent W_SNOW ≥ 0.01 kg/m^2 is interpreted as snow for a grid box (mostly on the edge of a snow-covered area), the surface temperature is >0 °C due to exchange processes. In the next time step the temperature will be corrected to 0 °C by the release of heat of fusion and the snow cover is going to vanish, i.e. W_SNOW gets a quantity <0.01 kg/m^2. If no further snow fall occurs at this grid box during the averaging period, the monthly or even yearly averages have an apparent snow temperature higher than the melting point (see also W_SNOW, SNOW_COV).

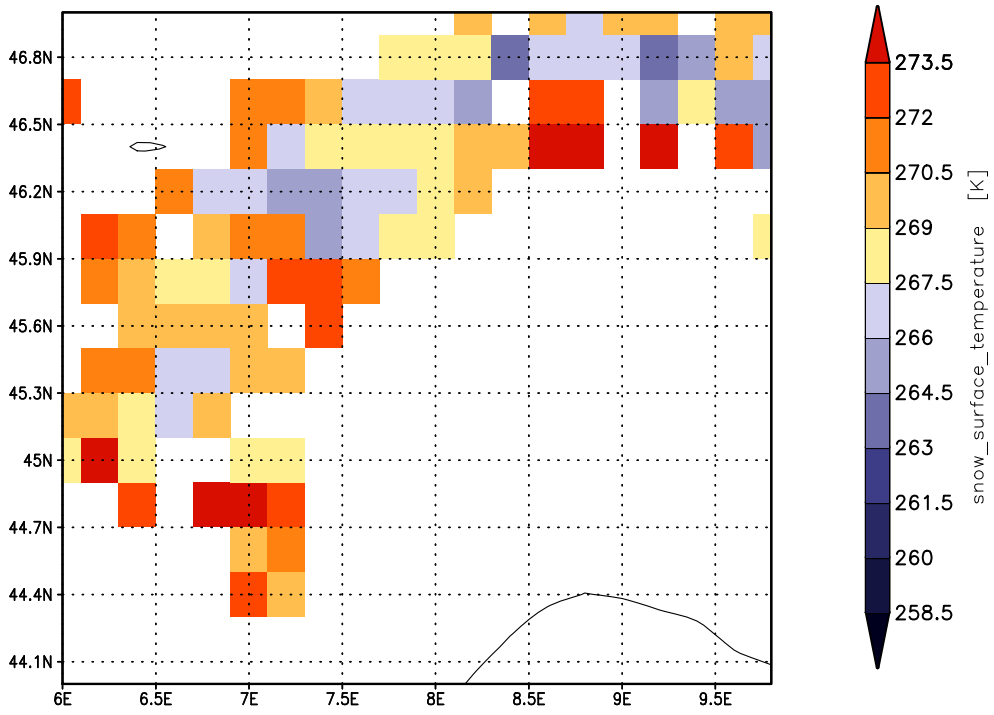

Figure 41 Monthly mean of snow surface temperature [K] over the western Alps for the model month of Oct. 1960. Scenario: CLM C20_1 (D3).

The validity of T_SNOW can only be assessed regarding the parameter W_SNOW and SNOW_COV.

T_SO

Soil temperature. For each soil layer. Note: soil temperature is the bulk temperature of the soil, not the surface (skin) temperature. The dataset acronym indicates the lower bound of the soil layer while the data values themselves are representative for the whole layer. All soil parameters are stored once a day at midnight. This results in rather low temperature values in the upper layers (_0001, _0004) and partly higher values at medium layers (_0010, _0022, _0046, _0084) where the temperature cycle is retarded. The vertical profiles are only typical for night-time hours and do not reflect the day-time heating of the upper layers. This is also true for monthly and yearly mean values.

U
U-component of the wind on each pressure level.

U_10M
U-component of wind at 10 m height.

V
V-component of wind on each pressure level.

VIO3
Vertical integrated ozone amount. The equivalent pressure of atmosphere ozone content, where "content" indicates a quantity per unit area. The "atmosphere content" of a quantity refers to the vertical integral from the surface to the top of the atmosphere. For the content between specified levels in the atmosphere, standard names including "content of atmosphere layer" are used. The equivalent pressure of a particular constituent of the atmosphere is the surface pressure exerted by the weight of that constituent alone. Constant or slowly varying fields.

VMAX_10M

Maximum wind speed at 10 m height calculated from the gust parameterisation.

VMAX_10M is determined as the maximum value of turbulent gusts and convective gusts. Turbulent gusts are "derived from the turbulence state in the atmospheric boundary layer", convective gusts are "estimated from the wind speed which is transported by the downdraft from higher levels to the ground and the wind speed associated to the downdraft itself" (Schulz and Heise, 2003). Convective gusts are restricted to a maximum value of 30 m/s. This value is sometimes reached in CLM scenario simulations.

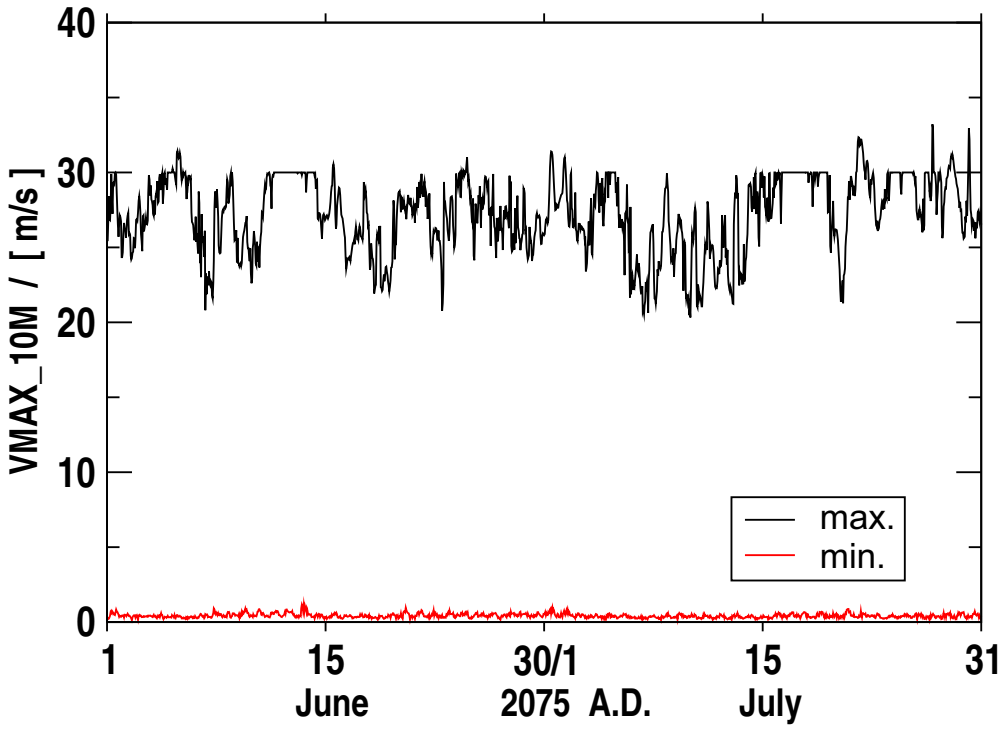

Figure 42 Maximum and minimum wind speed at 10 m in [m/s] for the model months June/July in the year 2075. Scenario: CLM B1_2 (D3).

The figure shows a timeseries of the minimum and maximum values of VMAX_10M in the model region with peculiar time periods with a constant maximum value of 30 m/s The absolute maximum value for B1_2 was found at model date 2008-11-24 21 UTC with a value of more than 57 m/s.

V_10M
V-component of wind at 10 m height.

WIND_DIR
Wind direction at 10m height.

WIND_SPEED
Wind speed. Post processed value of the wind speed at 10 m height. Calculated from the vector components as the mathematical norm: WIND_SPEED= $\sqrt{\text{U\_10M}^2 + \text{V\_10M}^2}$.

The deceleration of wind speed from sea to land appears to be too strong. An example is the mistral which is well represented in the model over the Gulf of Lion. But there is almost no enhancement in wind speed over land, i.e. within the Rhone delta and in the channel between Massif Central and Pyrenees.

The following figures show monthly mean wind speed for a selected month and two figures from the European wind atlas showing wind speed distribution over land and over sea. Although the simulation is a snapshot of a single month and the observations are statistics, it is obvious that the abating of wind speed in particular for Scotland and at the coastal region of Northern Germany and Southern France is different.

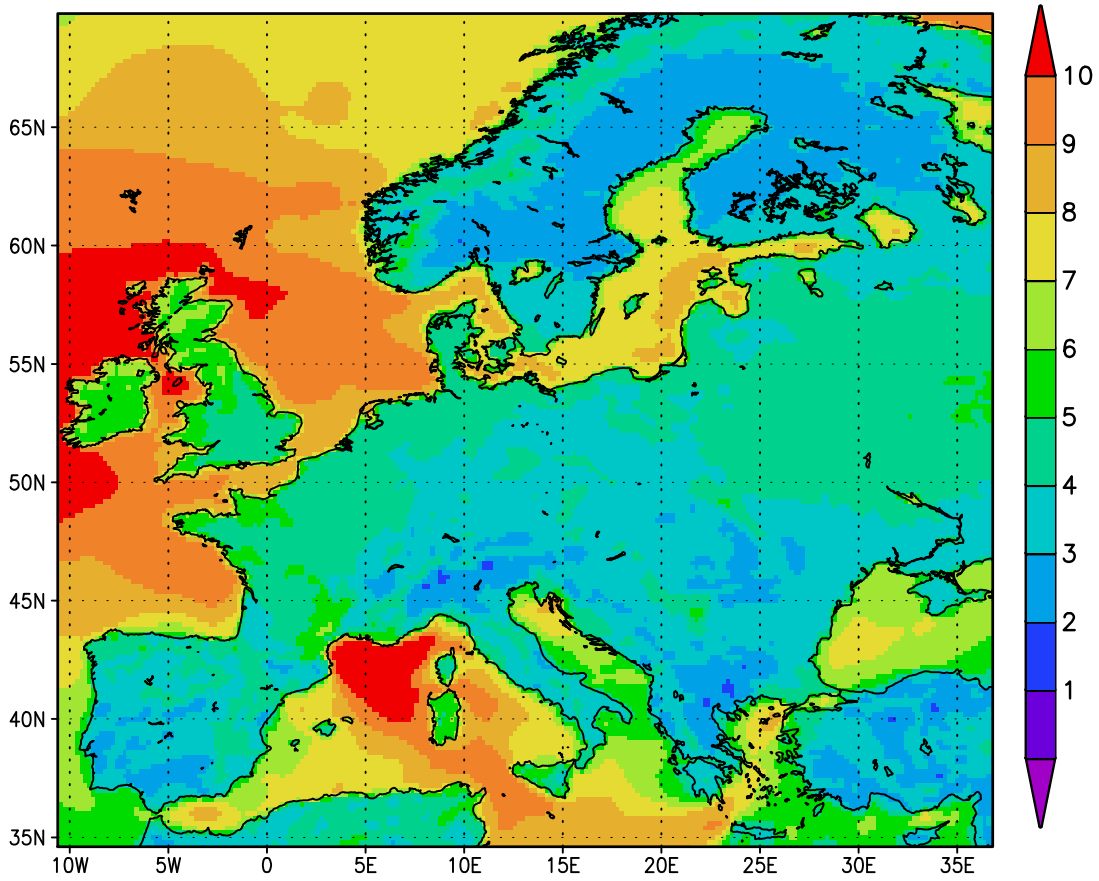

Figure 43 Monthly mean wind speed in [m/s] for the scenario CLM C20_1 (D3) for the model month of October in 1965.

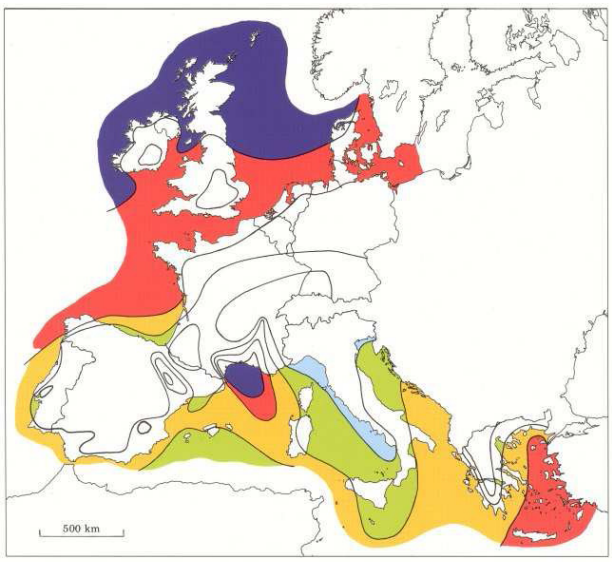

Wind resources over open sea (more than 10 km offshore) for five standard heights

	10 m		25 m		50 m		100 m		200 m	
	m s^{-1}	Wm^{-2}	m s^{-1}	Wm^{-2}	m s^{-1}	Wm^{-2}	m s^{-1}	Wm^{-2}	m s^{-1}	Wm^{-2}
	> 8.0	> 600	> 8.5	> 700	> 9.0	> 800	> 10.0	> 1100	> 11.0	> 1500
	7.0-8.0	350-600	7.5-8.5	450-700	8.0-9.0	600-800	8.5-10.0	650-1100	9.5-11.0	900-1500
	6.0-7.0	250-300	6.5-7.5	300-450	7.0-8.0	400-600	7.5- 8.5	450- 650	8.0- 9.5	600- 900
	4.5-6.0	100-250	5.0-6.5	150-300	5.5-7.0	200-400	6.0- 7.5	250- 450	6.5- 8.0	300- 600
	< 4.5	< 100	< 5.0	< 150	< 5.5	< 200	< 6.0	< 250	< 6.5	< 300

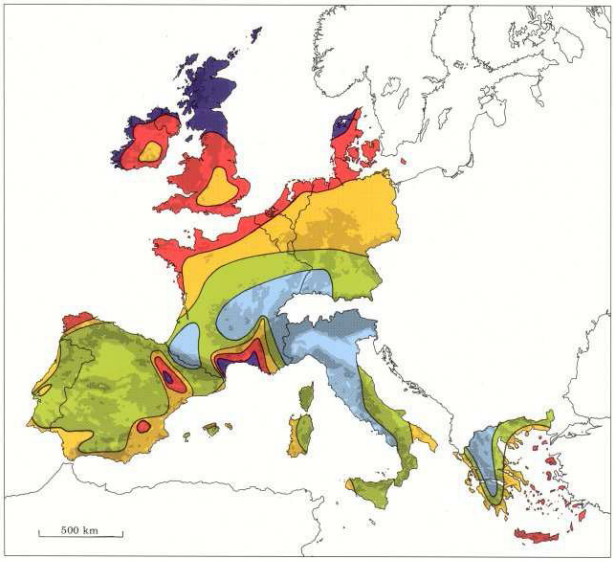

Wind resources[1] at 50 metres above ground level for five different topographic conditions

	Sheltered terrain[2]		Open plain[3]		At a sea coast[4]		Open sea[5]		Hills and ridges[6]	
	m s^{-1}	Wm^{-2}	m s^{-1}	Wm^{-2}	m s^{-1}	Wm^{-2}	m s^{-1}	Wm^{-2}	m s^{-1}	Wm^{-2}
	> 6.0	> 250	> 7.5	> 500	> 8.5	> 700	> 9.0	> 800	> 11.5	> 1800
	5.0-6.0	150-250	6.5-7.5	300-500	7.0-8.5	400-700	8.0-9.0	600-800	10.0-11.5	1200-1800
	4.5-5.0	100-150	5.5-6.5	200-300	6.0-7.0	250-400	7.0-8.0	400-600	8.5-10.0	700-1200
	3.5-4.5	50-100	4.5-5.5	100-200	5.0-6.0	150-250	5.5-7.0	200-400	7.0- 8.5	400- 700
	< 3.5	< 50	< 4.5	< 100	< 5.0	< 150	< 5.5	< 200	< 7.0	< 400

Figure 44 From the European Wind Atlas. Courtesy of Risø National Laboratory, Roskilde, Denmark. (Troen and Petersen, 1989).

It is recommended to make more comparisons to ensure that the wind field is realistically simulated in coastal regions, particularly with respect to wind energy issues.

W_I

Canopy water amount, where "amount" means mass per unit area, "water" means water in all phases including frozen, i.e. ice and snow, and "canopy" means the plant or vegetation canopy. The canopy water is the water on the canopy.

W_ICE_*depth*

Soil frozen water content. Frozen subset of the total water content of the soil W_SO. Thickness of the liquid water equivalent of the frozen water content of each soil layer.

The *depth* part of the acronym indicates the lower bound of the soil layer while the data values themselves are representative for the whole layer.

The figure presents time series of the maximum of soil frozen water content in the model region for the two realisations of A1B (minimum is alway zero), i.e. that grid-box with maximum content in the whole domain for a given year. The general warming predicted in the scenarios is clearly manifest in the strong reduction of frozen soil water content in the model region at 94 cm depth.

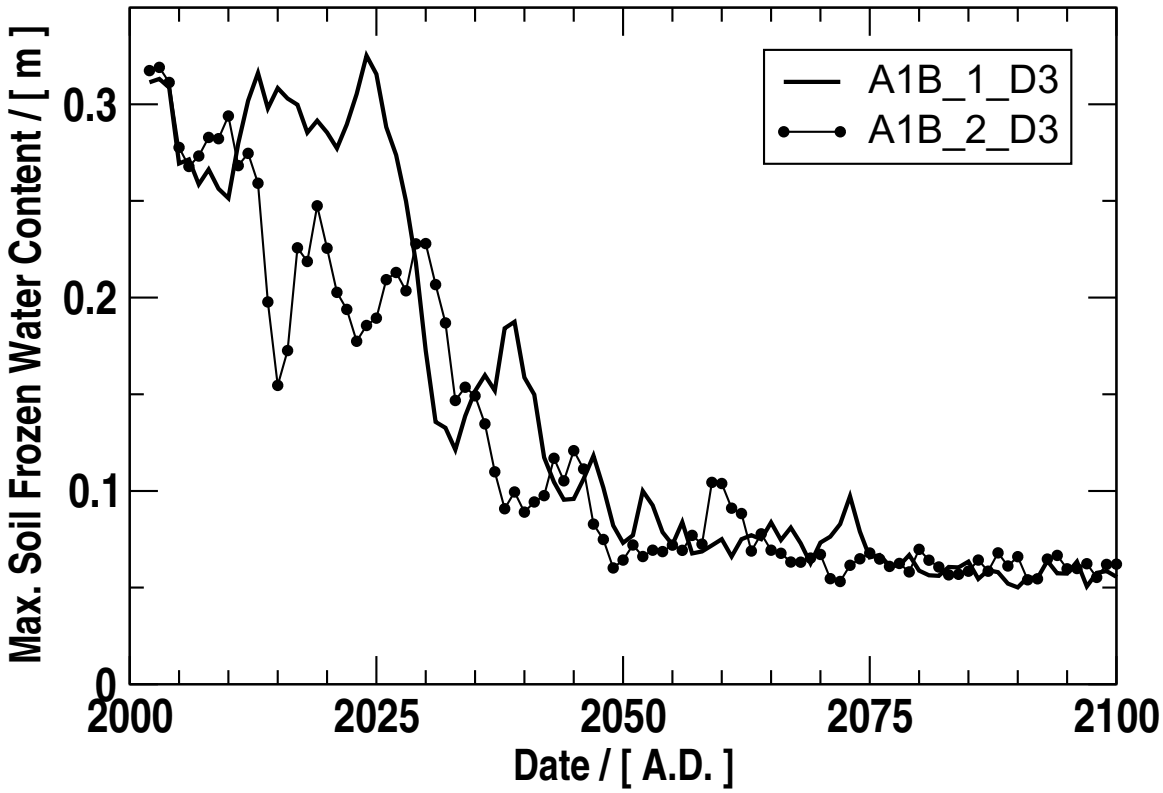

Figure 45 Maximum soil frozen water content between 0.94 – 1.90 m depth for the projection of the 21st century by the scenarios given in the legend.

W_ICE_DAYS
Number of days with frozen soil.

W_SNOW
Surface snow amount. Liquid water equivalent of the vertical extent of snow having the same mass per unit area. Surface amount refers to the amount on the ground, excluding that on the plant or vegetation canopy.

W_SNOW < 0.01 kg/m^2 (liquid water equivalent of 1 cm snow cover in grid box) is used to mask out T_SNOW and to count the days with snow (SNOW_COV) in time interval (monthly and yearly).

(see also T_SNOW, SNOW_COV)

W_SO_*depth*
Soil water content. Total water content of each soil layer. Liquid water equivalent of water in all phases contained in each soil layer, i.e. the extent of a layer of liquid water having the same mass per unit area.

The *depth* part of the acronym indicates the lower bound of the soil layer while the data values itselves are representative for the whole layer.

Technical-Report-Reference: *Reprinted in

Report 1 - 2 Please order the reference list from **Modelle und Daten**
Max-Planck Institut für Meteorologie, Bundesstrasse 53, D-20146 Hamburg, Germany

Report No. 1 **The Adjoint of TM2**
December 2001 Michael Voßbeck, Thomas Kaminski, Ralf Giering, Martin Heimann

Report No. 2 **Climatology and Internal Variability in a 1000-Year Control Simulation with the Coupled Climate Model ECHO-G**
March 2004

Seung-Ki Min*, Stephanie Legutke, Andreas Hense, Won-Tae Kwon

ISSN 1619-2257